

633-3

402788

NAVWEPS REPORT 8141

1 MARCH 1963

NAVWEPS REPORT 8141

ACTIA

CATACOM

quarterly report:

FOUNDATIONAL RESEARCH PROJECTS

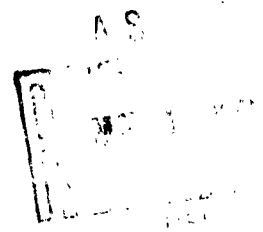
OCTOBER--DECEMBER 1962

402788



NAVAL ORDNANCE LABORATORY CORONA

CORONA, CALIFORNIA



FOR ERRATA

AD _____

402 788

THE FOLLOWING PAGES ARE CHANGES

TO BASIC DOCUMENT

AD 402788

5 June 1963

ERRATUM

QUARTERLY REPORT: FOUNDATIONAL RESEARCH PROJECTS,
OCTOBER-DECEMBER 1962, NAVWEPS Report 8141, U. S. Naval
Ordnance Laboratory, Corona, California, 1 March 1963.

On page 68, immediately preceding the last paragraph, the line should
read:

$b = 0.387$ millivolts

NAVAL ORDNANCE LABORATORY CORONA

W. R. KURTZ, CAPT., USN
Commanding Officer

F. S. ATCHISON, Ph. D.
Technical Director

FOREWORD

This report includes papers on various aspects of work performed during the second quarter of fiscal year 1963 under the Foundational Research Program, whose aim is "to stimulate original work by scientific and technical personnel at the Naval Ordnance Laboratory Corona, in all fields of science and technology." The projects are supported by WepTask R360 FR-104/211-1/R011-01-001. Additional support is provided the High Temperature Polymer Program by WepTask RMGA-41-031/211-1/F009-07-002.

C. J. HUMPHREYS
Head, Research Department

CONTENTS

	<u>Page</u>
FERROMAGNETIC RESEARCH	
Spin Wave Damping Constants for Disordered Crystals, by C. A. Roberts	1
Mean Free Path of Magnons, by C. A. Roberts	20
HIGH TEMPERATURE POLYMER PROGRAM	
Synthetic Studies, by D. L. Herring and C. M. Douglas	21
INFRARED ATOMIC SPECTRA	
Observation and Interpretation of 4f-5g Transitions in the Spectra of Alkalies and Noble Gases, by C. J. Humphreys and E. Paul, Jr.	29
NONAQUEOUS ELECTROCHEMISTRY	
The Electroreduction of Nitrobenzene in Liquid Ammonia Solutions, by W. S. Harris	47
Ionic Melt Electrochemistry, by R. E. Panzer	53
NONLINEAR TRANSMISSION LINES	
The Semigeneralization of the Transmission Line Equations, by J. R. Alday	55
SEMICONDUCTOR MICROWAVE MICROELECTRONICS	
Substrates, Circuitry, and Semiconductors, by R. W. Yancey.	59
SEMICONDUCTOR PHYSICS	
Accurate Measurements of a Magnetic Field by Means of a III-V Hall Effect Device, by K. I. Crowder and H. Piller	67
SOLID STATE SPECTROSCOPY	
The Infrared Absorption Spectrum of Ce^{3+} in $LaCl_3$, by R. A. Buchanan, H. H. Caspers, and J. Murphy	73
Symmetry Coordinates for $LaCl_3$, by J. Murphy and H. H. Caspers	86
SPECTRAL EMITTANCE OF SOLIDS	
Spectral Emittance Measurements of Some Commercial Transparent Solids, by D. L. Stierwalt, D. D. Kirk, and J. B. Bernstein	103

FERROMAGNETIC RESEARCH

SPIN WAVE DAMPING CONSTANTS FOR DISORDERED CRYSTALS

by

C. A. Roberts

Because the damping constants for spin wave excitation are mostly phenomenological in nature, a desirable theoretical objective is to calculate these constants in terms of fundamental constants of disordered crystals.

The excitation of spin waves in ferromagnetic films has been amply demonstrated.¹ However, at the present time there is relatively little understanding of the splitting of the resonance peaks and the nature of the damping. The purposes of the calculations presented in this report are to determine (1) the frequency shift of the normal modes (spin wave modes), and (2) the damping of the spin wave due to the disorder of the sample.

The ideas used in these calculations are based on the recent work of Maradudin et al.² who calculated the frequency spectra for a disordered lattice. Their model is a one-dimensional lattice of N atoms, in which we consider $N - n$ of the atoms to be of mass m and n atoms of mass M . We now consider the m -atoms to be the host lattice and the M -atoms to be distributed at random. If we define a mean mass as

$$M_T = Pm + (1 - P)M$$

then we can consider an average mass M perturbed by the probability P that the l th atom is m and the probability $1 - P$ that the $l + k$ atom is M .

¹C. Kittel, Phys. Rev., Vol. 110, p. 1295 (1958).

²A. A. Maradudin, G. H. Weiss, and D. W. Jepsen, J. Math. Phys., Vol. 2, pp. 349-369 (1960).

In the case of spin waves in a crystal, there is a similar disordered situation. Here the characteristic that is random is either the exchange constant or the z component of the spin.

Let us examine the microscopic equations of motion for a one-dimensional spin wave.

$$\dot{\vec{S}}_k = \frac{1}{i\hbar} [\vec{S}_k, H_I]$$

where

$$H_I = 2J \sum_{i < j} \vec{S}_i \cdot \vec{S}_j$$

Using the semiclassical approximations,³ we have

$$\hbar \dot{\vec{S}} = 2J [\vec{S} \times (6\vec{S} + a^2 \nabla^2 \vec{S})] \quad (1)$$

where a is interatomic spacing and where the quantity in parentheses is H_{eff} , the effective field at the j atom due to all other spins in the structure. Since $\vec{S} \times 6\vec{S} = 0$, equation (1) reduces to

$$\dot{\vec{S}} = \frac{2Ja^2}{\hbar} [\vec{S} \times \nabla^2 \vec{S}] \quad (2)$$

In component form, we have

$$\dot{S}_x = -\frac{2Ja^2}{\hbar} S_z \nabla^2 S_y$$

$$\dot{S}_y = \frac{2Ja^2}{\hbar} S_z \nabla^2 S_x$$

$$\dot{S}_z \cong 0$$

S_z is assumed to be constant in space-time and equal to S_0 .

The equation for S_x is

³C. Kittel, Solid State Physics, New York: John Wiley and Sons, Inc. (1956).

$$\ddot{S}_x = -\left(\frac{2Ja^2 S_o}{\hbar}\right)^2 \nabla^4 S_x \quad (3)$$

For the continuous case in which $S_x \sim e^{i(\omega t - kx)}$, the equation is

$$-\omega^2 S_{ox} = -\left(\frac{2Ja^2 S_o}{\hbar}\right)^2 k^4 S_{ox}$$

or

$$\omega^2 = \frac{2Ja^2 S_o}{\hbar} k^2 \quad (4)$$

where $k = 2\pi/\lambda$.

The dispersion relation for long wavelength spin waves is given by

$$E = \hbar\omega = 2Ja^2 S_o k^2$$

The finite difference equation for S_x is

$$\ddot{S}_{x_l} = -\left(\frac{2Ja^2 S_o}{\hbar}\right)^2 \left[S_{l+2}^x + S_{l-2}^x - 4(S_{l+1}^x + S_{l-1}^x) + 6S_l^x \right] \quad (5)$$

for

$$S_{x_l} \sim S_{x_{ol}} e^{i(\omega t - k l a)} = S_{x_{ol}}(t) e^{-ik l a} \quad (6)$$

where $k_o a = 2\pi/N$. For periodic boundary conditions, we have

$$S_{x_{N+l}} = S_{x_l} \quad (7)$$

and as the general solution

$$S_{x_l} = \frac{1}{\sqrt{N}} \sum_{k=-\frac{N}{2}+1}^{k=+\frac{N}{2}} Q_k \exp\left(\frac{2\pi i k l}{N}\right) \quad (8)$$

where N is the number of atoms between periodic boundaries. Thus

$$S_{x_l} = S_{x_l}^* \quad \text{and} \quad Q_k = Q_{-k}^*$$

Since

$$\frac{1}{N} \sum_l \exp \left[\frac{2\pi i}{N} l(k - k') \right] = \Delta(k - k') = \begin{cases} 1 & k = k' \\ 0 & k \neq k' \end{cases}$$

$$\sum_l S_{x_l} S_{x_l} = \frac{1}{N} \sum_k \sum_{k'} \sum_l Q_{tk} Q_k \exp \left[\frac{2\pi i}{N} l(k - k') \right] = \sum_k |Q_k|^2 \quad (9)$$

Upon substituting equation (8) into equation (5), the finite difference equation for the spins, we get

$$\begin{aligned} \sum \ddot{Q}_k \exp \left(\frac{2\pi i k l}{N} \right) = & - \left(\frac{2JS_o}{\hbar} \right)^2 \sum \ddot{Q}_k \left\{ \exp \left[\frac{2\pi i k}{N} (l + 2) \right] \right. \\ & + \exp \left[\frac{2\pi i k}{N} (l - 2) \right] - 4 \exp \left[\frac{2\pi i k}{N} (l + 1) \right] \\ & \left. - 4 \exp \left[\frac{2\pi i k}{N} (l - 1) \right] + 6 \exp \left(\frac{2\pi i k}{N} \right) \right\} \end{aligned} \quad (10)$$

For each k we then have

$$\ddot{Q}_k = -2 \left(\frac{2JS_o}{\hbar} \right)^2 Q_k \left(\cos \frac{4\pi k l}{N} - 4 \cos \frac{2\pi k}{N} + 3 \right) \quad (11)$$

and with trigonometric substitutions

$$\ddot{Q}_k + 4 \left(\frac{2Ja^2 S_o}{\hbar} \right)^2 \left(1 - 2 \cos \frac{2\pi k}{N} + \cos^2 \frac{2\pi k}{N} \right) Q_k = 0 \quad (12)$$

Note that for $2\pi k/N < 1$ or $k_o a < 1$, equation (12) reduces to $\frac{1}{4} \left(\frac{2\pi k}{N} \right)^4$, and the normal expression for long wavelength spin waves becomes

$\ddot{Q}_k + \left(\frac{JS_o}{\hbar} \right)^2 (ka)^4 Q_k = 0$. The dispersion relation in this motion, and for subsequent work, is then

$$\omega_k^2 = \omega_m^2 \left(1 - \frac{\omega_o^2 2\pi k}{N} \right)^2 \quad (13)$$

where

$$\omega_m^2 = \frac{2JS_o}{\hbar} \quad (14)$$

Let us now consider the effect of perturbing the normal order of a homogeneous line of spins. By this is meant that the environment of a particular lattice site is changed as one proceeds down the line.

The average exchange is defined as

$$J = PJ_1 + (1 - P)J_2 \quad (15)$$

which means that the environment of atom 1 has a probability P and that of atom 2 has a probability $1 - P$. The equation of motion for the system is then

$$\begin{aligned} \ddot{S}_{x_l} = & - \left(\frac{2J}{\hbar^2} \right)^2 \left[S_{l+2}^x + S_{l-2}^x - 4(S_{l+1}^x + S_{l-1}^x) + 6S_l^x \right] \\ & - \left(\frac{2J}{\hbar^2} \right)^2 (J_l - J)^2 \left[S_{l+2}^x + S_{l-2}^x - 4(S_{l+1}^x + S_{l-1}^x) + 6S_l^x \right] \end{aligned} \quad (16)$$

where J_l is the exchange constant of the l th atom. When $J_l = J$, the normal equations for a homogeneous line are recovered. Upon substituting the normal modes into equation (16), we have

$$\begin{aligned} \sum_k \ddot{Q}_k \exp\left(\frac{2\pi i k l}{N}\right) = & - \sum_k \omega_k^2 Q_k \exp\left(\frac{2\pi i k l}{N}\right) \\ & - \sum_k \left(\frac{2Ja^2}{\hbar^2} \right)^2 \left(\frac{J_l}{J} - 1 \right)^2 Q_k \exp\left(\frac{2\pi i k l}{N}\right) \end{aligned} \quad (17)$$

After multiplying both sides of equation (17) by $\frac{1}{\sqrt{N}} \sum_{k'} \exp\left(-\frac{2\pi i k' l}{N}\right)$ and

then summing over l , we have

$$\frac{1}{N} \sum_{k^*} \sum_{\ell} \ddot{Q}_k \exp \left[\frac{2\pi i (k - k') \ell}{N} \right] = - \frac{1}{N} \sum_{k\ell} \omega_k^2 Q_k \exp \left[\frac{2\pi i}{N} (k - k') \ell \right] \\ - \frac{1}{N} \sum_k \sum_{\ell} 4\gamma J a^2 k \left(\frac{J_{\ell}}{J} - 1 \right)^2 Q_k \exp \left[\frac{2\pi i}{N} (k - k') \ell \right]$$

By using the orthogonality property of the exponentials of equation (9), the resulting equation for the $Q_{k'}$ is

$$\ddot{Q}_{k'} + \omega_k^2 Q_{k'} = - \frac{1}{N} \sum_k \sum_{\ell} \omega_k^2 \left(\frac{J_{\ell}}{J} - 1 \right)^2 Q_k \exp \left[\frac{2\pi i}{N} (k - k') \ell \right] \quad (18)$$

In the more compact form, we have

$$\ddot{Q}_k + \omega_k^2 Q_k = - \sum_{k'} \Phi_{kk'} Q_{k'} \quad (19)$$

where

$$\Phi_{kk'} = - \frac{\omega_k^2}{N} \sum_{\ell=2}^N \left(\frac{J_{\ell}}{J} - 1 \right)^2 \exp \left[\frac{2\pi i}{N} (k - k') \ell \right] = 0 \quad (20)$$

if all $J_{\ell} = J$. Here $\Phi_{kk'}$ can be considered as a negative pumping term of the type that is found in parametric amplifier equations. In the special case in which all $\Phi_{kk'} = 0$ except Φ_{kk} , and $\Phi_{kk} = \Phi_0 \cos 2\omega t$, equation (19) takes the form

$$\ddot{Q} + (\omega^2 - \Phi_0 \cos 2\omega t) Q = 0 \quad (21)$$

This equation has the approximate solution

$$Q = \exp \left(- \frac{\Phi_0 t}{4\omega} \right) \left[\left(\sin \omega t - \cos \omega t + \frac{\Phi_0}{16\omega^2} \right) (\sin 3\omega t - \cos 3\omega t) \right] \quad (22)$$

Thus Q is damped by Φ_0 .

The following method for the solution of equation (19) is the same as that used by Maradudin et al.,² with the exception of some small

modifications. Since their method is not widely used, it is discussed at length below.

The transform of $Q_k(t)$ is

$$q_k(S) = \int_0^{\infty} e^{-St} Q_k(t) dt \quad (23)$$

With this expression, equation (19) takes the form

$$q_k(S) = \frac{SQ_k(0) + \dot{Q}_k(0)}{S^2 + \omega_k^2} - \frac{1}{d_k} \sum_{k_1} \Phi_{kk_1} q_{k_1}(S) \quad (24)$$

where

$$d_k = S^2 + \omega_k^2$$

This, of course, is still an integral equation in $q_{k_1}(S)$.

Upon iterating equation (24), we have

$$q_k(S) = D_{kk}(S) c_k(S) + \sum_{m \neq k} D_{km}(S) C_m(S) \quad (25)$$

where

$$c_k(S) = SQ_k(0) + \dot{Q}_k(0)$$

and

$$D_{km}(S) = \frac{S_{km}}{d_k} - \frac{1}{d_k d_m} \left(\Phi_{km} - \sum_{k_1} \frac{\Phi_{kk_1} \Phi_{k_1 m}}{d_{k_1}} + \sum_{k_1 k_2} \frac{\Phi_{kk_1} \Phi_{k_1 k_2} \Phi_{k_2 m}}{d_{k_1} d_{k_2}} \dots \right) \quad (26)$$

Next, the authors² define the operator $G_k(S)$ as

$$G_k(S) = \Phi_{kk} - \sum_{k_1}' \frac{\Phi_{k'k_1} \Phi_{k_1k}}{d_{k_1}} + \sum_{k_1 k_2}' \frac{\Phi_{kk_1} \Phi_{k_1 k_2} \Phi_{k_2 k}}{d_{k_1} d_{k_2}} \dots \quad (27)$$

where the prime means that no summation index k_1 shall equal k .

The relationship of D_k to G_k is simply

$$D_k = \frac{1}{d_k + G_k} \quad (28)$$

so that the solution to the inverse transformation is

$$q_k(S) = \frac{G_k(S)}{d_k + G_k} + \sum_{m \neq k} \frac{G_m(S)}{d_k + G_k} \quad (29)$$

where only the diagonal part of the operator D_{km} is used.

The ensemble average of $q_k(S)$, the average over all atom sites, is

$$\langle q(S) \rangle = \left\langle \frac{G_k(S)}{d_k + G_k} \right\rangle + \sum \left\langle \frac{G_m(S)}{d_k + G_k} \right\rangle \quad (30)$$

and

$$\left\langle \frac{1}{d_k + G_k} \right\rangle = \frac{1}{d_k + \langle G_k \rangle} \quad (31)$$

The solution is then just the inverse transformation to $\langle Q_k(t) \rangle$.

The reason for using only diagonal terms is that the average is performed only over $\langle Q_k(t) \rangle$ and not over $\langle Q_k(t) Q_h(t) \rangle$. In the latter expression, the diagonal terms do contribute.

Thus we find that

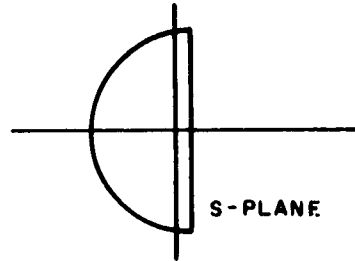
$$\langle Q_k(t) \rangle = \frac{1}{2\pi i} \int_{-i\infty+\epsilon}^{+i\infty+\epsilon} e^{St} \langle q_k(S) \rangle dS \quad (32)$$

or

$$\langle Q_k(t) \rangle = \frac{1}{2\pi i} \left(\int \frac{e^{St} C_k(S) dS}{d_k + \langle G_k \rangle} + \int e^{St} \sum_{m \neq k} \frac{C_m(S)}{d_k + \langle G_{km} \rangle} dS \right) \quad (33)$$

The second term vanishes for $m \neq k$.

The contour for equation (32) is the usual Bromwich contour for inverse Laplace transforms, as shown below.



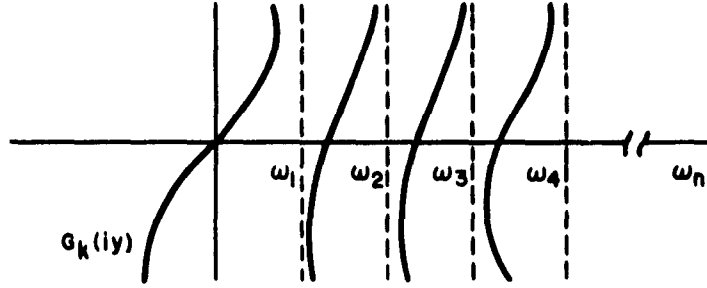
The behavior of $\langle Q_k(t) \rangle$ is governed principally by the denominators of equation (33). The expression

$$G_k(S) = \Phi_{kk} - \sum_{k_1 \neq k}^N \frac{\Phi_{kk_1} \Phi_{k_1 k}}{S^2 + \omega_k^2} \text{ for } S > 0$$

is the first approximation to equation (27) and has a finite number of poles. Since $S^2 + d_k + \langle G_k \rangle$ will have a finite number of zeros, the perturbed system will tend to oscillate. For an infinite number of particles, the pole density becomes infinite in a finite length ($\omega_{m_1} - \omega_m$). If we substitute iy for S ,

$$G_k(iy) = \Phi_{kk} - \sum_{k_1 \neq k}^N \frac{\Phi_{kk_1} \Phi_{k_1 k}}{\omega_{k_1}^2 - y^2} \quad (34)$$

There are $2N$ poles between $\omega_{m_1} - \omega_m$ at $y = \pm \omega_1 \pm \omega_2 \dots$



As can be seen from the plot of equation (34), there is an infinite number of poles as $N \rightarrow \infty$.

$$\begin{aligned} \omega_{k_1} - \omega_{k_2} = & \sqrt{4\gamma J} \left[1 + \cos \frac{2\pi(k+1)}{N} \right. \\ & \left. - \cos \frac{2\pi(k+1)}{N} - 1 + \cos \frac{2\pi k}{N} + \cos \frac{2\pi k}{N} \right] \end{aligned} \quad (35)$$

From equation (35) we obtain

$$\Delta\omega_{k_1} = \sqrt{4\gamma J} \left[\cos \frac{2\pi}{N}(k+1) - \cos \frac{2\pi}{N}k + \cos \frac{2\pi(k+1)}{N} - \cos \frac{2\pi}{N}k \right]$$

For N large, this becomes

$$\Delta\omega_k = \sqrt{4\gamma J} \left(\frac{2\pi}{N} \right)^2 \quad \text{for } 2k+1$$

and, as $N \rightarrow \infty$ and $2\pi k_1 a \rightarrow 0$

$$\Delta\omega_k \cong 2\sqrt{\gamma J} \left(\frac{2\pi}{N} \right)^2 \quad \text{for fixed } k_{0a} < 1 \quad (36)$$

The expression for $\langle Q_k(t) \rangle$ is

$$\begin{aligned} \langle Q_k(t) \rangle = & \frac{Q_k(c)}{2\pi i} \int_{c-i\infty}^{c+i\infty} \frac{S e^{St}}{S^2 + \omega_k^2 + \langle G_k(S) \rangle} dS \\ & + \frac{\dot{Q}_k(0)}{2\pi i} \int_{c-i\infty}^{c+i\infty} \frac{e^{St} dS}{S^2 + \omega_k^2 + \langle G_k(S) \rangle} \end{aligned} \quad (37)$$

Now consider the integral

$$\frac{1}{2\pi i} \int_{c-i\infty}^{c+i\infty} \frac{e^{St} dS}{S^2 + \omega_k^2 + \Phi_{kk}} - \sum_{k_1} \frac{\Phi_{kk_1} \Phi_{kk}}{S^2 + \omega_{k_1}^2} \quad (38)$$

which, on passing to the limit, becomes

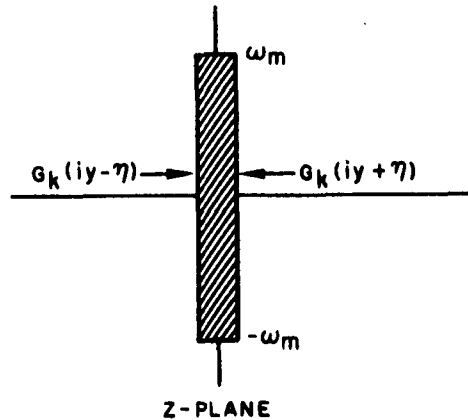
$$\frac{1}{2\pi i} \int_{c-i\infty}^{c+i\infty} \frac{e^{St} dS}{S^2 + \omega^2(k) + \Phi_{kk}} - \frac{1}{2\pi} \int \frac{K(kk_1)}{S^2 + \omega(k_1)^2} dk_1 \quad (39)$$

As $S \rightarrow y$ and $c \rightarrow 0$, we have

$$\frac{1}{2\pi i} \int_{c-i\infty}^{c+i\infty} \frac{e^{St} dS}{-y^2 + \omega^2(k) + \Phi(k)} - \frac{1}{2\pi} \int \frac{K(kk_1) dk_1}{\omega^2(k_1) - y^2} \quad (40)$$

This expression reveals the fact that the integral does not have a simple pole and so the integral in the denominator prevents the integrand from being analytic across the imaginary axis.

The cut is introduced in the S -plane from ω_m to $-\omega_m$.



Thus

$$\lim_{\eta \rightarrow 0^+} G_k(iy \pm \eta) = -K_k(y) \pm iJ_k(y) \quad (41)$$

where

$$K_k(y) = -\Phi_{kk} + \sum_{k_1} \frac{\Phi_{kk_1} \Phi_{k_1 k}}{(\omega_{k_1}^2 - y^2)_p} \quad (42)$$

and

$$J_k(y) = \pi \sin y \sum_{k_1} \Phi_{kk_1} \Phi_{k_1 k} \delta(\omega_{k_1}^2 - y^2) \quad (43)$$

Upon changing variables, $s = iy + c$ as $c \rightarrow 0^+$, and we obtain

$$I_k(t) = \frac{1}{2\pi} \int_{-\infty}^{+\infty} \frac{e^{iyt}}{-y^2 + \omega_k^2 - \langle K_y(y) \rangle + i \langle V_k(y) \rangle} dy \quad (44)$$

The denominator of the integral is just the average of the operator

$$D_k(s) = \frac{1}{s^2 + \omega_k^2 + G_k}$$

which can be written as

$$D_k(z) = [t - z - g(z)]^{-1}$$

and which has dissipative properties.⁴

Equation (44) can be written as

$$I_k(t) \equiv \frac{1}{2\pi} \int_{-\infty}^{+\infty} \frac{e^{iyt}}{U_k(y) + iV_k(y)} dy \quad (45)$$

⁴N. M. Hugenholtz, The Many Body Problem, New York: John Wiley and Sons, Inc., pp. 33-35 (1959).

where

$$\langle V_k(y) \rangle = 0 \text{ for } |y| > y_0 \quad y_0 = |\omega_n| \quad (46)$$

that is, the imaginary part of the denominator vanishes for regions beyond the maximum frequency. Also,

$$\langle U_k(y) \rangle = -y^2 + \omega_k^2 + \langle K_k(y) \rangle = 0 \text{ for } y > y_0 \quad (47)$$

If the probability value P for a lattice site is equal to 1 or 0, then $V_k(y) = 0$ for all y and $U_k(y)$ reduces to $-y^2 + \omega_k^2 = 0$, and the normal unperturbed frequencies are recovered.

It is the finite and nonvanishing part of $\langle V_k(y) \rangle$ that gives rise to dissipation. This is dissipation in the following sense: The state of the system changes in time τ irreversibly goes into a more complicated configuration, but there is no violation of the conservation of energy.

The argument of Hugenholtz⁴ can be used to estimate the long time behavior of the integral. It must be emphasized that since his method would give a vanishing result for the normal modes, it would not give the complete time dependence of the system.

If we expand $U_k(y) + iV_k(y)$ about the points $y = +y_k$ and $y = -y_k$ and note that $U_k(y_k) = 0$,

$$I_k(t) \cong \frac{1}{2\pi} \int_{-\infty}^{+\infty} e^{iyt} \left[\frac{1}{U_k(y_k) + (y - y_k)U_{k'}(y_k) + iV_k(y)} + \frac{1}{U_k(-y_k) + (y + y_k)U_{k'}(-y_k) + iV_k(-y_k)} \right] dy \quad (48)$$

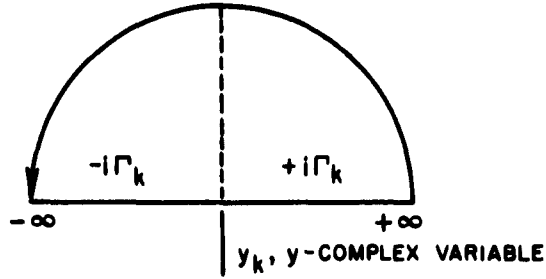
for $4k > 0$. Combining these terms with the given notations

$$N_k = \frac{1}{|U_{k'}(y_k)|} \quad \text{and} \quad \Gamma_k = N_k V_k(y_k) \quad (49)$$

we have

$$U_k(y) = f(y^2) \quad \text{and} \quad U_{k'}(-y) = -U_{k'}(y) \quad (50)$$

which may be plotted as



Thus

$$I_k(t) = -\frac{N_k}{2\pi} \int e^{iyt} \left(\frac{1}{y - y_k - i\Gamma_k} - \frac{1}{y + y_k - i\Gamma_k} \right) dy \quad (51)$$

$$I_k(t) \simeq 2N_k e^{-\Gamma_k t} \sin y_k t \quad (52)$$

The perturbed spin wave mode is then

$$\langle Q_k(t) \rangle \sim 2N_k \left[Q_k(0) e^{-\Gamma_k t} y_k \cos y_k t + \dot{Q}_k(0) e^{-\Gamma_k t} \sin y_k t \right] \quad (53)$$

Upon substitution of the above equation in the expression (8) for the normal modes, we have

$$S_{x_l} = \frac{1}{\sqrt{N}} \sum_{k=-(N/2)+1}^{k=+N/2} 2N_k \dot{Q}_k(0) e^{-\Gamma_k t} \sin y_k t \exp\left(\frac{2\pi i k l}{N}\right) \quad (54)$$

If we assume $\dot{Q}_k(0) \neq 0$ and $Q_k(0) = 0$, then

$$S_{x_l} = \frac{1}{\sqrt{N}} \sum 2N_k \dot{Q}_k(0) e^{-\Gamma_k t} \exp \left[i \left(y_k t - \frac{2\pi i k l}{N} \right) \right] \quad (55)$$

This is the general solution to spin waves propagating in a disordered medium, where

$2N_k \dot{Q}_k(0) = A_k$ amplitude

Γ_k = damping constant

and y_k = the shifted normal mode frequency, which is determined from

$$-y_k^2 = +\omega_k^2 + \langle G_k(iy + \eta) \rangle \text{ as } \eta \rightarrow 0^+ \quad (56)$$

Physically, the disordered spin wave medium damps a normally propagating spin wave for long periods of time.

It must be emphasized that this is not the only mechanism that brings about a finite amplitude to a spin wave resonance.

The ensemble average of

$$\Phi_{kk_1} = \frac{\omega_k^2}{N} \sum_{\ell=1}^N \left(\frac{J_\ell}{J} - 1 \right)^2 \exp \left[\frac{2\pi i(k - k_1)\ell}{N} \right] \quad (57)$$

becomes

$$\begin{aligned} \langle \Phi_{kk_1} \rangle &= \frac{\omega_k^2}{N} \sum_{\ell=1}^N \left[P \left(\frac{J_\ell}{J} - 1 \right)^2_{J_\ell=1} + (1 - P) \left(\frac{J_\ell}{J} - 1 \right)^2_{J_\ell=J_2} \right] \exp \left[\frac{2\pi i}{N} (k - k_1)\ell \right] \\ &= \frac{\omega_k^2}{N} \left[P \left(\frac{J_1}{J} - 1 \right)^2 + (1 - P) \left(\frac{J_2}{J} - 1 \right)^2 \right] \Delta(k - k_1) \\ &= \frac{\omega_k^2}{N} U_1 \Delta(k - k_1) \end{aligned} \quad (58)$$

The average for $\langle \Phi_{kk_1} \Phi_{k_1 k_2} \rangle$ is calculated in the same manner as that used by Maradudin et al., that is, we separate the diagonal terms from the nondiagonal terms and sum and average separately.

$$\begin{aligned} \langle \Phi_{kk_1} \Phi_{k_1 k_2} \rangle &= \frac{\omega_{k_1}^2 \omega_{k_2}^2}{N^2} \sum_j \left\langle \left(\frac{J_j}{J} - 1 \right)^2 \left(\frac{J_\ell}{J} - 1 \right)^2 \right\rangle \\ &\quad \cdot \exp \left\{ -\frac{2\pi L}{N} \left[(k - k_1)j + U_{k_1} + k_2 \right] \ell \right\} \\ &= \frac{\omega_{k_1}^2 \omega_{k_2}^2}{N^2} \left\{ \sum_{j=1}^N \left\langle \left(\frac{J_j}{J} - 1 \right)^4 \right\rangle \exp \left[-\frac{2\pi i}{N} (k - k_2)j \right] \right\} \end{aligned} \quad (\text{Contd.})$$

$$\sum_{j \neq l} \left\langle \left(\frac{J_j}{J} - 1 \right)^2 \left(\frac{J_l}{J} - 1 \right)^2 \right\rangle \quad (59)$$

$$\cdot \exp \left\{ -\frac{2\pi i}{N} [(k - k_1)j + (k_1 - k_2)l] \right\}$$

We now average each term separately.

$$\begin{aligned} \langle \Phi_{kk_1} \Phi_{k_1 k_2} \rangle &= \frac{\omega_{k_1}^2 \omega_{k_2}^2}{N^2} \left(\left\langle \left(\frac{J_l}{J} - 1 \right)^4 \right\rangle \sum_{j=1}^N \exp \left[-\frac{2\pi i}{N} (k - k_2)j \right] \right. \\ &\quad \left. + \left\langle \left(\frac{J_l}{J} - 1 \right)^2 \right\rangle^2 \sum_{j \neq l} \exp \left\{ -\frac{2\pi i}{N} [(k - k_1)j + (k_1 - k_2)l] \right\} \right) \quad (60) \end{aligned}$$

Next, we add and subtract the diagonal term

$$\langle \Phi_{kk_1} \Phi_{k_1 k_2} \rangle = \frac{\omega_{k_1}^2 \omega_{k_2}^2}{N^2} \left[\frac{\mu_2 - \mu_1^2}{N} + \mu_1^2 \Delta(k - k_1) \right] \cdot \Delta(k - k_2) \quad (61)$$

where

$$\begin{aligned} \mu_1 &= P \left(\frac{J_1}{J} - 1 \right)^2 + (1 - P) \left(\frac{J_2}{J} - 1 \right)^2 \\ \mu_2 &= P \left(\frac{J_1}{J} - 1 \right)^4 + (1 - P) \left(\frac{J_2}{J} - 1 \right)^4 \end{aligned}$$

With these results, we can now find explicit expressions for the damping constants.

The solution for the shift of the normal mode frequency is reached in the following manner: From equation (56), with $\langle U_k \rangle = 0$, we have

$$-y_k^2 + \omega_k^2 = -\langle \Phi_{kk} \rangle + \sum_{k_1} \frac{\langle \Phi_{kk_1} \Phi_{k_1 k} \rangle}{(\omega_{k_1}^2 - y^2)_p}$$

where the averages may be obtained from equations (58) and (61). Then

$$y_k^2 = \omega_k^2 \left[1 - \mu_1 - (\mu_2 - \mu_1^2) \frac{1}{N} \sum_{k_1} \frac{\omega_{k_1}^2}{(\omega_{k_1}^2 - i y_k^2)_p} \right]$$

Treating the sum as small, we have to the first order

$$y_k = \omega_k \left[1 - \mu_1 - \frac{1}{2} (\mu_2 - \mu_1^2) \frac{1}{N} \sum_{k_1} \frac{\omega_{k_1}^2}{(\omega_{k_1}^2 - \omega_k^2)_p} \right]$$

or

$$y_k = (1 - \mu_1) \omega_m \left(1 - \cos \frac{ka}{N} \right)^{\frac{1}{2}} - \frac{1}{2} \omega_m \left(1 - \cos \frac{ka}{N} \right)^{\frac{1}{2}} (\mu_2 - \mu_1^2) \frac{1}{N} \sum_{k_1} \frac{\omega_{k_1}^2}{(\omega_{k_1}^2 - \omega_m^2)_p}$$

We may proceed in the manner of Maradudin et al. and calculate the shift in the zero point energy, but that is not of interest here.

The damping constant Γ_k was given in equation (49) as

$$\Gamma_k = N_k V_k(y_k)$$

where y_k is the shifted normal mode frequency and, from equation (43),

$$V_k(y_k) = \langle J_k(y_k) \rangle = \left\langle \pi \sin y \sum_{k_1} \Phi_{kk_1} \Phi_{k_1k} \delta(\omega_k^2 - y_k^2) \right\rangle$$

Using the specific results for the spin wave problem as given by equation (61) for $\langle \Phi_{kk_1} \Phi_{k_1k_2} \rangle$, we have

$$\begin{aligned} V_k(y_k) &= \pi \omega_k^2 (\mu_2 - \mu_1^2) y_k \frac{1}{N} \sum_{k_1} \omega_{k_1}^2 \delta(\omega_{k_1}^2 - y_k^2) \\ &= \pi \omega_k^2 (\mu_2 - \mu_1^2) \frac{1}{N} \sum_{k_1} \omega_m^2 \left(1 - \cos \frac{2\pi k}{N} \right) \delta(\omega_{k_1}^2 - y_k^2) \end{aligned}$$

Using the relation

$$\omega_k^2 = \omega_m^2 \left(1 - \cos \frac{2\pi k}{N}\right)^2$$

we obtain

$$V_k(y_k) = \pi \omega_k^2 (\mu_2 - \mu_1^2) \frac{1}{\pi} \int_0^\pi \omega_m^2 \left(1 - \cos \frac{2\pi k}{N}\right)^2 \cdot \delta \left[\omega_m^2 \left(1 - \cos \frac{2\pi k}{N}\right)^2 - y^2 \right] dy$$

where $Q \rightarrow \pi k/N$. We let

$$X^2 = \omega_m^2 (1 - \cos 2Q)^2$$

and solve for $\cos 2Q$. If we use the fact that $0 \leq \omega_k \leq \omega_m$ and the relation

$$\delta(X^2 - y^2) = \frac{1}{2y} [\delta(X - y) + \delta(X + y)]$$

then

$$\begin{aligned} V_k(y) &= \pi \omega_k^2 (\mu_2 - \mu_1^2) \frac{1}{2\pi y} \int \frac{X^2 \delta(X - y)}{\omega_m \sqrt{1 - (1 - X/\omega_m)^2}} \\ &= \pi \omega_k^2 (\mu_2 - \mu_1^2) \frac{1}{2\pi \omega_m} \frac{y}{\sqrt{1 - (1 - y/\omega_m)^2}} \quad 0 \leq y \leq \omega_m \\ &= 0 \quad y \geq \omega_m \end{aligned}$$

The other function needed for the damping constant is

$$N_k^{-1}(y) = |U_{k'}(y_k)|$$

Since

$$U_k(k) = -y_k^2 + \omega_k^2 - \langle K_k(y) \rangle$$

we can approximate $|U_{k'}(y)|$:

$$|U_{k'}(y)| \approx |-2y_k - \langle K_{y'}(y) \rangle| \approx 2\omega_k$$

to the first order for $y_k \approx \omega_k$. By combining the terms, the damping constant for spin waves as a function of wave number is

$$\Gamma_k = \frac{\pi \omega_k (\mu_2^2 - \mu_1^2)}{4\pi} \frac{\omega_k}{\omega_m} \frac{1}{\sqrt{1 - \left(1 - \frac{\omega_k}{\omega_m}\right)^2}}$$

and for $\omega_k = \omega_m$

$$\Gamma_m = \frac{1}{4} (\mu_2^2 - \mu_1^2) \omega_m$$

This is to be compared with the case of phonons where

$$\Gamma_m = \infty$$

For long wavelength spin waves, with $ka \ll 1$

$$\Gamma_k = \frac{1}{4} (\mu_2^2 - \mu_1^2) \omega_m (1 - \cos ka) \sqrt{\frac{1}{2} \frac{\omega_k}{\omega_m}}$$

or

$$\Gamma_k = \frac{1}{16} (\mu_2^2 - \mu_1^2) \omega_m (ka)^3$$

$$\omega_m = \frac{2JS_0}{\hbar} \approx 2 \times 10^{13} \text{ sec}^{-1}$$

$$\mu_2^2 - \mu_1^2 = P(1 - P) \left[\left(\frac{J_1}{J} - 1 \right)^2 + \left(\frac{J_2}{J} - 1 \right)^2 \right]$$

where J_1 and J_2 are the exchange constants for each component. Thus

$$\Gamma_k = 10^{13} P(1 - P) \left[\left(\frac{J_1}{J} - 1 \right)^2 + \left(\frac{J_2}{J} - 1 \right)^2 \right] (ka)^3$$

for long wavelength spin waves.

Note that spin wave energy is proportional to $(ka)^2$ and spin wave velocity is proportional to ka , therefore the rate of energy transfer is

proportional to $(ka)^3$. For example, if $\lambda \sim 100 \text{ \AA}$, $a \sim 1 \text{ \AA}$ and $\Gamma_k \sim 10^9 \text{ sec}^{-1}$.

MEAN FREE PATH OF MAGNONS

by

C. A. Roberts

The lifetime of the magnon is

$$\tau_k = \Gamma_k^{-1} = \frac{4\omega_m \sqrt{1 - (1 - \omega_k/\omega_m)^2}}{\omega_k^2 (\mu_1 - \mu_2)^2}$$

The mean free path as a function of number is

$$l_k = V_g \tau_k \quad \text{where} \quad V_g = \frac{d\omega}{dk} = \text{group velocity}$$

Thus

$$l_k = 4 \left(\frac{\omega_m}{\omega_k} \right)^2 \frac{\sin ka \sqrt{1 - (1 - \omega_k/\omega_m)^2}}{\mu_1 - \mu_2}$$

for spin waves with $ka \ll 1$, and for $ka = 1/100$

$$l_k = 1.6 \times 10^{-3} \text{ cm}$$

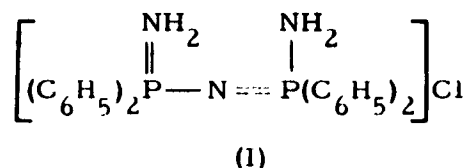
HIGH TEMPERATURE POLYMER PROGRAM

SYNTHETIC STUDIES

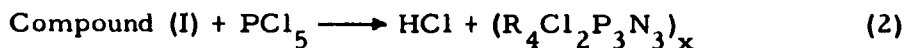
by

D. L. Herring and C. M. Douglas

It was initially postulated by the authors that

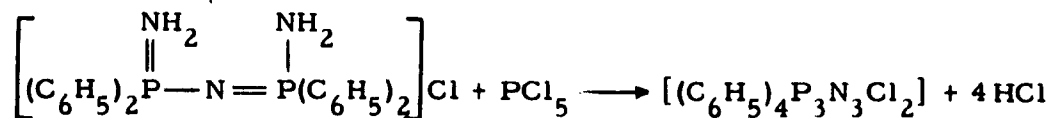


would react with the three classes of pentavalent phosphorus halides according to the following equations:



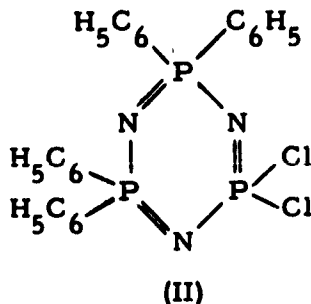
and yield the corresponding cyclic trimer, along with higher polymers. The preparation of $[(\text{C}_6\text{H}_5)_2\text{PN}]_3$ by the equation (1) method has been described.¹ This report gives an account of the preparation of $[(\text{C}_6\text{H}_5)_4\text{P}_3\text{N}_3\text{Cl}_2]$ by means of equation (2).

When compound (I) reacted with PCl_5 under vacuum over the range 135-145°C, about 75% of the amount of HCl was evolved that would be expected from the reaction



¹NAVWEPS Report 7229, Quarterly Report: Foundational Research Projects, April-June 1962, pp. 19-31 (August 1962).

From the product mixture, some $(\text{PNCl}_2)_3$ was isolated, together with a 24% yield of a white crystalline compound (m. p. $142-143^\circ\text{C}$, lit. m. p. $137-140^\circ\text{C}$), which was identified on the basis of its infrared spectrum (Figure 1) and an elemental analysis as the tetraphenyl geminal dichlorophosphonitrilic cyclic trimer²

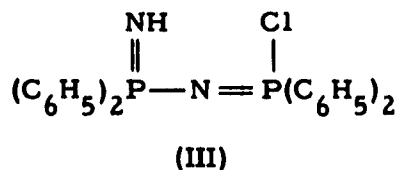


The isolation of the geminal dichloride caused considerable difficulty because of its extreme solubility in all the solvents tried. However, this route to the geminal dichloride appears to be an improvement over the Friedel-Crafts method,² which required a reaction period of six weeks and gave lower yields.

In a second experiment, compound (I) reacted with PCl_5 in CH_3CN and again yielded the geminal dichloride (II), but the yield was less than the amount isolated in the first experiment described above.

In a preliminary experiment, compound (I) reacted with $\text{C}_6\text{H}_5\text{PCl}_4$ under vacuum at $140-145^\circ\text{C}$ and gave a new $[(\text{C}_6\text{H}_5)_2\text{PN}]_x$ compound (m. p. $163-164^\circ\text{C}$), together with a polymeric material which analyzed only approximately for $[(\text{C}_6\text{H}_5)_5\text{P}_3\text{N}_3\text{Cl}]$.

In a series of four experiments in which reaction times were varied from 45 to 90 hours, $(\text{C}_6\text{H}_5)_2\text{PCl}$ reacted with $\text{NH}_2\text{NH}_2 \cdot \text{HCl}$ in refluxing tetrachloroethane³ and yielded $[(\text{C}_6\text{H}_5)_2\text{PN}]_3$ and a compound that was tentatively identified as



²R. A. Shaw and F. B. G. Wells, Chem. and Ind., pp. 1189-1190 (1959).

³H. Sisler, H. Ahuja, and N. Smith, Inorganic Chemistry, Vol. 1, pp. 84-88 (1962).

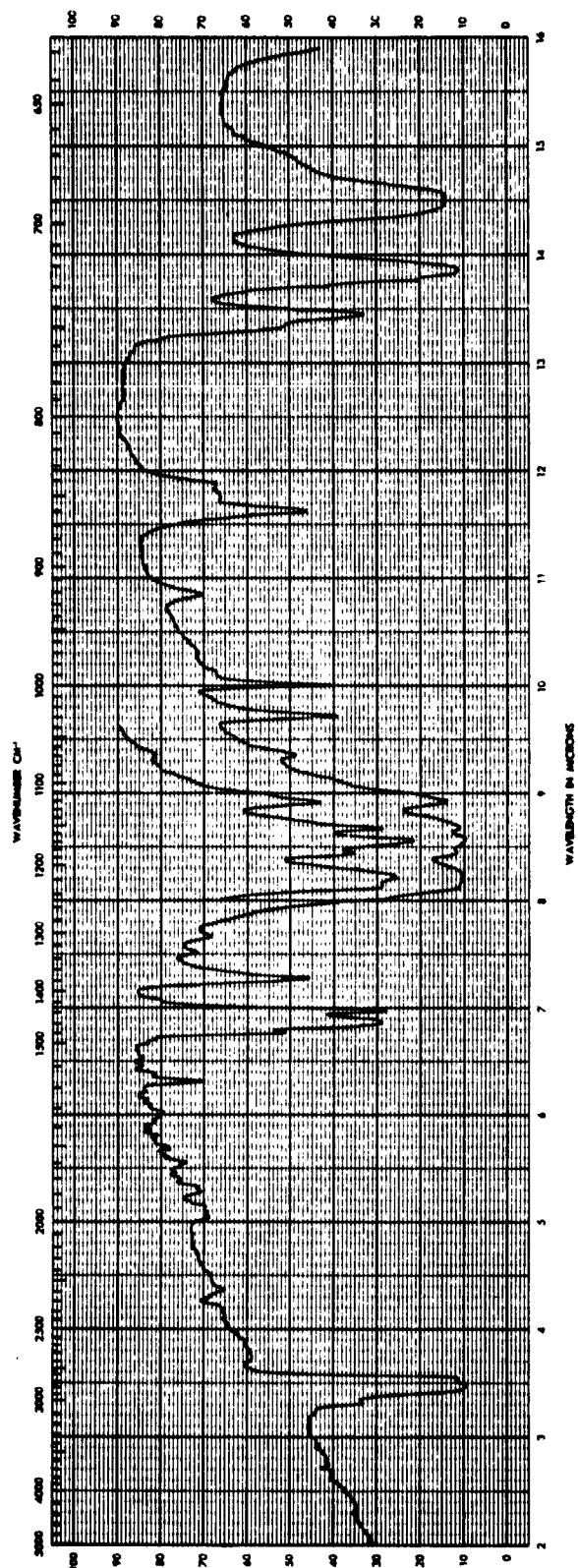
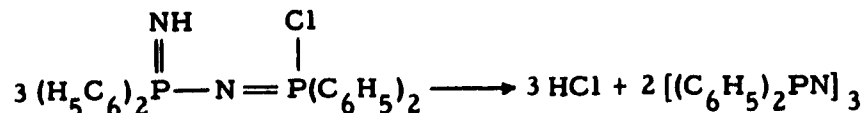


FIGURE 1. Infrared Spectrum of the Tetraphenyl Geminal Dichlorophosphonitrilic Cyclic Trimer

Pyrolysis of compound (III) under vacuum over the range 240-250°C, which may be described according to the equation:

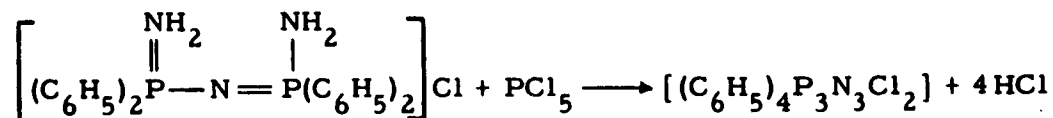


yielded $[(\text{C}_6\text{H}_5)_2\text{PN}]_3$.

EXPERIMENTAL

Reaction of Compound (I) with PCl_5 Under Vacuum

In the drybox, 5.71 g (0.0126 mole) of compound (I) was mixed with 2.63 g (0.0126 mole) of PCl_5 , and the mixture was introduced into a heavy-wall glass ampoule. The ampoule was removed from the drybox, attached to the vacuum line, and gradually heated in an oil bath. The reaction mixture melted at bath temperature, 110-120°C, and evolution of hydrogen chloride commenced at 135-140°C. The reaction was continued for 8 hours at 140-145°C, with continuous removal of the HCl. The yield of HCl was 830 ml/STP, or 74% of the amount anticipated for the reaction



The ampoule was detached from the vacuum line and opened to the air. A small amount of white crystalline material which had sublimed into the neck of the ampoule was identified by its melting point (109-110°C, Fisher-Johns m. p. block) and infrared spectrum as $(\text{PNCI}_2)_3$.

The solid material remaining in the ampoule was extracted with boiling benzene. A portion of the reaction mixture was benzene-insoluble and was removed from the solution by filtration. The insoluble fraction was extracted with 400 ml of hot ligroine (boiling range 65-75°C). When the ligroine solution was allowed to stand undisturbed for several days, crystals were formed which melted sharply at 171°C. No other analytical data are available as yet.

The benzene was removed from the soluble portion of the reaction product. The light-tan residue was extracted repeatedly with ligroine (boiling range 90-120°C). Prolonged fractional crystallization from the ligroine solution yielded 1.51 g (24%) of compound (II).

Calcd. for $C_{24}H_{20}P_3N_3Cl_2$: C, 56.1; H, 3.9; P, 18.1; N, 8.2; Cl, 13.8;
m.p. 137-140°C

Found: C, 56.2; H, 4.0; P, 18.2; N, 8.3; Cl, 13.8
m.p. 142-143°C

The material that was not soluble in ligroine softened over the range 80-100°C.

Found: C, 54.8; H, 4.9; P, 18.3; N, 8.4; Cl, 10.4; O, 2.3

Reaction of Compound (I) with PCl_5 in CH_3CN

In the drybox, 4.2 g (0.009 mole) of compound (I), dissolved in 100 ml of acetonitrile, reacted with 1.9 g (0.009 mole) of freshly sublimed PCl_5 in the manner previously described.⁴ One of the products isolated in this experiment was a material which was recrystallized from ligroine (boiling range 90-120°C). Its melting points were 137-139°C (Fisher-Johns m.p. block) and 142-143°C (sealed tube). This material was identified as the geminally substituted dichlorotetraphenyl phosphonitrilic trimer.

Calcd. for $C_{24}H_{20}P_3N_3Cl_2$: C, 56.1; H, 3.9; P, 18.1; N, 8.2; Cl, 13.8

Found: C, 56.3; H, 3.9; P, 18.1; N, 8.4; Cl, 13.6

Preparation of Phenyltetrachlorophosphorane

In the drybox, 50.4 g (0.281 mole) of phenyldichlorophosphine was dissolved in 500 ml CCl_4 which had been dried by distillation from P_2O_5 . The solution was introduced into a 1-liter stainless steel bomb fitted with a valve and vacuum line connection. The bomb was attached to the vacuum line, cooled to -196°C, and charged with 20 g (0.281 mole) of chlorine. The bomb was then allowed to warm to room temperature. After 72 hours it was emptied into a liter flask in the drybox. Because of the great solubility of $C_6H_5PCl_4$ in CCl_4 , it was necessary to evaporate the solution to near dryness before the product could be isolated (m.p., sealed tube, 75-76°C; lit. 75°C).

Reaction of Compound (I) with Phenyltetrachlorophosphorane

In the drybox, 5.11 g (0.011 mole) of compound (I) was mixed with 2.82 g (0.011 mole) of $C_6H_5PCl_4$ and introduced into a heavy-wall glass ampoule. The reaction tube was attached to the vacuum line and gradually heated to 175°C. The mixture fused at 90-95°C and began to evolve

⁴NAVWEPS 7237, Quarterly Report: Foundational Research Projects, July-September 1962, p. 48 (December 1962).

HCl at 120°C. During the 8-hour heating cycle the HCl was continuously removed (total amount recovered, 720 mm/STP). The reaction product was then extracted with benzene and 0.59 g of $[(C_6H_5)_2PN]_4$ was recovered by fractional crystallization. The benzene was evaporated and the crude product extracted with ligroine. The first fraction recovered from the ligroine solution was a small amount of crystalline material that melted sharply at 163-164°C.

Calcd. for $[(C_6H_5)_2PN]_x$: C, 72.3; H, 5.1; P, 15.6; N, 7.0

Found: C, 72.1; H, 5.1; P, 15.6; N, 6.8

A material which appeared to be amorphous (softening point 95-100°C) was also precipitated from the ligroine solution.

Calcd. for $(C_6H_5)_5P_3N_3Cl$: C, 65.0; H, 4.5; P, 16.8; N, 7.5; Cl, 6.3

Found: C, 66.78; H, 4.69; P, 16.8; N, 6.37; Cl, 4.62

Reaction of Diphenylchlorophosphine with Hydrazine Monohydrochloride in Tetrachloroethane

Four experiments were conducted to test the reaction of $(C_6H_5)_2PCl$ and $NH_2NH_2 \cdot HCl$ in tetrachloroethane. Reaction times varied from 45 to 90 hours, but the results were essentially the same. The following is a typical experiment.

To 21.0 g (0.3 mole) of $NH_2NH_2 \cdot HCl$ slurried in 200 ml of boiling tetrachloroethane was added dropwise, with stirring, a solution containing 66.3 g (0.3 mole) of $(C_6H_5)_2PCl$ in 200 ml of tetrachloroethane. After the mixture was stirred at reflux temperature for 72 hours, a precipitate of $NH_2NH_2 \cdot HCl$ and NH_4Cl was removed by filtration. Next, the excess tetrachloroethane was removed under vacuum and an amber-colored mixture of solids remained. The mixture of residual solids was extracted with 1 liter of dry acetone, and the insoluble material was removed by filtration. From the acetone solution, 7.2 g (11%) of a white granular mixture (m.p. 217-230°C) was isolated by recrystallization. The material was probably the desired compound,

$$\begin{array}{c} \text{NH} \quad \text{Cl} \\ || \quad | \\ (C_6H_5)_2P-N=P(C_6H_5)_2 \end{array}$$

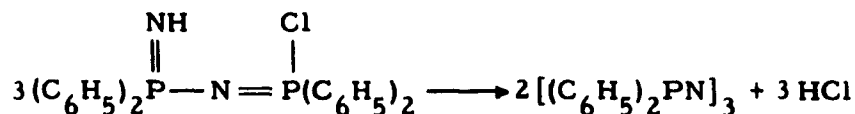
contaminated with some oxygen-containing impurity.

Calcd. for $C_{24}H_{21}P_2N_2Cl$: C, 66.6; H, 4.9; N, 6.4; P, 14.2; Cl, 7.9

Found: C, 68.8; H, 5.1; N, 6.2; P, 13.2; Cl, 5.1; O, 1.6

The acetone-insoluble material was then extracted with 1 liter of boiling benzene and the insoluble material was removed by filtration. From the resulting solution, by the process of fractional recrystallization, 3.2 g (5%) of a white crystalline material (m.p. 267-269°C) was isolated. Concentration of the remaining benzene solution yielded 10.3 g (18%) of $[(C_6H_5)_2PN]_3$ (m.p. 224-226°C).

When a sample of the unknown material was pyrolyzed under vacuum at 240-250°C, 95% of the HCl required for the reaction



was collected. The resulting solid product was identified as $[(C_6H_5)_2PN]_3$ (m.p. 217-222°C). The conversion of this material into $[(C_6H_5)_2PN]_3$ in the above pyrolysis experiment strongly suggests that it is the com-

pound $(C_6H_5)_2\overset{\overset{NH}{\parallel}}{P}-N=\overset{\overset{Cl}{|}}{P}(C_6H_5)_2$. However, a quantitative analysis of the elements was only approximate for this compound.

Calcd. for $C_{26}H_{21}P_2N_2Cl$: C, 66.5; H, 4.9; P, 14.3; N, 6.5; Cl, 7.9

Found: C, 66.5; H, 4.9; P, 14.4; N, 8.9; Cl, 5.6

INFRARED ATOMIC SPECTRA

OBSERVATION AND INTERPRETATION OF 4f-5g TRANSITIONS IN THE SPECTRA OF ALKALIS AND NOBLE GASES

by

C. J. Humphreys and E. Paul, Jr.

The experimental program during recent months has emphasized the observation of selected spectra in the 4-micron region. Owing to repeated detector failures, the amount of data accumulated has been relatively small. It has been sufficient, however, to demonstrate the feasibility of observation in this region. Furthermore, the interpretation of new data on the spectra of the noble gases has demonstrated the validity of the treatment of one aspect of the theory of complex spectra, something heretofore impossible owing to lack of observations in a region previously unexplored by high-resolution methods.

Discussion of the experiments is limited to a few comments, since in essentials the methods remain the same as previously reported. Microwave-excited electrodeless source tubes with inblown windows oriented end-on have proved satisfactory for the region covered. The response of coolable lead sulfide cells mounted in miniature Dewars of a variety of designs is found not to fall off to a significant extent for wavelengths short of 4 microns. The location of the practical limit near this point still permits observation of essentially all the interesting features of the spectra under study. A much more serious handicap associated with the use of these detectors is a tendency of the Dewars to lose vacuum or even to fracture, something apparently associated with the cooling and heating cycle. Some consideration is being given to developing new designs for the Dewars since the loss of time from detector failure is becoming intolerable.

It has also been necessary to replace the 15,000 lines-per-inch grating with one of 7,500 lines per inch, since the former can only reach 3.3 microns in the first order in the Littrow arrangement. The relatively small dispersion associated with practical scanning speeds is not so much of a handicap as it might appear when working near 4 microns. With reasonable effort the chart features can be measured to not much better than 1 Å. It is noted, however, that at 4 microns a change of 1 Å is equivalent to a wave-number variation of 0.06 cm^{-1} .

In an earlier period of radiometric observation of line emission spectra connected with the name of Paschen,¹ a feature was found in several spectra, notably those of the alkalis, near 4 microns. It was interpreted as the transition between the unresolved doublet levels associated with the f- and g-configurations. The line, shifting slightly to shorter wavelengths with elements of increasing atomic number, was very near to that associated with the transition between the fifth and fourth orbits of hydrogen, which was discovered by Brackett² more than ten years later. Illustrated here is a kind of degeneracy related to all atomic spectra, resulting from the essentially hydrogenic character of levels from peripheral configurations. It is expected, therefore, that a fairly conspicuous feature may be observed near 4 microns, of a complexity dependent on the electron configuration. The precision of Paschen's observations was surprisingly good when one considers the energy limitation of his thermal detectors and the fact that the lines are of only moderate intensity.

A short section of cesium record, shown in Figure 1, illustrates the feature in question, another Ritz combination in Cs I, and two argon lines. The wavelength of the Cs I line of lesser intensity is calculable from Kleiman's³ energy-level values. The first-order Ar I lines are included among those described in the following section of this report.

The features appearing in the record are:

	λ, A	σ, cm^{-1}	Transition
Cs I	39177.66	2551.779	$5p^6 7p^2 P_{0\frac{1}{2}}^\circ - 5p^6 8s^2 S_{0\frac{1}{2}}$
Cs I	39418	2536.2	$5p^6 4f^2 F^\circ - 5p^6 5g^2 G$
Ar I	39659.75	2520.76	$4f[1\frac{1}{2}]_{1,2} - 5g[2\frac{1}{2}]_{2,3}^\circ$
Ar I	39899.65	2505.60	$4f[4\frac{1}{2}]_{4,5} - 5g[5\frac{1}{2}]_{5,6}^\circ$

Of much greater theoretical interest are the features associated with the transitions, occurring in the 4-micron region, between the levels originating respectively in the configurations $p^5 f$ and $p^5 g$ of the noble atmospheric gases. These configurations are analogous with pf and pg, which are characteristic of fourth-group elements, notably germanium,

¹F. Paschen and R. Götze, Seriengesetze der Linienspektren, Berlin: Springer (1922).

²F. S. Brackett, Astrophys. J., Vol. 56, p. 154 (1922).

³H. Kleiman, J. Opt. Soc. Am., Vol. 52, p. 441 (1962).

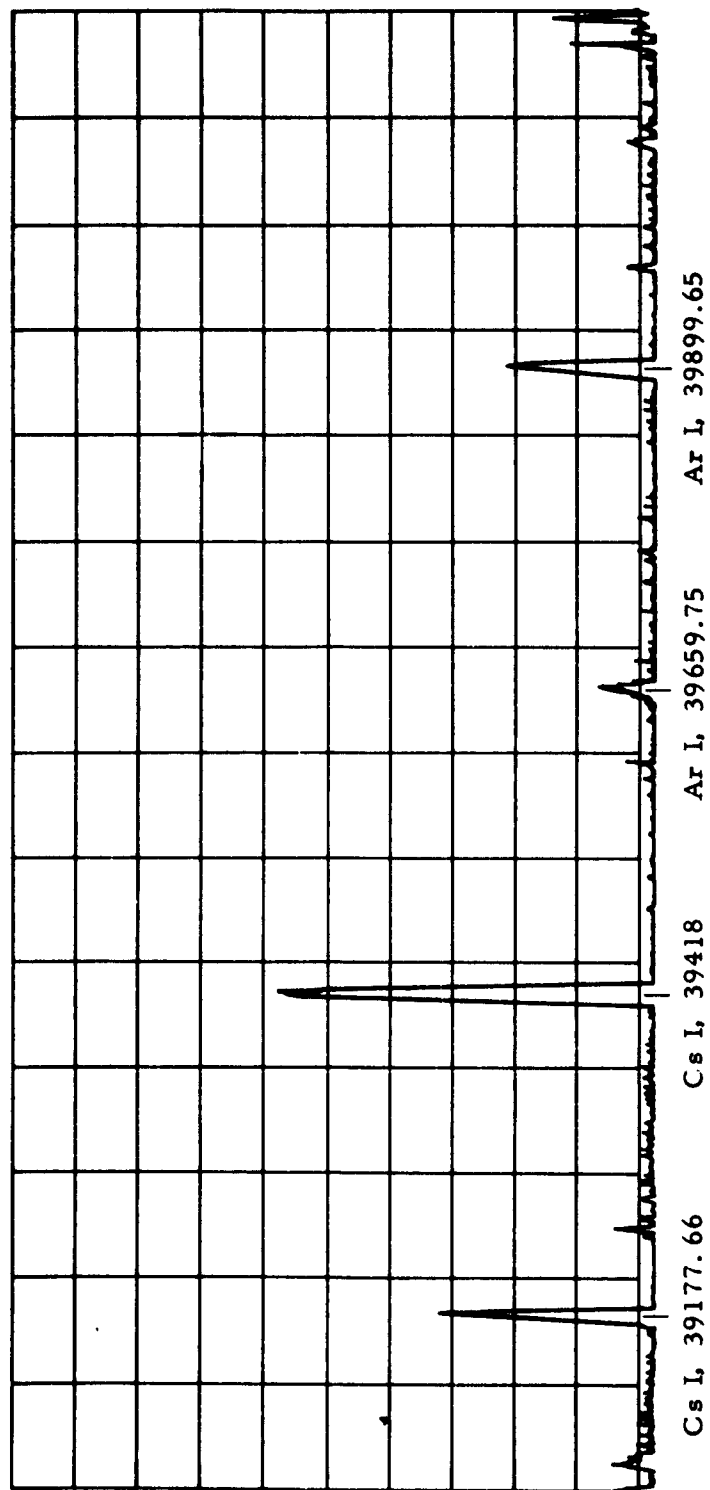


FIGURE 1. The First Spectrum of Cesium in the 4-Micron Region,
Showing First-Order Argon Lines Originating in the Carrier Gas

which has been the subject of an investigation by the authors⁴ in cooperation with K. L. Andrew of Purdue University. Application of the Pauli exclusion principle to configurations involving a given number, designated n , of p -electrons leads to the same number of levels with the same set of J -values as that obtained for $(6 - n)$ p -electrons. In general, the order of the J -values is reversed for the complementary cases. When the outer electron assumes large l -values, as in the instances of f or g , the distribution and quantum number characterization of the levels are described closely by the pair-coupling approximation, probably first formulated by Shortley and Fried⁵ in 1938 for the d^9f and d^9g configurations in Cu II and for the p^5d and p^5f configurations in the rare gases. A general treatment of intermediate or Jl coupling was given by Racah⁶ in 1942. Our own recent work on the experimental determination of the p^5f levels of Ar I is described in an earlier report⁷ in which the physical conditions appropriate to the application of the Racah theory for intermediate or Jl coupling—namely, electrostatic interaction relatively weak compared with the spin-orbit interaction of the parent ion but strong compared with the spin coupling of the external electron—lead to two groups of close pairs of levels, the groups being separated by the interval between the two levels of the ion limit. In the extreme case where the spin coupling of the external electron is vanishingly small, the components of the close pairs coalesce so that instead of twelve levels for the configurations under discussion the number would be expected to be reduced to six, each with two J -values. Owing to a degeneracy that appears in the evaluation of the energies of the levels associated with the ion limit $^2P_{0\frac{1}{2}}^{\circ}$, the number is further reduced to five.

Shortley and Fried derived approximate theoretical expressions for the energies of the levels of the p^5d and p^5f configurations for pure pair coupling in terms of the energy parameters, or Slater integrals, under the limiting assumptions that only the leading term in the electrostatic interaction and the splitting factor of the parent configuration need be considered.

Accordingly, instead of the usual six significant energy parameters, only three were left, namely:

⁴NAVWEPS Report 7190, Quarterly Report: Foundational Research Projects, April-June 1961, p. 11 (1961).

⁵G. H. Shortley and B. Fried, Phys. Rev., Vol. 54, p. 749 (1938).

⁶G. Racah, Phys. Rev., Vol. 61, p. 537 (1942).

⁷NAVWEPS Report 7219, Quarterly Report: Foundational Research Projects, January-March 1962, p. 11 (1962).

F_0 , giving the location of the group of levels

F_2 , the electrostatic interaction integral, leading to the distribution of the double levels

ζ_p , the splitting factor⁸ of the parent ion, permitting evaluation of the separation of the two level groups

The tabulation of the quantum designations of the levels arising from the p^5f configuration in pair coupling, including the appropriate vector summations, together with the energy formulas derived by Shortley and Fried, is displayed in Table 1. Undoubtedly owing to the lack of illustrative data, Shortley and Fried did not work out the derivation for p^5g . In fact, at the time they had little to work on to verify their treatment of the p^5f configuration. The following prophetic statement, interesting in retrospect after twenty-five years, is quoted: "The only observations of p^5f are in argon where there are sketchy data for a number of these configurations. At most, five of the twelve levels are observed and not even the J-values of these are certain. It may be that the above formulas can be of use in interpreting these observations. Perhaps the five observed levels, four lower and one upper, are at the positions of the five collapsed levels given by these formulas."

Atomic Energy Levels, compiled by Moore,⁹ lists both experimental and calculated energy levels from the p^5f configurations. The latter are from an unpublished manuscript by Edlén. In 1956, Eriksson¹⁰ published a paper entitled "Coupling of Electrons with High Orbital Angular Momentum, Illustrated by $2p\ n f$ and $2p\ n g$ in N II." A set of formulas for the pg configuration was derived by a treatment essentially identical with that employed by Shortley and Fried. Eriksson had included the effect of interaction between levels converging to different ion limits. This included an extra term in each of two of the energy equations. By leaving off the extra term—something later justified by treatment of the data—and changing the algebraic signs of the coefficients of F_2 and ζ_p in accordance with the inversion of levels associated with complementary equivalent-electron configurations, the Eriksson expressions convert to a form equivalent to those derived by Shortley and Fried. Table 2 is developed for the p^5g configuration in the same form as Table 1 for the p^5f configuration.

A detailed treatment of the derivation of the energy formulas is not included here. The referenced articles may be consulted. For a

⁸S. Goudsmit and C. J. Humphreys, Phys. Rev., Vol. 31, p. 960 (1928).

⁹C. E. Moore, Atomic Energy Levels, Natl. Bur. Standards Circular 467 (1949).

¹⁰K. B. S. Eriksson, Phys. Rev., Vol. 102, p. 102 (1956).

TABLE 1. Shortley-Fried Approximation for $p^5 f$
(Taken from Phys. Rev., Vol. 54, p. 749, 1938)

j_1	l	K	J	Energy
3/2	3	9/2	5,4	$F_0 - 1/2\zeta_p - 5F_2$
3/2	3	7/2	4,3	$F_0 - 1/2\zeta_p + 10F_2$
1/2	3	7/2	4,3	$F_0 + \zeta_p$
1/2	3	5/2	3,2	$F_0 + \zeta_p$
3/2	3	5/2	3,2	$F_0 - 1/2\zeta_p + 3F_2$
3/2	3	3/2	2,1	$F_0 - 1/2\zeta_p - 12F_2$

TABLE 2. Approximation for $p^5 g$, Based on Shortley-Fried Treatment

j_1	l	K	J	Energy
3/2	4	11/2	6,5	$F_0 - 1/2\zeta_p - 28F_2$
3/2	4	9/2	5,4	$F_0 - 1/2\zeta_p + 49F_2$
1/2	4	9/2	5,4	$F_0 + \zeta_p$
1/2	4	7/2	4,3	$F_0 + \zeta_p$
3/2	4	7/2	4,3	$F_0 - 1/2\zeta_p + 22F_2$
3/2	4	5/2	3,2	$F_0 - 1/2\zeta_p - 55F_2$

more extensive discussion, the standard work of Condon and Shortley¹¹ is suggested.

Examination of the energy equations shows that only two unknowns need to be determined for a solution since ζ_p is related to the separation of the ion doublet by the relation $\Delta p^5 2P = 3/2\zeta_p$. Correct identification of any two transitions involving levels whose energy description includes F_2 permits evaluation of the parameters and derivation of the remaining levels, which can in turn be checked against appropriate transitions. Certain clues to the identification of the selected transitions are fairly obvious. Among the 4f-5g transitions, $4f[4\frac{1}{2}]_5 - 5g[5\frac{1}{2}]_6^\circ$ is certain to be the most intense. Of the array of pairs of f-levels, $4f[4\frac{1}{2}]_{5,4}$ and $4f[3\frac{1}{2}]_{4,3}$ have the smallest pair separations; in fact, neither has ever been resolved experimentally. This condition leads to the expectation that the features resulting from the double transitions

$$4f[4\frac{1}{2}]_{5,4} - 5g[5\frac{1}{2}]_{6,5}^\circ \quad \text{and}$$

$$4f[3\frac{1}{2}]_{4,3} - 5g[4\frac{1}{2}]_{5,4}^\circ$$

will be appreciably sharper than the others. Finally, based on the sequence of levels in each category, a feature common to the spectra of all the noble gases, the most intense transitions that form the diagonal of the supermultiplet come in the following order of increasing wave number:

$$4f[3\frac{1}{2}]_{4,3} - 5g[4\frac{1}{2}]_{5,4}^\circ$$

$$4f[2\frac{1}{2}]_{3,2} - 5g[3\frac{1}{2}]_{4,3}^\circ$$

$$4f[4\frac{1}{2}]_{5,4} - 5g[5\frac{1}{2}]_{6,5}^\circ$$

$$4f[1\frac{1}{2}]_{2,1} - 5g[2\frac{1}{2}]_{3,2}^\circ$$

These characteristics are all illustrated by Figure 2, a record of Ar I in the 4-micron region under the best available conditions of resolution. The entire procedure becomes an exceedingly simple and powerful classification tool in instances where pair coupling applies.

¹¹E. U. Condon and G. H. Shortley, Theory of Atomic Spectra, Cambridge University Press (1951).

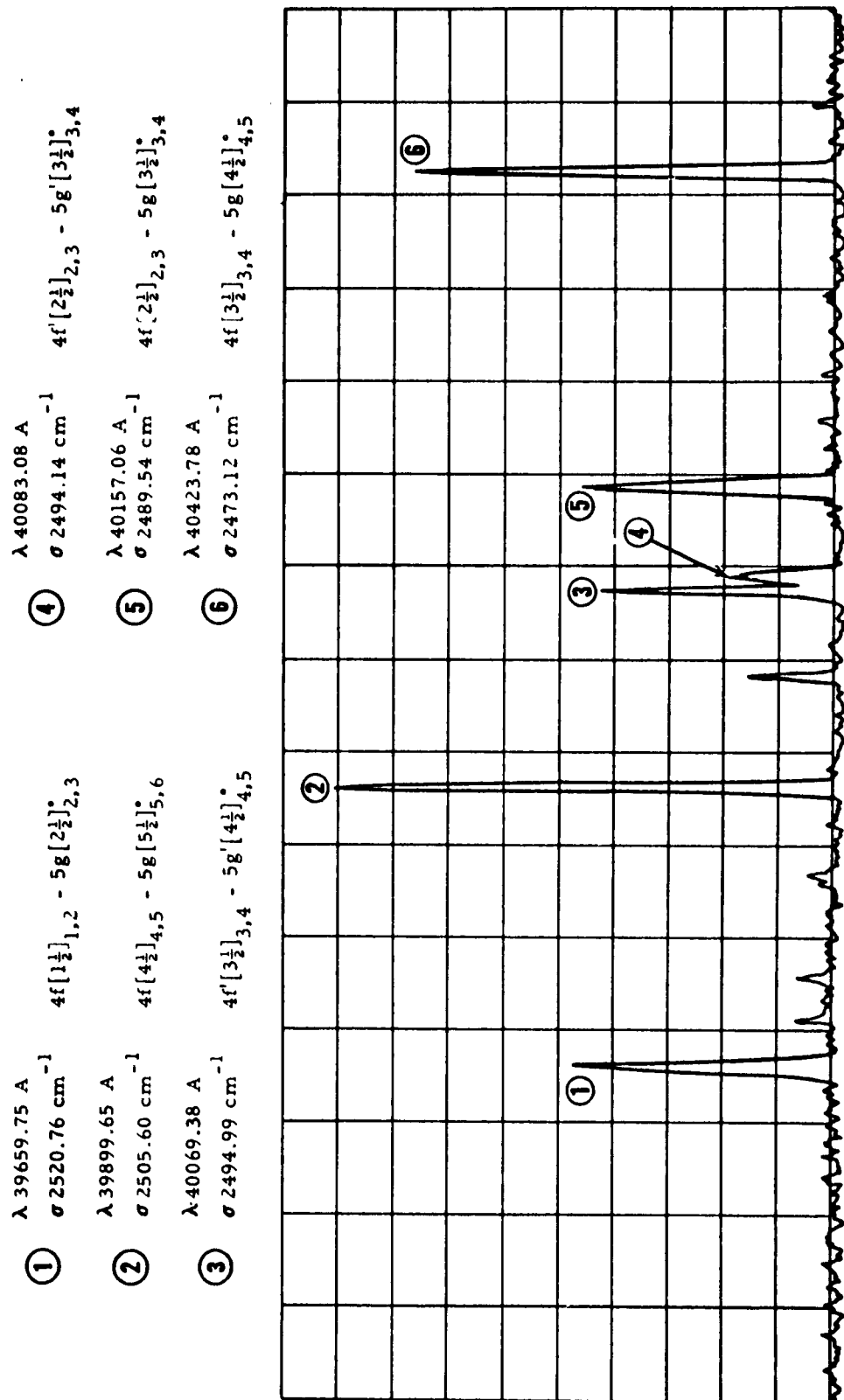


FIGURE 2. Section of a Recording of the First Spectrum of Argon in the 4-Micron Region, with Identifications of the 4f-5g Transitions

For various degrees of intermediate coupling where the other Slater parameters, namely, the exchange integrals and the spin coupling of the valence electron, are significant, similar treatments are useful but are much more involved, requiring iterated approximations to arrive at the best fit between the calculated eigenvalues of the Hamiltonian and the experimental energy levels of the atom.

Although this report is primarily concerned with the evaluation of levels originating in the p^5g configuration, a few comments are interjected regarding the character of the vector coupling associated with noble-gas configurations involving smaller l -values of the outer electron, specifically the configuration p^5f . In all the noble gases some degree of intermediate coupling is in evidence for all configurations of greater excitation than the normal state, which is associated with s^2p^6 .

The development of pair coupling proceeds much more rapidly for neon than for the other noble gases and is essentially complete with the configuration p^5f . The first detailed and complete description of the 4f-levels was based on the observation of the 3d-4f transitions by Humphreys and Kostkowski.¹² Eriksson¹⁰ used this material to illustrate his theoretical treatment but presented it only in graphic form. We are therefore inserting a tabulation of the experimental 4f-levels and the values calculated on the basis of the pair-coupling approximation, according to the equations in Table 1. This material is shown in Table 3. Also listed are the A. E. L. values, including unobserved values calculated by Edlén. The only significant difference between the observed values and those calculated on the basis of the pair-coupling hypothesis is that two coalesced pairs associated with the $^2P_{0\frac{1}{2}}^{\circ}$ limit are observed, instead of a complete collapse into a single level of four components.

It is noted also, with reference to Table 3 and the level tabulations for Ar I and Kr I that follow, that the calculated values depend somewhat on which experimental pair of levels is introduced into the calculations. A final publication is expected to include a description based on more measurements and adoption of level values derived from an average of results obtained from alternative sets of starting data. A clue to the degree of pair coupling is to be found from examination of the four collapsed pairs converging to the limit $^2P_{\frac{1}{2}}$. Because of the values of the coefficients of F_2 for the various pairs of levels in pure pair coupling, when the four energy values are arranged in a monotonic sequence the upper and lower pairs have exactly the same interval separating them.

¹²C. J. Humphreys and H. J. Kostkowski, J. Research Natl. Bur. Standards, Vol. 49, p. 73 (1952).

TABLE 3. The $2p^5 4f$ Levels in Ne I

Level	Observed by Humphreys & Kostkowski	Taken From <u>Atomic Energy Levels</u>	Assumed for Shortley-Fried Approximation*	Calculated by Shortley-Fried Equations
$2p^5 \left({}^2P_{1/2}^{\circ} \right) 4f \left[1\frac{1}{2} \right]_{1,2}$	167054.70	167054.49	167054.70	
$4f \left[4\frac{1}{2} \right]_{4,5}$	167062.28	[167062.5]		167062.45
$4f \left[2\frac{1}{2} \right]_{2,3}$	167071.03	167071.08		167071.31
$4f \left[3\frac{1}{2} \right]_{3,4}$	167079.06	[167079.1]	167079.06	
$2p^5 \left({}^2P_{0/2}^{\circ} \right) 4f' \left[3\frac{1}{2} \right]_{3,4}$	167848.33	- - -		} 167848.49
$4f' \left[3\frac{1}{2} \right]_{2,3}$	167848.62	167848.67		

*Based on Humphreys-Kostkowski values.

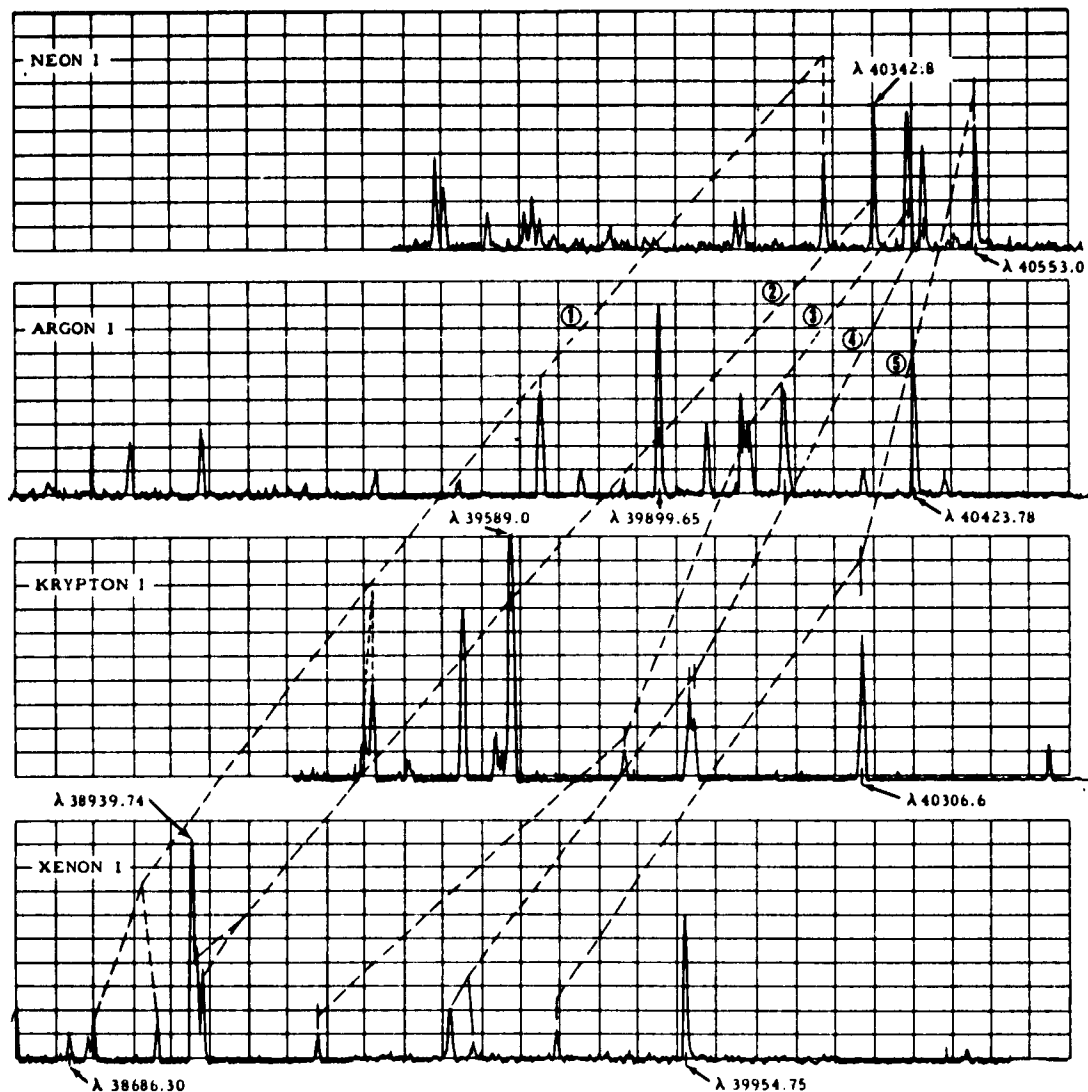
This condition is realized to well within the experimental error for these four levels of Ne I. Increasing departure is noted for the other noble gases. In Xe I the 4f-levels fit the pair-coupling relationship rather poorly. Another indication is the separation of the pair having the double J-value 1, 2. Unresolvable in Ne I, it is interferometrically separable in Ar I with an interval of 0.40 cm^{-1} , it is easily resolvable in Kr I with an interval of 0.88 cm^{-1} , but in Xe I it shows a relatively wide separation of 9.67 cm^{-1} . Similarly, the 4f-level pair having the double J-value 2, 3, unresolvable in Ne I and Ar I, is resolved in favorable instances in Kr I and separated by 3.0 cm^{-1} in Xe I. The 4f-level with J-values 4, 5 is resolvable only in Xe I.

In order to compare the characteristic features of the multiple group of lines associated with the 4f-5g transitions, a set of sections of records for the various noble-gas spectra, aligned as to wavelength, has been assembled as Figure 3. Particularly to be noted are the shift of the multiple group to shorter wavelengths with increasing atomic number, and the transition from a broadening of unresolved features to partial and finally complete resolution, also with increasing wave number. With reference to transitions between levels converging to the ion limit, $^2P_{0\frac{1}{2}}^{\circ}$, a partially resolved feature is noticeable only in Ar I. Of the two pairs of 4f'-levels in this spectrum, one is much closer than the other, 0.35 cm^{-1} for the f' $_{2,3}$ pair as against 0.05 cm^{-1} for the f' $_{3,4}$ pair. This accounts for the double feature with one sharp and one diffuse component. In the instance of Kr I, the 5g' complex is above the first ion limit, and in Xe I, both the 4f' - and 5g' -levels are above this limit. In both instances, although the structure should be resolvable, only one feature is observed that is probably associated with the most intense transition.

Taking up now the consideration of the 5g-levels determined from the 4f-5g transitions, observation of which has supplied the experimental material for this study, it is found that these levels in Ne I, Ar I, and Kr I all conform to the pair-coupling approximation within the limits of observational error.

The corresponding Xe I transitions have been observed but it has not been found possible to sort out the levels by a similar treatment. Evidently the departure from pair coupling is too great in this instance so that a more detailed treatment involving additional parameters will be required. This will be reserved for a future report.

The results of the determinations of the 5g-levels of Ne I, Ar I, and Kr I are now presented in order by means of arrays shown as Tables 4, 5, and 6. In each instance the 4f-levels are shown in the left-hand column in the same order. The g-levels are arranged monotonically at the top of the page. The arrangement of the set of double



- | | | | |
|---|--|---|---|
| ① | $4f[1\frac{1}{2}]_{1,2} - 5g[2\frac{1}{2}]_{2,3}^{\circ}$ | ④ | $4f[2\frac{1}{2}]_{2,3} - 5g[3\frac{1}{2}]_{3,4}^{\circ}$ |
| ② | $4f[4\frac{1}{2}]_{4,5} - 5g[5\frac{1}{2}]_{5,6}^{\circ}$ | ⑤ | $4f[3\frac{1}{2}]_{3,4} - 5g[4\frac{1}{2}]_{4,5}^{\circ}$ |
| ③ | $4f'[3\frac{1}{2}]_{3,4} - 5g'[4\frac{1}{2}]_{4,5}^{\circ}$
$4f'[2\frac{1}{2}]_{2,3} - 5g'[3\frac{1}{2}]_{3,4}^{\circ}$ | | |

FIGURE 3. Superposed Sections of Recordings of the Spectra of Neon, Argon, Krypton, and Xenon, with Correlation of Analogous Features

TABLE 4. NeI Array—Transitions of the Class $2p^5 4f - 2p^5 5g$

$\begin{array}{c} \text{g-levels} \rightarrow \\ \text{f-levels} \downarrow \\ \text{A. E. L.} \end{array}$	$G_{4,5}$	$G_{3,4}$	$G_{5,6}$	$G_{2,3}$
167079.06 $Z_{3,4}$	169544.30 assumed	169542.90 calc.	169540.31 calc.	169538.90 assumed
167071.03 $Y_{2,3}$	2465.24 $\left\{ \begin{array}{l} \text{obs.} \\ \text{assumed} \end{array} \right.$	- - -	- - -	- - -
167062.28 $V_{4,5}$	- - -	2471.80 obs. 2471.87 calc.	x	- - -
167054.70 $X_{1,2}$	- - -	- - -	2478.08 obs. 2478.03 calc.	- - -
	x	- - -	x	2484.20 $\left\{ \begin{array}{l} \text{obs.} \\ \text{assumed} \end{array} \right.$
$\begin{array}{c} \text{g'-levels} \rightarrow \\ \text{f'-levels} \downarrow \end{array}$	$G'_{4,5}; G'_{3,4}$			
167848.33 $U_{3,4}$	170332.26 calc.	2473.93 calc.	2473.66 obs.	
167848.62 $U_{2,3}$		2473.64 calc.	2473.78 av. calc.	

TABLE 5. Ar I Array—Transitions of the Class $3p^5 4f - 3p^5 5g$

g-levels \rightarrow f-levels \downarrow A. E. L. \downarrow		$G_{4,5}$	$G_{3,4}$	$G_{5,6}$	$G_{2,3}$
120249.917	$4U_3$	- - -	122719.46 av. obs. 122719.46 calc.	122712.78 assumed	122709.17 calc.
120249.955*	$4U_4$	2473.12 ^{obs.} {assumed}	2469.63 obs. 2469.50 calc.	- - -	- - -
120230.104	$4Y_2$	- - -	- - -	- - -	- - -
120229.791*	$4Y_3$	- - -	2489.54 obs. 2489.67 calc.	x	2479.79 obs. 2479.38 calc.
120207.216	$4V_4$	- - -	- - -	- - -	- - -
120207.175*	$4V_5$	2515.84 obs. 2515.90 calc.	- - -	2505.60 ^{obs.} {assumed}	- - -
120188.274	$4X_1$	x	- - -	x	- - -
.473 (av.)					
120188.672	$4X_2$		- - -		2520.76 obs. 2520.70 calc.
g' -levels \rightarrow f' -levels \downarrow		$G'_{4,5}$	$G'_{3,4}$		
121654.621	$4Z_2$	124148.31 obs. 124148.57 calc.	124148.42 obs.		
121654.275*	$4Z_3$		2494.14 obs. 2494.30 calc.		
121653.279	$4W_3$	2494.99 obs. 2495.25 calc.			
121653.321*	$4W_4$				

* f-level of largest J used to calculate σ in transitions.

TABLE 6. Kr I Array—Transitions of the Class $4p^5 4f - 4p^5 5g$

<div>g-levels→</div> <div>f-levels↓ A. E. L.↑</div>		$G_{4,5}$ 108528.50 assumed	$G_{3,4}$ 108523.72 calc.	$G_{5,6}$ 108514.87 assumed	$G_{2,3}$ 108510.10 calc.
106048.19	$4W_{3,4}$	2480.31 assumed	2475.69 obs. 2475.53 calc.	- - -	- - -
106022.425	$4Y_2$	- - -	2501.47 obs. 2501.30 calc.	x	- - -
106021.657	$4T_3$	- - -	2502.12 obs. 2502.06 calc.		- - -
105989.60	$4U_{4,5}$	2538.96 obs. 2538.90 calc.	- - -	2525.27 assumed	- - -
105965.258	$4X_1$	x	- - -	x	2544.83 obs. 2544.84 calc.
105966.379	$4X_2$		- - -		2543.75 obs. 2543.72 calc.
<div>g'-levels→</div> <div>f'-levels↓ J</div>		$G'_{4,5}; G'_{3,4}$ 113890.83 calc.			
111379.21	3				
111378.7	4				
111381.98	2				
111381.10	3				
111380.25 (av.)		2510.74 obs. 2510.58 calc.			

J-values with respect to the monotonic sequences is uniform for all the noble gases and the pattern is maintained for both the 4f and 5g arrays.

A summary compilation of the values of the energy parameters for the 5g configurations for the elements neon, argon, and krypton, as derived on the basis of the selected starting data, appears in Table 7.

TABLE 7. Energy Parameters for the p^5g Configuration

Element	ζ_p, cm^{-1}	F_0, cm^{-1}	F_2, cm^{-1}
Neon	520.33	169801.93	0.05192
Argon	954.70	123193.87	0.13363
Krypton	3580.67	110310.16	0.17701

In some noted instances, other Ritzian combinations appear on the records. Some of these may be seen in the various sections of Figure 3. The availability of such transitions is advantageous for data reduction because the wavelengths associated with them are precisely calculable. In most instances the wavelengths were measured by introducing a superposed second-order argon spectrum.

Finally, some observations have been made on He I by using a source tube containing a helium-neon mixture. Figure 4 displays a record from this source superposed on one from a pure neon source. Three features attributed to He I are identified as:

$\lambda, \text{air, \AA}$	$\sigma, \text{vac., cm}^{-1}$	Transition
40364.2	2476.77	$4d^3D - 5f^3F^\circ$
40395.6	2474.84	$4d^1D - 5f^1F^\circ$
		$4f^3F^\circ - 5g^3G$
40477.9	2469.81	$4f^1F^\circ - 5g^1G$

The wavelengths of the first two listed helium lines, particularly the singlet transition, differ somewhat from those calculated from level values as published in Atomic Energy Levels. It is expected that some revision of level values, as determined by further measurements, will

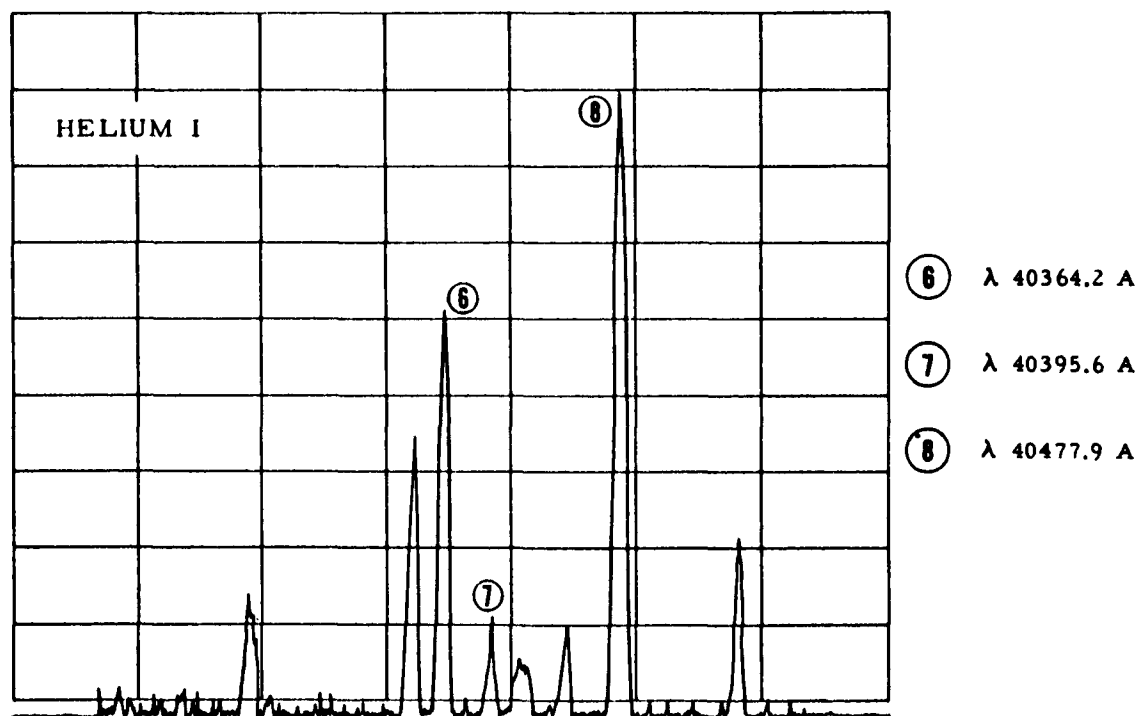
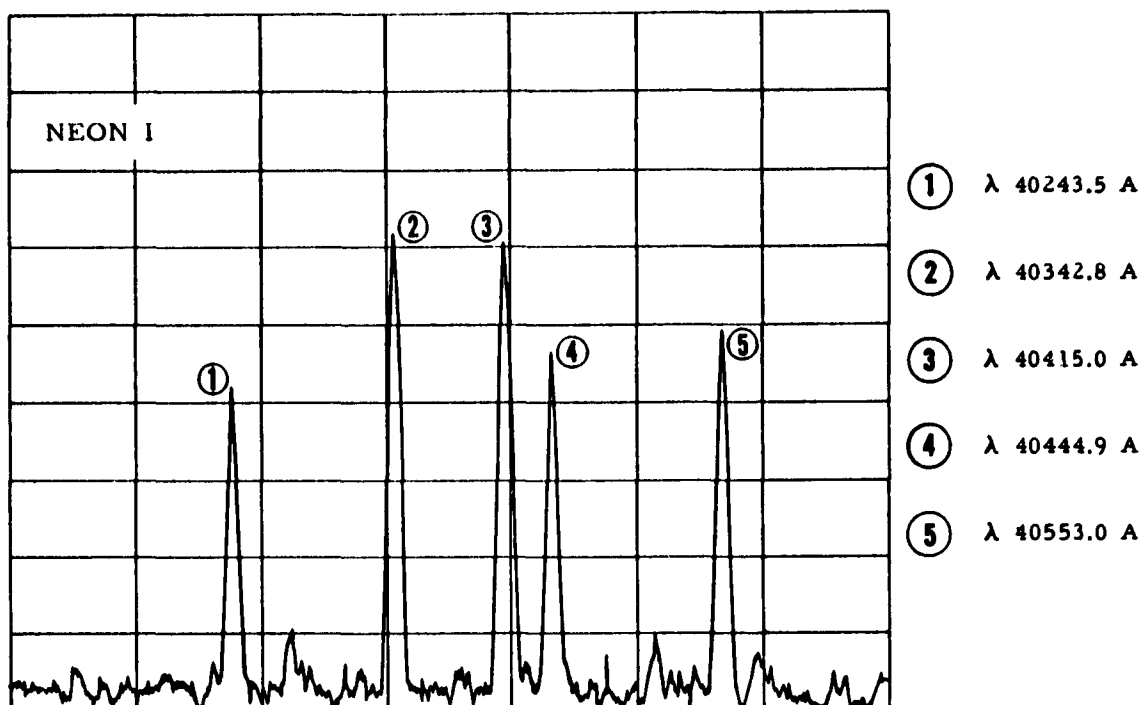


FIGURE 4. Section of a Recording of the Spectrum of a Helium-Neon Mixture Compared with a Recording of the Spectrum of Neon Covering the Same Wavelength Interval Near 4 Microns

be required. The interpretation of the third feature is not verifiable by intercombinations and possible ambiguity is indicated. The validity of the interpretation of the triplet combination seems unquestionable owing to the nearly hydrogenic character of the high levels. It is noted that the Brackett line of hydrogen has a wavelength of 40511 Å.

The authors are indebted to K. L. Andrew of Purdue University for suggesting the use of the Shortley-Fried approximation in the interpretation of the experimental data, and to R. D. Cowan of the University of California, Los Alamos Scientific Laboratory, for valuable discussions.

NONAQUEOUS ELECTROCHEMISTRY

THE ELECTROREDUCTION OF NITROBENZENE IN LIQUID AMMONIA SOLUTIONS

by

W. S. Harris

For some time it has been known qualitatively that the m-dinitrobenzene (abbreviated here as m-DNB) cathode, when used in current-producing cells and batteries, performs better in an acid (NH_4SCN) than in a neutral (KSCN) environment. This phenomenon was investigated as a part of NOLC's study of the reduction mechanism of aromatic nitro compounds in liquid ammonia solutions. The results from this investigation were utilized to recalculate the maximum energy to be expected from the electrochemical cell $\text{Li}/\text{electrolyte in } \text{NH}_3/\underline{\text{m}}\text{-DNB}$.

EXPERIMENTAL

The apparatus and method are the same as reported in previous quarterly reports¹ and in NAVWEPS 7241.²

RESULTS

m-Dinitrobenzene behaves quite differently when reduced in acid liquid ammonia solutions than when reduced in neutral liquid ammonia solutions. This behavior is shown in Figure 1a. At low rates, in acid solutions the useful yield is the expected 8 electrons per molecule; in neutral solutions the useful yield is about 2 electrons. The useful yield

¹ NAVWEPS 7214, Quarterly Report: Foundational Research Projects, October-December 1961, pp. 29-35 (March 1962); and NAVWEPS 7229, Quarterly Report: Foundational Research Projects, April-June 1962, pp. 33-39 (August 1962).

² NAVWEPS 7241, The Electroreduction of Aromatic Nitro Compounds in Nonaqueous Solutions. Part I: The Reduction of Nitrobenzenes in Acid Liquid Ammonia Solutions, by W. S. Harris and G. B. Matson (December 1962).

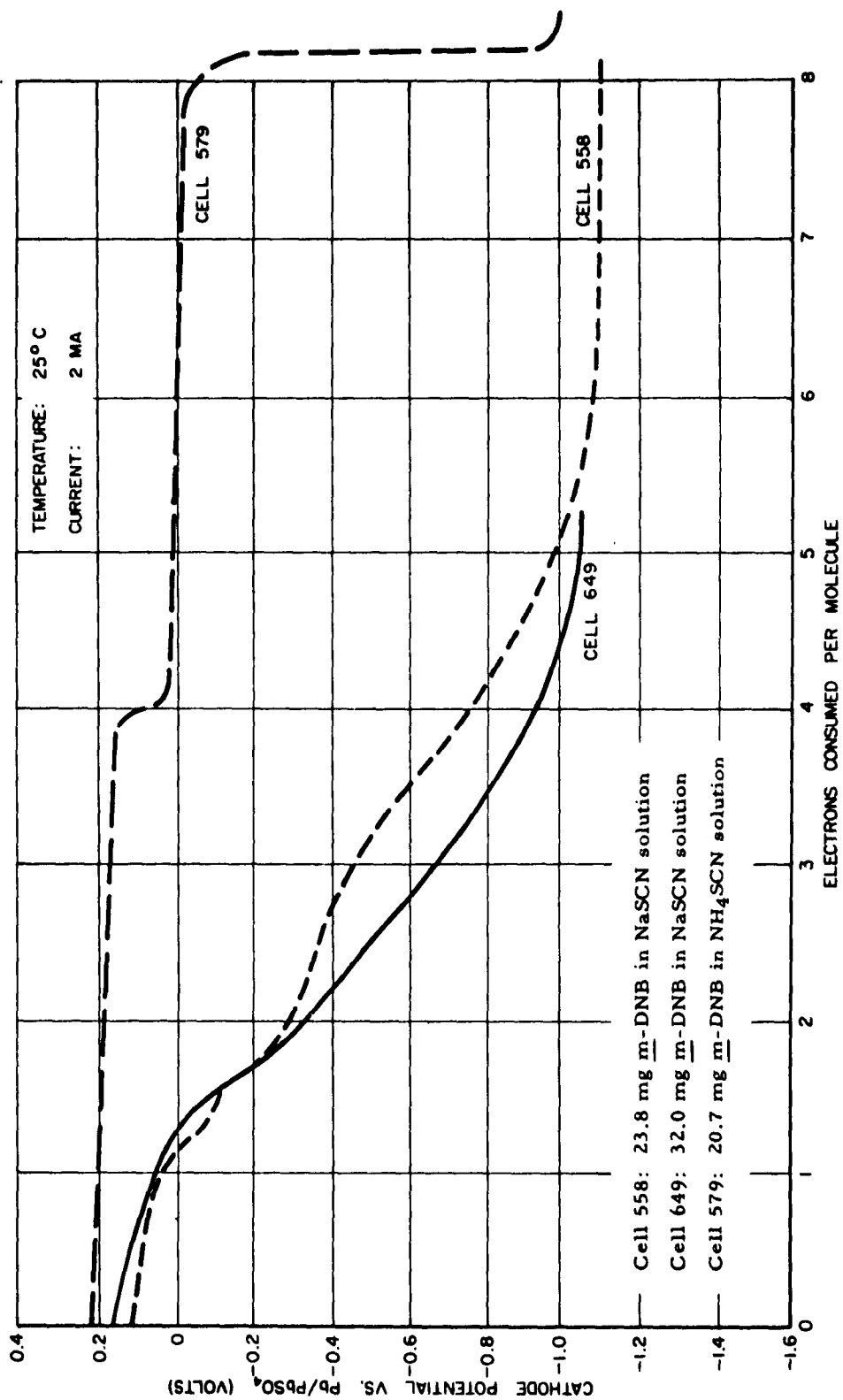


FIGURE 1a. Low-Rate Reduction of m-DNB in Liquid Ammonia Solutions

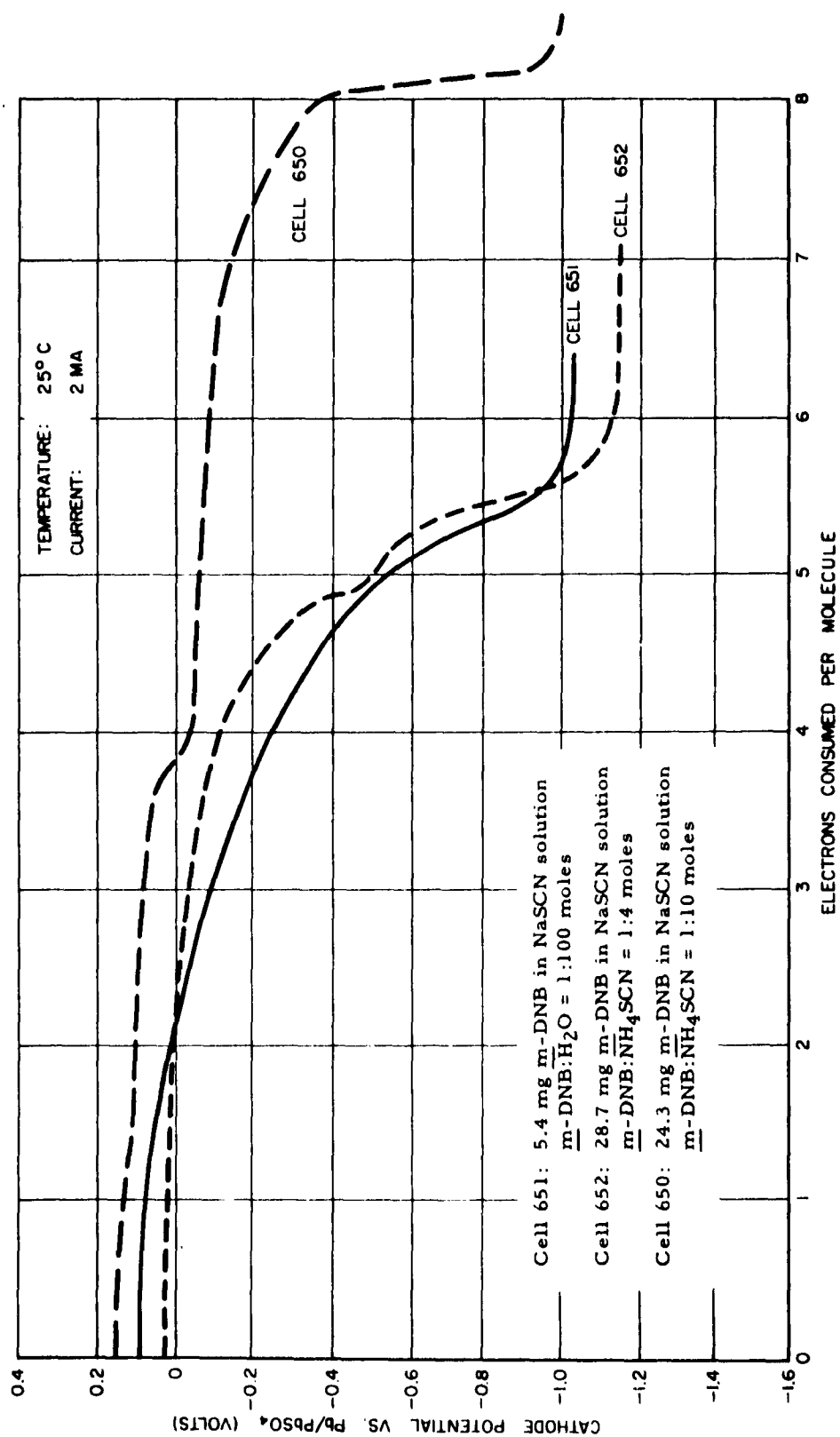


FIGURE 1b. Low-Rate Reduction of m-DNB in Liquid Ammonia Solutions

is the number of electrons used until a 0.4-volt³ drop in cathode potential occurs.

The addition of strong acids (in ammonia), such as NH_4SCN , to the neutral solution increases the utilization of electrons approximately in proportion to the amount of acid added. When a weaker acid is added, a much greater amount must be used to give the same effect. This is illustrated in Figure 1b. Cells 651 and 652 gave similar results but contained different relative amounts of added acid. Cell 652 used the strong acid NH_4SCN with an acid:m-DNB mole ratio of 4. Cell 651 used the weak acid H_2O at a ratio of 100.

The addition of sufficient strong acid to the neutral solution to bring the acid:m-DNB mole ratio to 10 results in a discharge curve that is virtually the same as in acid solution, with the exception of a slight drop in voltage.

CONCLUSIONS

From these investigations, several conclusions are drawn for well-stirred solutions at very low current densities:

- (1) m-DNB is incompletely reduced in neutral solutions.
- (2) Acid is needed for the complete 8-electron reduction of m-DNB.
- (3) The concentration of acid appears to be of minor importance.

It is postulated that these conclusions will have the following effects upon hardware type cells:

- (1) m-DNB will be utilized best in cells having a $\text{NH}_4^+:\text{m}$ -DNB mole ratio of 8 or higher.
- (2) Cells containing smaller amounts of NH_4^+ than this ratio may be expected to have variable lives and voltages that depend upon the amount of NH_4^+ present in the cathode.
- (3) Because NH_4^+ is an essential part of the reaction, it must be included in any weight calculation that includes the m-DNB cathode.

³ This value is arbitrary and cannot be related to battery voltage regulation.

CALCULATIONS

Because H^+ participates in and is necessary for the reaction



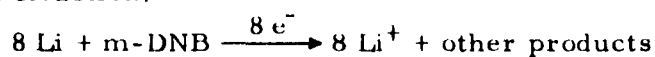
it must be included in any energy density calculation for cells utilizing m-DNB as a cathode material. Energy density calculations for the system Li/electrolyte in $\text{NH}_3/\underline{m}\text{-DNB}$, based upon various assumptions, are given below.

Calculation No. 1

Assumptions:

- (1) Need for H^+ is disregarded.
- (2) 100% efficiencies.
- (3) Working voltage is same as E^0 (2.6 volts, estimated).

Cell Reaction:



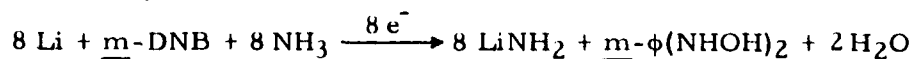
$$\text{Watt-hours/pound}^4 = 1100$$

Calculation No. 2

Assumptions:

- (1) Source of H^+ is NH_3 ; i. e., $\text{NH}_3 \longrightarrow H^+ + \text{NH}_2^-$
(H_2O would give a similar result.)
- (2) 100% efficiencies.
- (3) Working voltage is same as E^0 .

Cell Reaction:



$$\text{Watt-hours/pound} = 705$$

Calculation No. 3

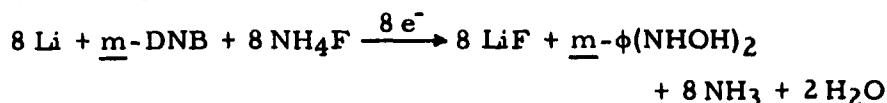
Assumptions:

- (1) Source of H^+ is NH_4^+ from NH_4F .⁵
- (2) 100% efficiencies.
- (3) Working voltage is same as E^0 .

⁴One watt-hour/pound = 7.94 joules/gram.

⁵ NH_4F was arbitrarily taken as one of lightest H^+ sources. It is, however, insoluble in NH_3 .

Cell Reaction:



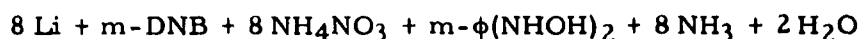
Watt-hours/pound = 482

Calculation No. 4

Assumptions:

- (1) Source of H^+ is the NH_4^+ from NH_4NO_3 .
- (2) 100% efficiencies.
- (3) Working voltage is same as E^0 .

Cell Reaction:

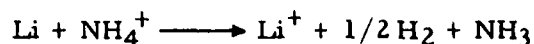


Watt-hours/pound = 295

Calculation No. 5

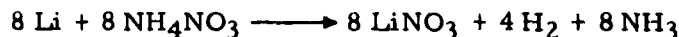
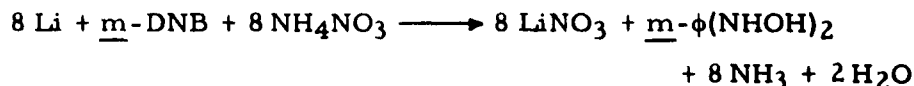
Assumptions:

- (1) Source of NH_4^+ is NH_4NO_3 .
- (2) 50% efficiencies.
- (3) Corrosion reaction at anode causes its inefficiency.



- (4) Lack of reaction causes inefficiency at cathode.
- (5) Working voltage is 2.2 volts at 100 ma/cm².

Cell Reactions:



Watt-hours/pound = 122

Calculation No. 5 is the best approximation for the system as it is now known in research-hardware type cells at room temperature. Assumption (3) is based upon a Li anode in a NH_4NO_3 - NH_3 environment. The corrosion would be much less in a neutral solution.

From the above calculations, it is seen that the dinitrobenzene cathode is penalized severely because of its need for acid. To achieve better energy it is necessary to find (1) strong acids with lower equiva-

lent weights or (2) cathode materials that do not require acid or that can use weaker acids such as H_2O .

IONIC MELT ELECTROCHEMISTRY

by

R. E. Panzer

Investigations in ionic melts reported in the last quarterly report have been continued. Problems of instrumentation and preparing electrolyte pills were solved and all necessary cell components, i. e., anodes, anolyte pills, catholyte pills, cathodes, and insulators, were prepared.

Fifty-four factorial cell experiments were run at the rate of 18 cells per day. Each daily set was operated at one of three temperatures: 200, 250, or 300°C. These temperatures differ from the original plan of 175, 250, or 325°C, the change being necessitated by problems encountered in preliminary cell tests. Statistical evaluation and analysis of the data from these cell tests are in process.

A literature search for prospective low melting electrolytes is continuing. Several mixtures of thiocyanates and other salts appeared quite promising in preliminary evaluation of melting point, conductivity, stability, and unreactivity with cell components. Results of these studies will be reported later.

In conjunction with studies of electrochemical polarization in practical cell systems, efforts are being made to apply modified techniques of voltammetry at constant current (chronopotentiometry). Problems under study are reproducible electrode areas and their positioning in the cell, and concentration limits in ionic melt voltaic cells. Circuitry has been developed and tested by using short time (<1 second) electrolysis with oscilloscope recording. Additionally, longer electrolysis times of up to 5 seconds have been used with a fast strip chart recorder. Presently, it is not known whether this technique will yield interpretable results in the practical ionic melt cells.

NONLINEAR TRANSMISSION LINES

THE SEMIGENERALIZATION OF THE TRANSMISSION LINE EQUATIONS

by
J. R. Alday

INTRODUCTION

In previous studies, attempts have been made to use the general linear form of the transmission line equations to describe the actions of a nonlinear transmission line. A lumped constant approach has also been attempted. Both of these approaches, although quite fruitful in some instances, are insufficient for fully describing the nonlinear line.

The analysis presented here is an attempt to generalize further the usual linear transmission line equations to include the case of active or magnitude-sensitive admittance elements. The term "semi-generalization" has been coined for use where only the admittance elements are considered active.

ANALYSIS

An equivalent circuit of infinitesimal length (Figure 1) is used here to develop the nonlinear transmission line equations in the same manner as it was used for the linear transmission line equations.

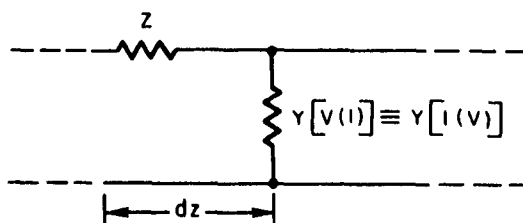


FIGURE 1. Equivalent Circuit

Let Z be the complex series impedance of the infinitesimal section of the transmission line and let $Y[V(I)]$ or $Y[I(V)]$ be a functional representation for the complex shunt admittance in I or V respectively. The terms $V(I)$ and $I(V)$ are indicative, respectively, of the voltage across and the current through the admittance element.

From Ohm's Law, the following equation may be written:

$$V = IZ_T = I \left\{ Z + \frac{1}{Y[V(I)]} \right\} \quad (1)$$

where V is the instantaneous input voltage signal, Z_T is the total impedance of the equivalent circuit, and I is the instantaneous current drawn by the circuit.

If V is allowed to change to $V + \Delta V$, there will be a corresponding change in I ; that is

$$V + \Delta V = (I + \Delta I) \left\{ Z + \frac{1}{Y[V(I + \Delta I)]} \right\} \quad (2)$$

Expanding equation (2) and subtracting equation (1) from it gives

$$\Delta V = \frac{I}{Y[V(I + \Delta I)]} - \frac{I}{Y[V(I)]} + \Delta I Z + \frac{\Delta I}{Y[\Delta(I + \Delta I)]}$$

Collecting terms and dividing both sides by ΔI yields

$$\frac{\Delta V}{\Delta I} = I \left\{ \frac{Y[V(I)] - Y[V(I + \Delta I)]}{\Delta I \cdot Y[V(I + \Delta I)] Y[V(I)]} \right\} + Z + \frac{1}{Y[V(I + \Delta I)]}$$

Observing that

$$Y[V(I)] - Y[V(I + \Delta I)] \equiv -\Delta Y[V(I)]$$

and passing to the limit results in

$$\lim_{\Delta I \rightarrow 0} \frac{\Delta V}{\Delta I} = \frac{dV}{dI} = -I \frac{dY[V(I)]}{dI} \cdot \frac{1}{Y^2[V(I)]} + Z + \frac{1}{Y[V(I)]}$$

Integrating¹ with respect to I yields

$$V = \frac{I}{Y[V(I)]} + ZI + \int \frac{dI}{Y[V(I)]}$$

¹The integration at the first term on the right-hand side is actually with respect to $Y[V(I)]$.

Now, inasmuch as the change in voltage per unit length of the infinitesimal section of line is equal to the voltage drops around the circuit,

$$\frac{\partial V(I)}{\partial z} = \frac{I}{Y[V(I)]} = \frac{\partial V}{\partial z} - ZI - \int \frac{dI}{Y[V(I)]}$$

Also, since the applied signal V is not a function of z , its derivative vanishes and

$$\frac{\partial V(I)}{\partial z} = - \int \left\{ Z + \frac{1}{Y[V(I)]} \right\} dI \quad (3)$$

Equation (3) is the semigeneralized form of the voltage transmission line equation.

In a very similar manner (the details of which are not included here), the semigeneralized current transmission line equation is found to be

$$\frac{\partial I(V)}{\partial z} = - \int \frac{dV}{Z + \frac{1}{Y[I(V)]}} \quad (4)$$

The usual equations

$$\frac{\partial V}{\partial z} = -ZI \quad (3a)$$

and

$$\frac{\partial I}{\partial z} = -YV \quad (4a)$$

where Z and Y are complex, can be similarly derived if it is assumed that Y is invariant with voltage.

For further generalization, assume that the time-dependent voltages and currents are Fourier in nature,² that is to say, they take on the respective forms

$$I = \sum_{n=1}^{\infty} I_n \exp \{i[n\omega t + \phi_n(t)]\} \quad 0 \leq t \leq \frac{2\pi}{\omega} \quad (5)$$

and

²This assumption is not only academically important. Its physical interpretation is at least this complex.

$$V = \sum_{n=1}^{\infty} V_n \exp \{i[n\omega t + \theta_n(t)]\} \quad 0 \leq t \leq \frac{2\pi}{\omega} \quad (6)$$

where

$n = 1, 2, 3, \dots$

I_n = maximum current magnitudes of the fundamental signal and its harmonics

V_n = maximum voltage magnitudes of the fundamental signal and its harmonics

$\phi_n(t)$ = complex current phase functions

$\theta_n(t)$ = complex voltage phase functions

Direct substitution of equations (5) and (6) into equations (3) and (4), with the change in variables $Y[V(I)] \equiv Y[I(V)] = Y(t)$, results in the semigeneralized equations

$$\frac{\partial V(t)}{\partial z} = - \int Z(t) \sum_{n=1}^{\infty} I_n i \left[n\omega + \frac{\partial \phi_n(t)}{\partial t} \right] \exp \{i[n\omega t + \phi_n(t)]\} dt \quad (7)$$

and

$$\frac{\partial I(t)}{\partial z} = - \int \frac{1}{Z(t)} \sum_{n=1}^{\infty} V_n i \left[n\omega + \frac{\partial \theta_n(t)}{\partial t} \right] \exp \{i[n\omega t + \theta_n(t)]\} dt \quad (8)$$

where

$$Z(t) = Z + \frac{1}{Y[V(I)]} = Z + \frac{1}{Y(t)}$$

CONCLUSIONS

The transmission line equations for a transmission line with active shunt admittances have been derived. It is felt that these equations, although more complex than those that do not consider the admittance elements, are representative of the properties of a nonlinear transmission line. Complete utilization of these equations is dependent upon their simultaneous solution.

SEMICONDUCTOR MICROWAVE MICROELECTRONICS

SUBSTRATES, CIRCUITRY, AND SEMICONDUCTORS

by

R. W. Yancey

The last quarterly report contained a brief discussion of some aspects of microwave semiconductor microelectronics. In continuation of this study to develop and determine properties of microwave functional circuits employing semiconductors, tunnel diodes were chosen as the major semiconductor device to be considered. The properties and advantages of tunnel diodes have been covered in most electronic publications and need not be repeated here. These devices are capable of operation beyond 100 Gc,¹ but commercial units are limited to 30 Gc. This 30-Gc limitation precludes the use of tunnel diodes in millimeter wave equipment which has a number of ordnance as well as other applications.

Consideration was given to taking advantage of the tunnel diodes' capabilities by fabricating the tunnel diodes directly into microwave structures to increase the frequency of operation into the millimeter wave region. A brief search revealed that tunnel diodes are made by the alloying process, which is simple and straightforward if an alloying furnace is available.

A trip to the Harry Diamond Laboratories (which was then the Diamond Ordnance Fuze Laboratory) resulted in the acquisition of sufficient information to build an alloying furnace and to perform the alloying process. (It should be mentioned that these first costs were borne by Code 71 during one of its programs that was later terminated. The work was then continued under Foundational Research funds.)

The decision was made to go ahead in this direction and to fabricate the diodes into microwave equipment. From the information and sample material obtained from DOFL, the furnace was constructed as follows.

¹C. A. Burrus, "Gallium Arsenide Esaki Diodes for High-Frequency Applications," J. Appl. Phys., Vol. 32, pp. 1031-1036 (1961).

The furnace (Figure 1) was made of stainless steel and glass, with a base 7 inches in diameter and approximately 4 inches high. The heating element is a filament made from a 0.010-inch nickel sheet 5/8 of an inch wide. The edges are bent up 1/16 inch at a 90-degree angle to give rigidity. The two leads on the left of the figure are external connections for thermocouple leads. The furnace is evacuated through the center hole in the base and the reduction atmosphere is admitted through the same hole. This is accomplished by an external glass "T." The filament current is supplied via its supporting posts which go through Teflon insulators to the base.

The closed furnace, with an over-all height of 6 inches, is shown in Figure 2. The handles exert pressure on the glass flange to effect a seal from an O-ring between the base and bell jar. The furnace proper is now complete.

The filament temperature-control unit is complete with the exception of the timer needed to give completely automatic alloying cycles. This control unit is capable of supplying 4 volts at 75 amp continuously, and 125 amp intermittently. The anticipated heater current is 30 to 50 amp. The timer will be adjustable to allow 30 to 50 seconds for preheating and 2 to 10 seconds for alloying. The control panel is shown in Figure 3, while Figure 4 shows a rear view of the control unit.

Briefly, the alloying process consists of placing the doped semiconductor wafer on a heat-generating element. On this wafer is placed the proper alloying material. Both are then placed in a reducing atmosphere (for germanium, gallium arsenide, or gallium antimonide, hydrogen is used) and preheated to 550 or 600°C for approximately 45 seconds. The temperature is then increased to approximately 700°C for 2 seconds, and the unit is allowed to return to room temperature. The high temperature produces the alloying which, when used with proper semiconductor wafers and alloying material, yields tunneling junctions.

Normally, a very highly doped semiconductor wafer must be used to produce germanium tunneling junctions. A doping level on the order of $2 \text{ to } 6 \times 10^{19} \text{ atom/cm}^3$ gives a resistivity of about 0.006 ohm-cm. The wafer thickness may vary from 0.002 to 0.010 inch. With n-type germanium, a common alloying material is indium. A small (0.0005-inch) sphere or wafer may be used.

In initial tests, 4 germanium tunnel diodes were made at a reduced pressure (approximately 0.001 mm Hg) without using the reduction atmosphere. Since no provisions were made for mounting these units, they are at best just samples.

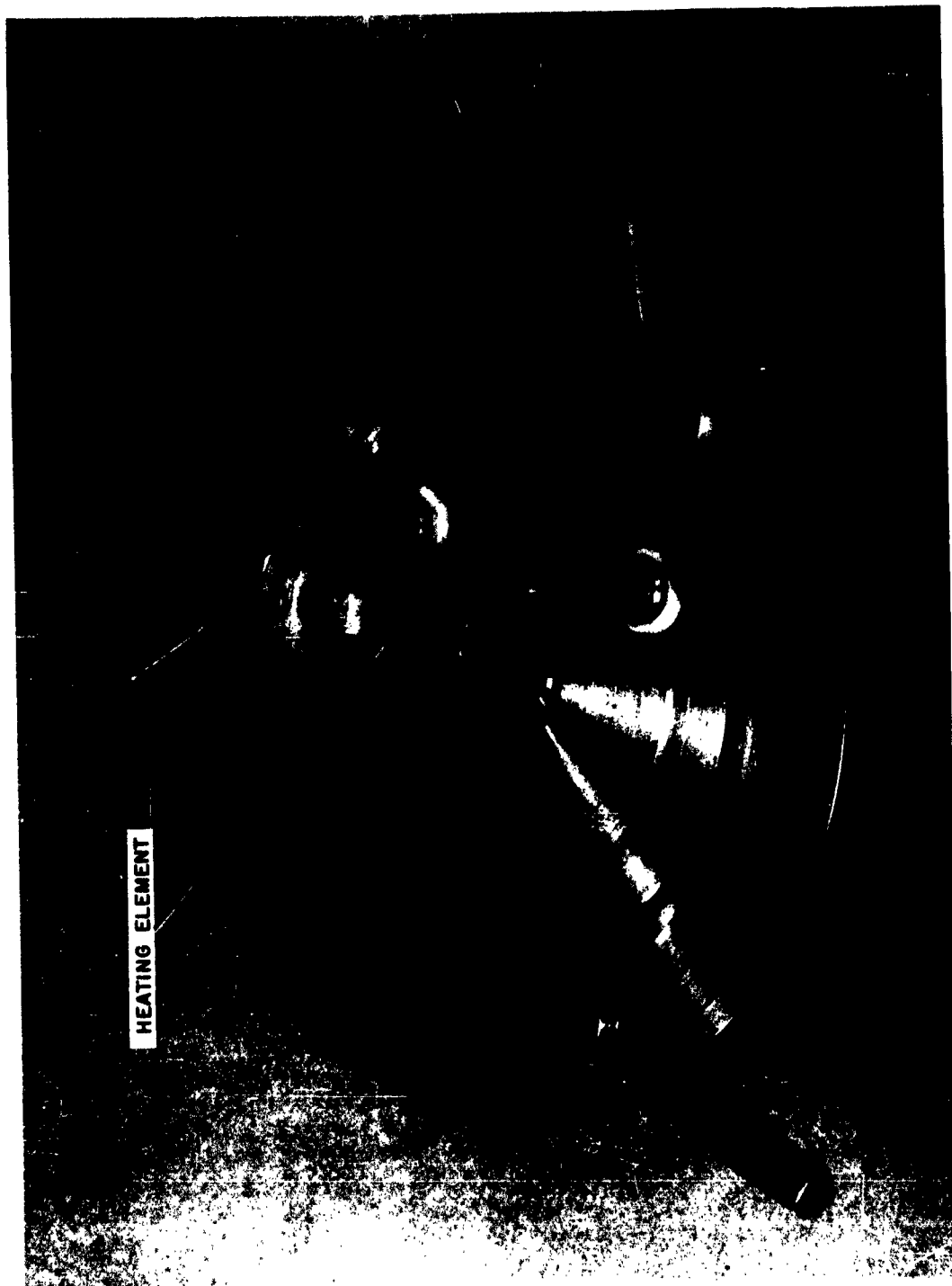


FIGURE 1. Alloying Furnace



FIGURE 2. Alloying Furnace with Cover

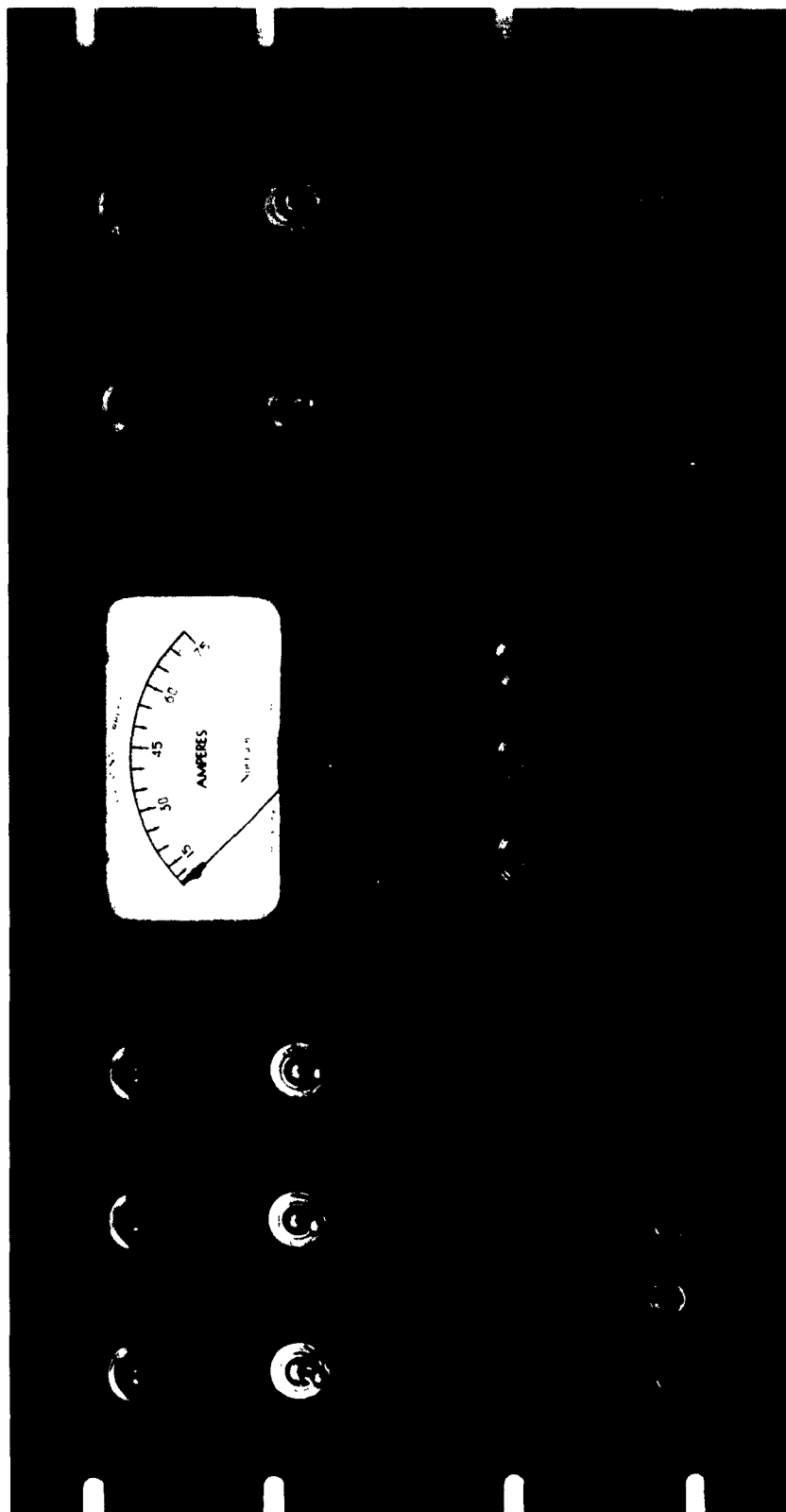


FIGURE 3. Front Panel of Temperature-Control Unit



FIGURE 4. Back View of Temperature-Control Unit

During the next quarter, the furnace control will be completed, tested, and calibrated. Full operation of the completed system is anticipated by the next reporting period.

SEMICONDUCTOR PHYSICS

ACCURATE MEASUREMENTS OF A MAGNETIC FIELD BY MEANS OF A III-V HALL EFFECT DEVICE

by

K. I. Crowder and H. Piller

INTRODUCTION

A current traveling through a material in the presence of a magnetic field experiences a Lorentz force normal to the magnetic field and current in the direction $\vec{J} \times \vec{B}$. Because the material constrains the electrons, an equal and opposite electromotive force is set up, $\vec{E} = R\vec{B} \times \vec{J}$. This electromotive force is the Hall voltage. Here R is the Hall coefficient. In a semiconductor with a high electron concentration, R is inversely proportional to this concentration, n , and therefore $R = 1/ne$, where e denotes the electronic charge. If the charge carriers are positive, R is taken to be positive and the analysis still holds. The sense of \vec{E} is thus determined by the sign of the carriers. The equation for R holds in III-V compound semiconductors since the density of states in the conduction band is low and the contribution of electrons to the conduction band by ionized impurity atoms is high in the temperature region where the Hall generator is used.

A Hall generator has many advantages over other methods of measuring magnetic field strength. In the presence of a magnetic field for a given current, it generates a voltage that is proportional to the current, J , and also the magnetic field, B . Its physical size is small; therefore, it samples a small portion of the field. The output voltage is determined by the average field strength over the area of the sample; hence the field may be measured in small gaps and small areas.

DISCUSSION

The voltage output is influenced by temperature, shunt resistance, input current, and magnetic field. The temperature dependence of the Hall constant R is equal to or less than 0.1% per degree centigrade in the region between 0 and 100°C. By using manganin wire for the shunt

resistance and large capacity batteries to supply the input current, the accuracy of the device may well be limited only by the temperature stability. Error due to this instability may be minimized by use of heat sinks such as copper tubes with water from a temperature-controlled bath circulating through them. It should be noted that orientation in the field changes the apparent thickness of the device by a factor of secant θ , where θ is measured between the lines of magnetic force and the face of the Hall generator. The voltage is proportional to cosine θ .

A Hall generator was obtained commercially from Instrument Systems Corporation (Siemens Type FA-21) and calibrated for the region between 2 and 10 kilogauss. A Leeds and Northrup potentiometer, Model K-3, was used to measure the output voltage, and a Harvey-Wells Corporation nuclear magnetic resonance precision gaussmeter system, Model G502, was used to measure the field. (A schematic diagram of the arrangement is shown in Figure 1.) The instrument had a built-in crystal calibrator which gave resonance lines at each megacycle frequency. Because the field could be determined quite accurately ($\pm 0.01\%$) at these points, they were chosen for the calibration of the Hall generator. The H^1 and the Li^7 probes were used.

The Hall voltage as a function of the magnetic field deviates from a linear behavior in a uniform and predictable manner for a given shunt resistance. The curve has an S shape that crosses a line through the origin at approximately 5 kilogauss and at 10 kilogauss (see Figure 2). This curve has the form

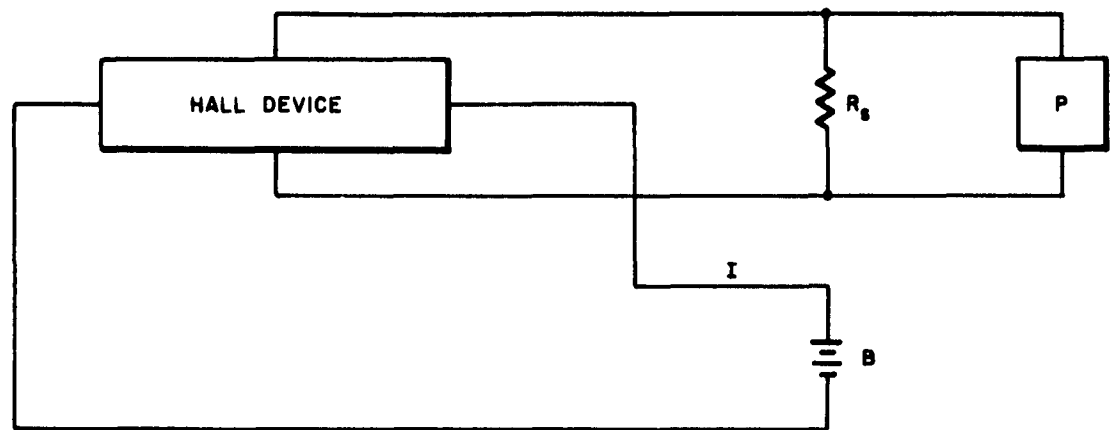
$$V_h = aB + b \sin(0.2 \pi B)$$

where V_h is the Hall voltage in millivolts, B is the magnetic field in kilogauss, and a and b are constants. The sine term is a small perturbation on the linear behavior of the Hall voltage vs. field; b will not exceed 1% of the value of the Hall voltage at 10 kilogauss if the proper shunt resistance is chosen. For this calibration

$$a = 4.661 \text{ millivolts/kilogauss}$$

$$b = 3.867 \text{ millivolts}$$

The best accuracy is obtained by a straight-line interpolation between calibration points. The precision in reading the Hall voltage was about $\pm 0.02\%$. The value of the magnetic field strength was known to be at least this accurate, and the accuracy in reading the voltage was between 0.05 and 0.10%. Accuracy here is determined by the ability to take repeated measurements of the same value; precision is determined by the number of places to which this measurement may be read on each attempt.



R_s - SHUNT RESISTOR
 P - LEEDS & NORTHRUP POTENTIOMETER, MODEL K-3
 B - LARGE CAPACITY WET CELL BATTERY
 I - INPUT CURRENT = 100 MA

FIGURE 1. Schematic Diagram

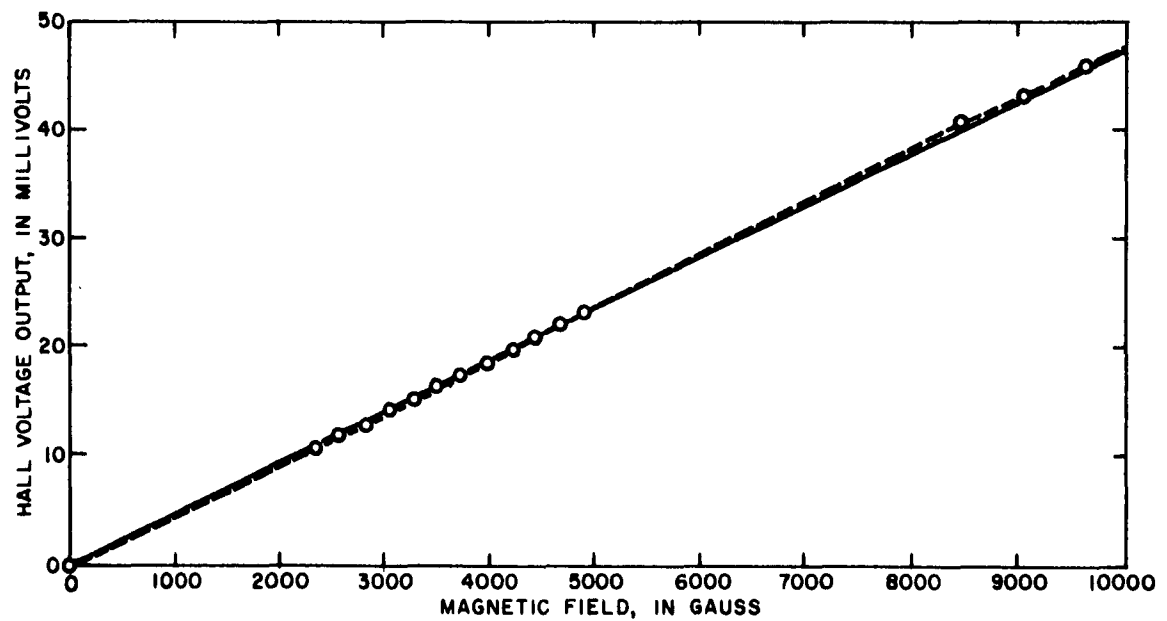


FIGURE 2. Graph of Hall Voltage vs. Magnetic Field, Showing Data Points, Best Fit Curve, and Best Fit Straight Line

The face of the Hall generator was estimated to be within 3 degrees of being normal to the field. This corresponds to an error of 0.1% or less. Error due to temperature change and instability of the current was negligible.

Because of difficulties in fabrication, the leads are not always attached on equipotential lines. Thus one may read a voltage across the Hall leads when the input current is flowing even though the field is off. This may also effect a voltage difference when the field is non-zero and the direction of the field is reversed. This voltage at zero field divided by the input current is defined as the "resistive zero component." For the device reported herein, this component was sufficiently small that it could not be measured.

SUMMARY OF RESULTS

The S curve deviated from a linear behavior by about 1% with respect to the value at 10 kilogauss. This may be improved by a factor of 3 by using the sinusoidal perturbation mentioned before. Voltage readings at calibration points one megacycle apart (adjacent) differ by less than 0.15%; hence the error in interpolating between adjacent calibration points is less than 0.1%. The use of more calibration points and better accuracy in orienting the device normal to the field would yield an error estimated at less than 0.05%. Table 1 lists the data obtained for the plot shown in Figure 2.

Care must be used, especially in high fields, to prevent the leads from forming large loops in the field. Even with the input current equal to zero, an induced voltage, U_i , may be set up.

$$U_i = A \frac{dB}{dt}$$

where A is the "inductive zero component" expressed in cm^2 and dB/dt is the time rate of change of the field. The induced current may easily be high enough to burn the leads or destroy the calibration of these thin film devices, or to do both.

TABLE 1. Calibration Data for Hall Generator*

Probe	Resonance Frequency ($\pm 0.01\%$), Mc	Equivalent Magnetic Field, kgauss	Hall Voltage, mv
H ¹	10	2.3487	10.723
	11	2.5835	11.826
	12	2.8184	12.938
	13	3.0533	14.060
	14	3.2881	15.180
	15	3.5280	16.303
	16	3.7578	17.430
	17	3.9927	18.563
	18	4.2276	19.696
	19	4.4624	20.852
	20	4.6973	21.998
	21	4.9322	23.154
Li ⁷	14	8.461	40.366
	15	9.065	43.119
	16	9.670	46.003
	17	10.274	48.552

* Type FA-21, Transverse Field Probe; manufactured by Siemens, Munich, Germany; obtained from Instrument Systems Corporation, College Point 56, Long Island, New York.

SOLID STATE SPECTROSCOPY

THE INFRARED ABSORPTION SPECTRUM OF Ce^{3+} IN LaCl_3

by

R. A. Buchanan, H. H. Caspers, and J. Murphy

INTRODUCTION

In a previous report¹ the problem of placing a trivalent cerium ion in LaCl_3 was considered. In particular, the effect of the crystalline field symmetry acting on the free-ion energy levels was developed and selection rules were used to predict the number of absorption lines due to the electronic transitions. These predictions were summarized in Figures 2 and 3 of the report.

The spectrum of Ce^{3+} in LaCl_3 in the spectral region from 1700 to 4500 cm^{-1} (2 to 6 microns) has now been obtained and will be reported. In addition, evaporated films of LaCl_3 have been prepared and their spectra taken in the infrared region between 60 and 700 cm^{-1} . A qualitative discussion of these spectra is included here.

The infrared spectrum of Ce^{3+} in CaF_2 has been presented by Feofilov² and by Kiss.³ Feofilov has noted the effects of charge compensation in his spectra, and Kiss has suggested that vibronic lines are present in his spectrum. No attempt was made to analyze these spectra by crystalline field theory, although Kiss noted a crystalline field splitting of about 1000 cm^{-1} . Hutchison and Wong⁴ reported the paramagnetic resonance spectrum of Ce^{3+} in LaCl_3 . Their work indicates which state is the ground state. This is essential information if predictions of the absorption spectrum are to be made.

¹J. Murphy, H. H. Caspers, and R. A. Buchanan, NAVWEPS Report 7237, Quarterly Report: Foundational Research Projects, July-September 1962, pp. 111-134 (December 1962).

²P. P. Feofilov, Optics and Spectroscopy, Vol. 6, p. 150 (1959).

³Z. J. Kiss, Phys. Rev., Vol. 127, p. 718 (1962).

⁴C. A. Hutchison, Jr. and E. Wong, J. Chem. Phys., Vol. 29, p. 754 (1958).

EXPERIMENTAL DETAILS

Crystals containing 0.1 and 5 mole-% of Ce^{3+} in LaCl_3 * were prepared by Professor Eugene Wong of the UCLA Physics Department. The preparation technique has been described in the literature.⁴

The crystals were ground to the desired shape with dry emery paper and polished on a cloth lap with rouge and benzene. The polished samples were mounted on the liquid helium Dewar sample-holder by means of spring clips. The edges of the sample were thickly coated with silicone vacuum grease to provide better thermal contact between the crystal and sample-holder at the lower temperatures. This entire operation was carried out in a drybox.

The liquid helium Dewar used in this experiment was designed specifically for use on a Cary Model 14 spectrophotometer. It cools the sample by conduction of heat through the solid copper sample-holder. Since the sample is not immersed directly in the liquid helium, the true sample temperature is unknown.

The spectra were recorded in the near infrared region by using the Cary Model 14b spectrophotometer equipped with PbS and cooled PbSe detectors and a 300 lines/mm grating. The resolution obtainable with this instrument depends upon many factors, which include the sample transmittance and the wavelength. In the unpolarized spectra being reported, the resolving power is approximately 1000.

DISCUSSION OF THE SPECTRA

Figure 1 shows the spectra of Ce^{3+} in LaCl_3 at room temperature, near liquid nitrogen temperature, and near liquid helium temperature. The principal effect of lowering the sample temperature is to narrow the absorption line widths and thus present a more resolved spectrum. The room temperature spectrum suggests that there are three groups of lines centered about 2250, 2900, and 3400 cm^{-1} . Upon being cooled with liquid helium, these groups of lines become more precisely defined and many components are observed. There are clearly more lines here than can possibly be explained by electronic transitions alone. The

*The 0.1 mole-% sample also contains about 0.1 mole-% of Gd^{3+} . Since the electronic structure of Gd^{3+} is such that no transitions occur in the 2-6 micron region, its presence will be ignored in the following discussion. It should be noted that the spectrum of the crystal that contains 5 mole-% Ce^{3+} in LaCl_3 but has no Gd^{3+} is essentially identical with this 0.1 mole-% Ce^{3+} sample.

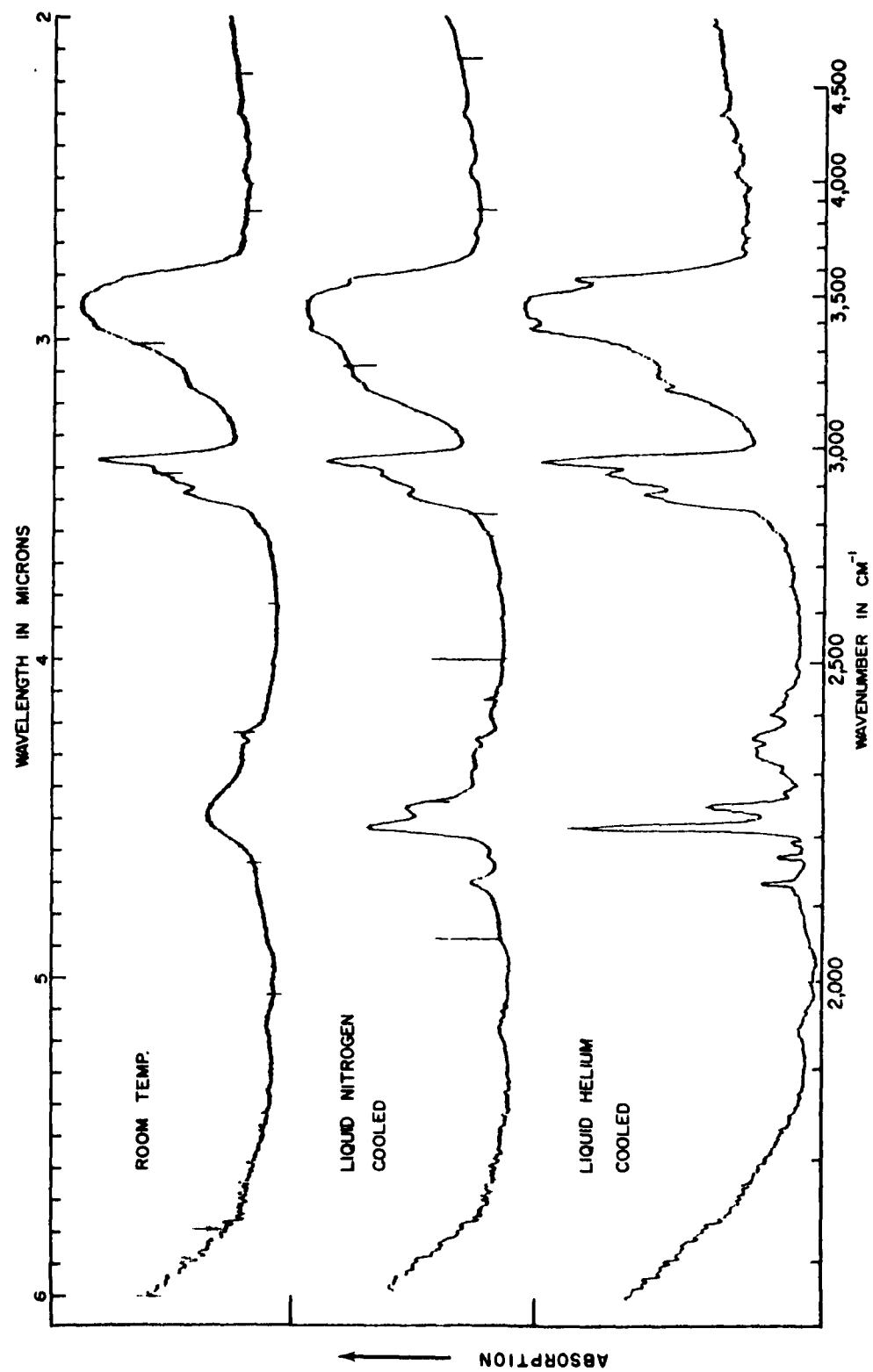


FIGURE 1. Unpolarized Absorption Spectra of 0.1 Mole-% Ce^{3+} in LaCl_3 at Room Temperature, Near 77°K, and Near 4.2°K

increase in absorption in the 1700 cm^{-1} (6 micron) region is due to an instrumental effect and is not characteristic of the crystal containing Ce^{3+} in LaCl_3 .

In order to determine the electric or magnetic dipole nature of these transitions, spectra were obtained by using a silver chloride plate polarizer. These spectra, which are presented in Figure 2, were made with the sample cooled by liquid helium. The crystalline c-axis was oriented perpendicular to the slit and to the direction of light propagation. Effects of polarization are present in these spectra. However, an unambiguous interpretation of these effects is not possible at this time, and the reasons for this may be experimental. The spectrum of the polarizer mounted in the sample compartment in such a way that the \vec{E} was perpendicular and parallel to the slit is shown in Figure 3. A large polarization of the spectrophotometer optical system is noted, and, in addition, a very curious crossing of the curves in the 1- to 2.5-micron region raises some question as to the validity of any polarization spectra taken on this machine. Nevertheless, the spectra of the polarizer seem well behaved for wavelengths between 2.6 and 6.0 microns, which is the region of primary interest in this investigation.

The crystalline c-axis was located by using crossed polaroids. The sample was mounted so that its c-axis was aligned with the horizontal plane and was perpendicular to the direction of propagation. The polarizer was then mounted externally on the liquid helium Dewar and aligned to be parallel and perpendicular to the horizontal direction. All of these alignments were made by eye and it is possible that some misalignment occurred, although many spectra were repeated after realignment of the polarizer and no essential changes in the spectra of Figure 2 were observed.

Perusal of the lowest temperature spectrum in Figure 1 shows that it is clearly inconsistent with any interpretation based only on electronic transitions of Ce^{3+} ions on a single symmetry site.¹ The possibility that Ce^{3+} ions occupy more than a single Ce site is excluded on the following grounds: (1) No multiplicity of sites has been reported for other trivalent rare-earth ions in LaCl_3 , and (2) Hutchison and Wong⁴ have studied the ground state of Ce^{3+} in LaCl_3 by paramagnetic resonance techniques and find no evidence for more than a single Ce^{3+} site.

If the symmetry of the La site were not C_{3h} , as was assumed in the previous quarterly report,¹ the number of multiplet levels in the crystal, and hence the number of spectral lines, would not be increased. The minimum degeneracy of the multiplets exists for C_{3h} symmetry since each level consists of a pair of Kramer's conjugate levels.

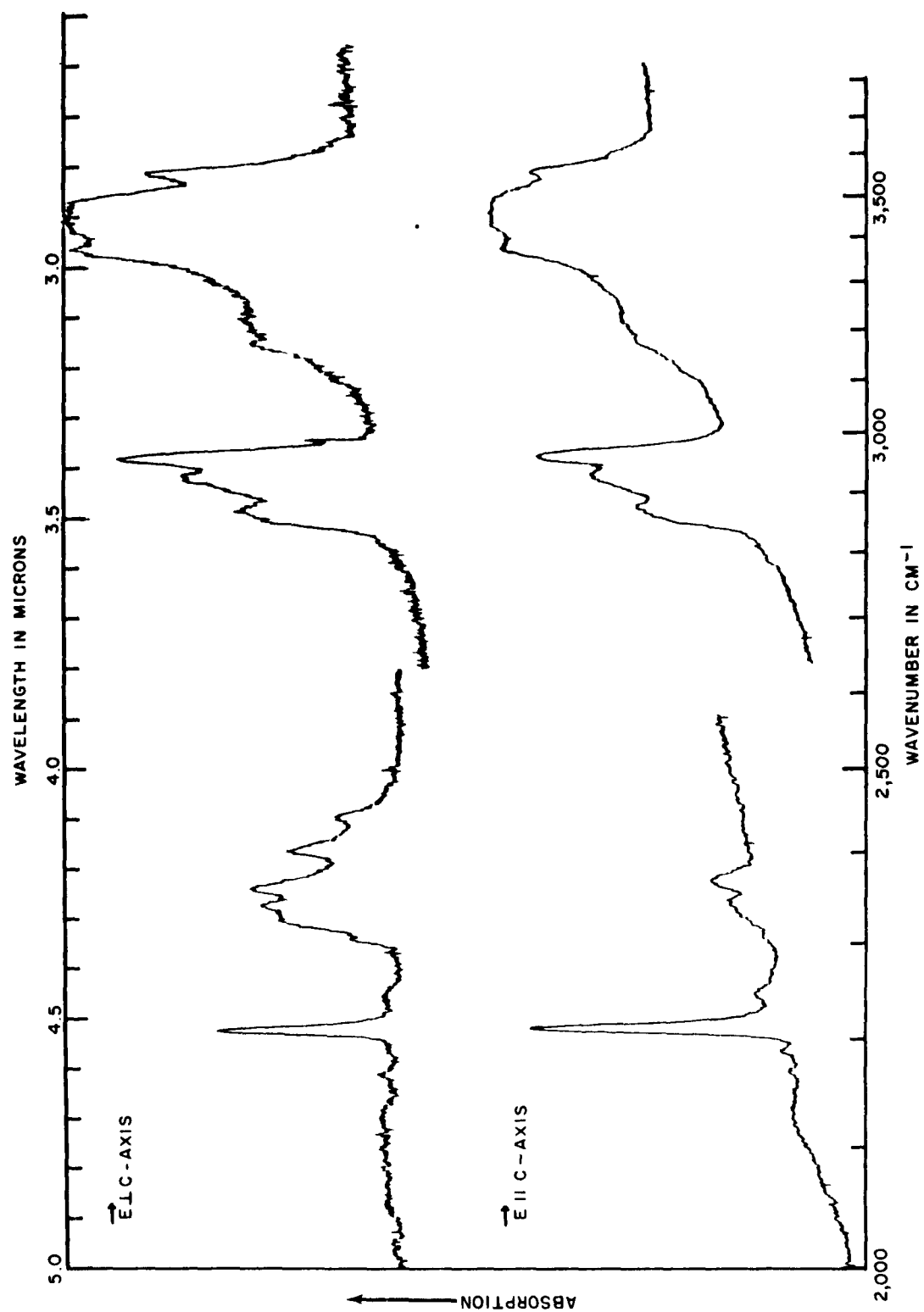


FIGURE 2. Polarized Absorption Spectra of Ce^{3+} in LaCl_3 Near 4.2°K

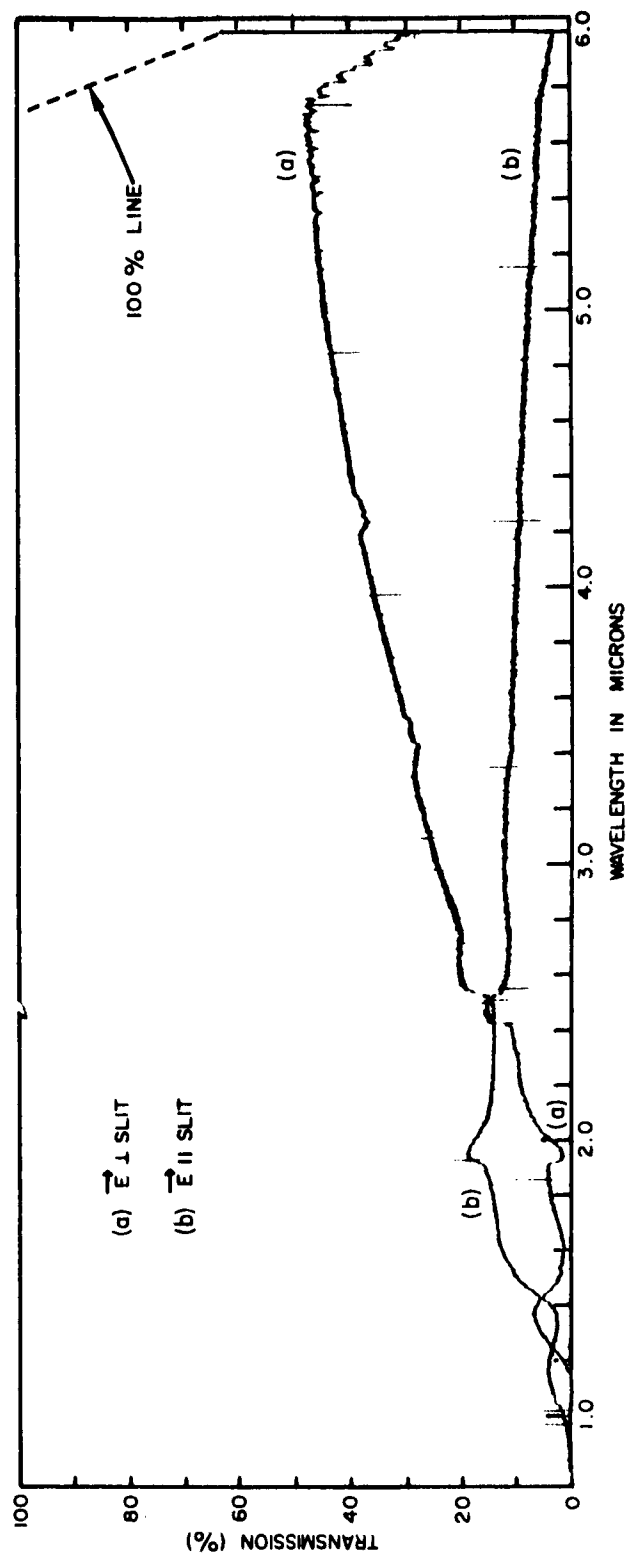


FIGURE 3. Transmission of a AgCl Plate Polarizer as Measured with the Cary Model 14b Spectrophotometer

If only sites of a single symmetry are available to the Ce^{3+} ion in the LaCl_3 lattice, it would seem that vibration electronic interactions are the only plausible explanation for the "extra" lines observed in the spectrum. Such an interaction results in the production of energy levels that are separated from an electronic level by the energy of a lattice vibration. Absorption lines associated with transitions to such levels are known as "vibronic" lines. The problem is to decide correctly which lines of the spectrum are "pure electronic" and which ones are "vibronic."

The spectra of a crystal of LaCl_3 containing 5 mole-% Ce^{3+} are presented in Figure 4. These spectra more clearly define the absorption lines in the 2250 cm^{-1} group. Again, the principal effect of lowering the sample temperature is to present a much more resolved spectrum. In addition to this, the intensities of the absorption lines near 2057 and 2100 cm^{-1} are reduced at the lower temperature. This fact labels these absorptions as being due to transitions that originate on an energy level above the ground state.

The absorption lines at 2131 and 2168 cm^{-1} appear to be narrower than most of the other lines. This suggests that they are likely candidates for assignment as pure electronic transitions. In support of this assignment, it is to be noted that lines are observed at 2210 and 2247 cm^{-1} . These lines are exactly 79 cm^{-1} above the assigned electronic lines. Such lines could be evidence that a 79 cm^{-1} lattice vibration is coupling to both the electronic transitions. Indeed, if one searches for 37 separations ($2168 - 2131 = 37\text{ cm}^{-1}$) in the region between 2250 and 2450 cm^{-1} , many such separations can be found. This is evidence that many other lattice vibrations are coupling to the upper electronic levels.

The possible existence of vibronic lines in the spectrum of Ce^{3+} in LaCl_3 has stimulated the investigation of the lattice vibrations of LaCl_3 . A complete group theoretical analysis, including the symmetry coordinates, will be presented in the following paper in this report. The number and activity of the normal modes of $\vec{k} = 0$ are summarized in Table 1. Three infrared active fundamental absorption bands are predicted. No infrared spectrum of LaCl_3 has previously been reported in the literature.

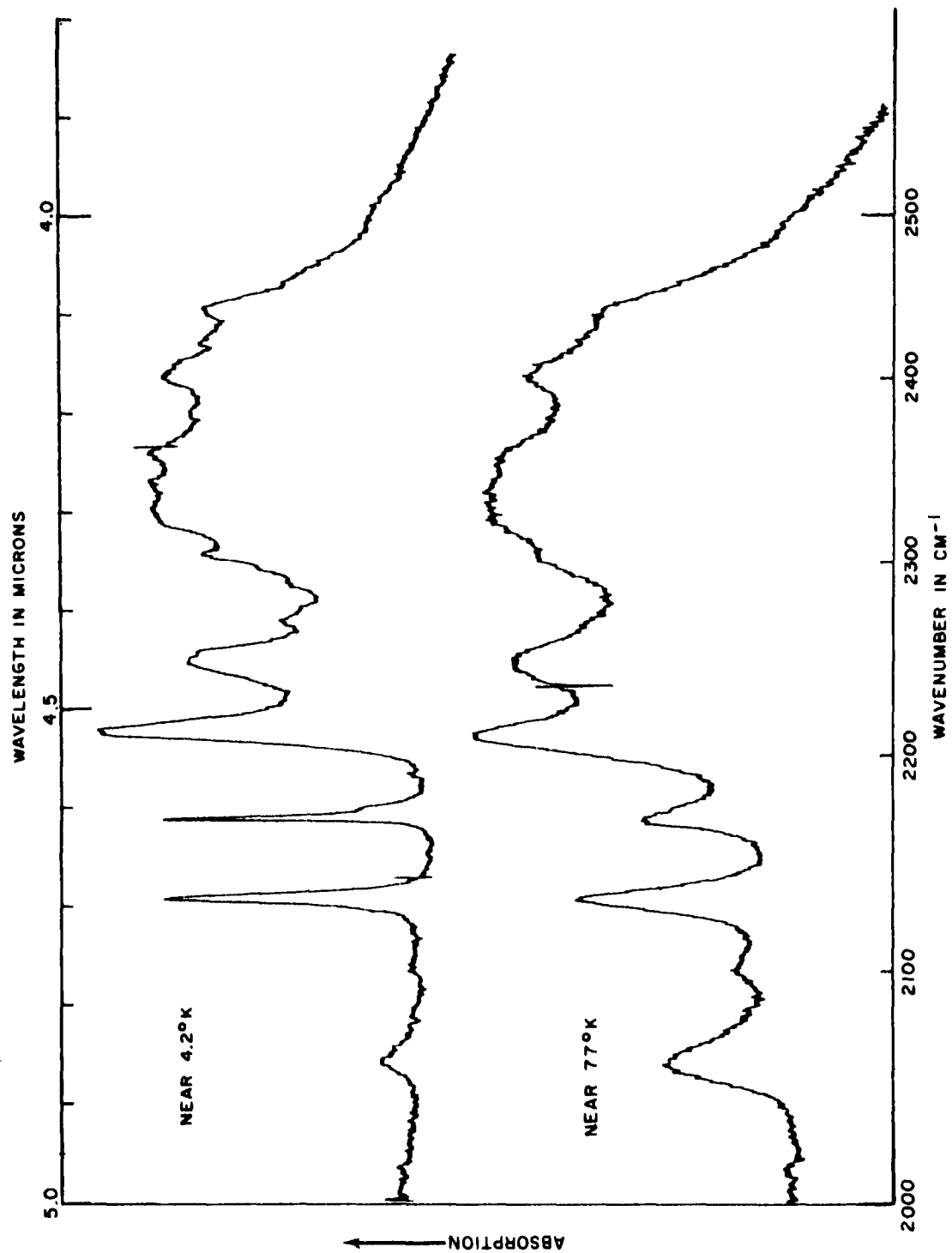


FIGURE 4. Unpolarized Absorption Spectra of 5 Mole-% Ce^{3+} in LaCl_3 Near 4.2°K and Near 77°K

TABLE 1. Selection Rules for Transition
From the Ground State

Operators	Representation of Modes	Type of Spectrum
$(a_{xx} + a_{yy}), a_{zz}$	$2 A_g$	Raman
a_{yz}, a_{zx}	$1 E_{1g}$	
$(a_{xx} - a_{yy}), a_{xy}$	$3 E_{2g}$	
T_z	$1 A_u$	Infrared
(T_x, T_y)	$2 E_{1u}$	
	$2 B_g$	Inactive
	$2 B_u$	
	$1 E_{2u}$	

LaCl₃ FILMS

Preparation

LaCl₃, particularly in thin films, reacts rapidly with atmospheric H₂O. In order to maintain a pure LaCl₃ sample, it was found necessary to prepare a vacuum cell in which to hold the evaporated film. The cell mounted in the evaporation apparatus is shown in Figure 5.

The films are prepared in the following manner: The entire vacuum cell in its open configuration and with polyethylene substrate exposed is placed in the evaporation chamber. Next, LaCl₃ crystals or powders are placed in the platinum boat located about 3 inches directly below the substrate. The evaporation chamber is evacuated to about 10^{15} torr and the boat heated sufficiently to cause the LaCl₃ to evaporate. When a film of the desired thickness is deposited on the substrate, the current to the boat is turned off and the vacuum cell closed and sealed by means of the external control shaft, which enters the evaporation chamber through O-ring seals. Air is allowed to enter the evaporation chamber, and the sealed vacuum cell containing the evaporated film is removed.

The spectrum was obtained in the 225 to 700 cm^{-1} region on a Beckman IR-7 spectrophotometer with a grating and CsI foreprism

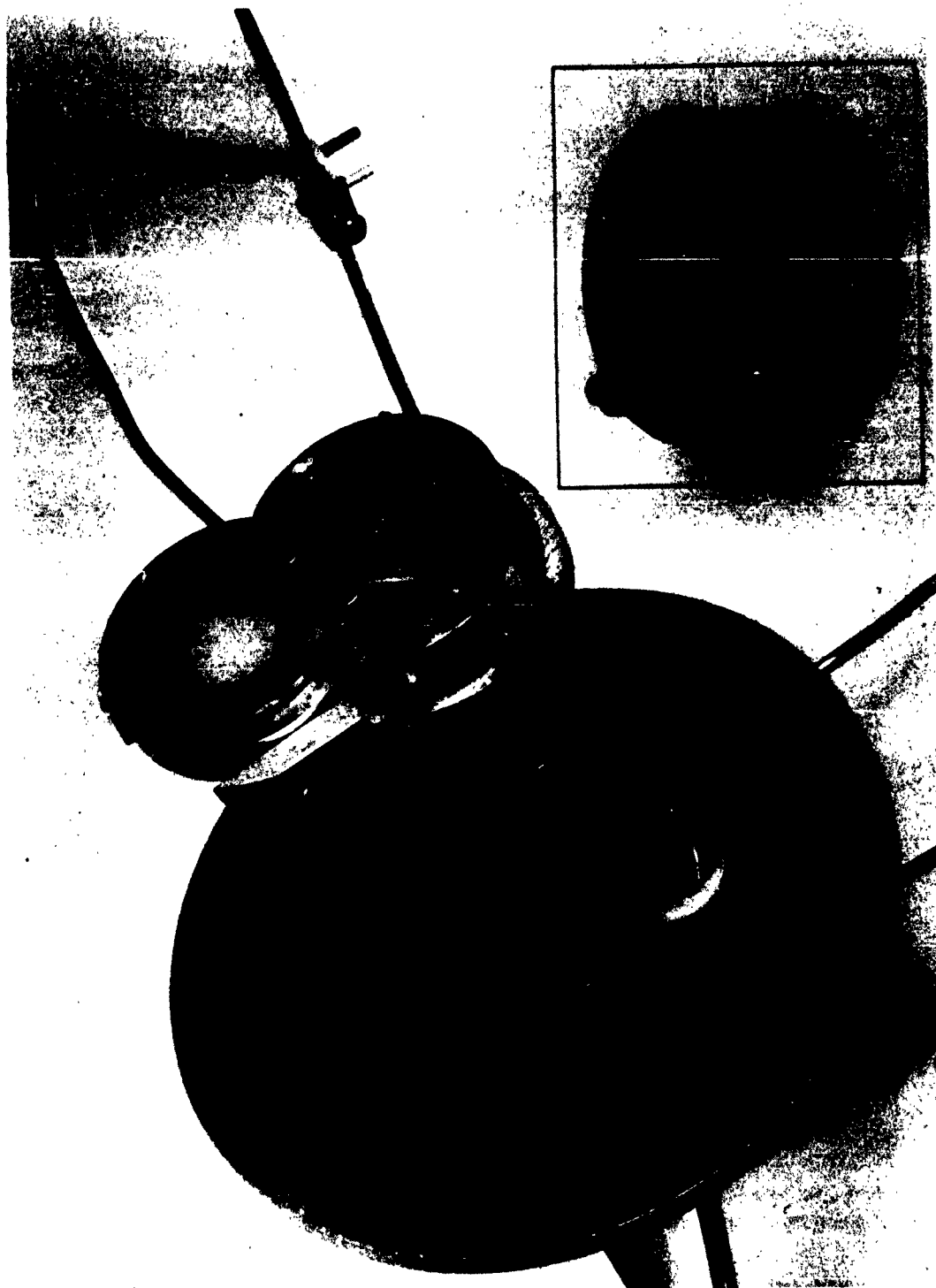


FIGURE 5. Vacuum Cell Mounted in Evaporation Apparatus. Cell is shown in open configuration exposing the polyethylene substrate. Insert shows the unmounted cell in its closed configuration.

interchange unit. The region from 60 to 225 cm^{-1} was covered with a Perkin-Elmer 98 monochromator converted for grating operation.

Spectra

The spectra of two evaporated LaCl_3 films are shown in Figure 6. These are preliminary spectra and instrumentation is now under construction that will permit a better definition and hence more precise wave-number assignment of the absorption bands.

In the double-beam IR-7 instrument, the vacuum cell with the sample was placed in the sample beam and three pieces of polyethylene were placed in the reference beam to compensate for the cell windows and substrate. In the Perkin-Elmer 98 monochromator, the transmission signal of the vacuum cell with sample was divided by the transmission signal of the three pieces of polyethylene at each wavelength to determine the percent transmission of the LaCl_3 film at that particular wavelength. The crosses on Figure 6 represent the percent transmission of the three pieces of 0.040-inch polyethylene.

The three absorption bands near 136, 165, and 212 cm^{-1} are apparently associated with the three infrared active $\vec{k} = 0$ modes (see Table 1). The evaporated films consist of randomly oriented crystallites and, therefore, polarization data are not available. Without polarization data, any assignments of the E_{1u} and A_u modes to the observed absorption bands are uncertain. Assignments of the E_{1u} and A_u modes may be possible by comparing the far infrared spectra of the isomorphous compounds LaBr_3 and UCl_3 with that of LaCl_3 . This work is now in progress.

It is of considerable interest to examine the vibronic spectrum of Ce^{3+} to see if these infrared active lattice frequencies couple to the electronic levels. Table 2 shows that the 136 and 212 cm^{-1} modes are present in the vibronic spectrum. The 165 cm^{-1} mode does not yield such good agreement. If a mode of 173 cm^{-1} is assumed, good agreement is obtained.

TABLE 2. Vibronic Spectrum of Ce^{3+}

Electronic cm^{-1}	+ Vibration cm^{-1}	= Predicted Vibronic cm^{-1}	Observed Vibronic cm^{-1}
2131	136	2267	2268
2131	173	2304	2302
2131	212	2343	2342
2168	136	2304	2302
2168	173	2341	2342
2168	212	2380	2381

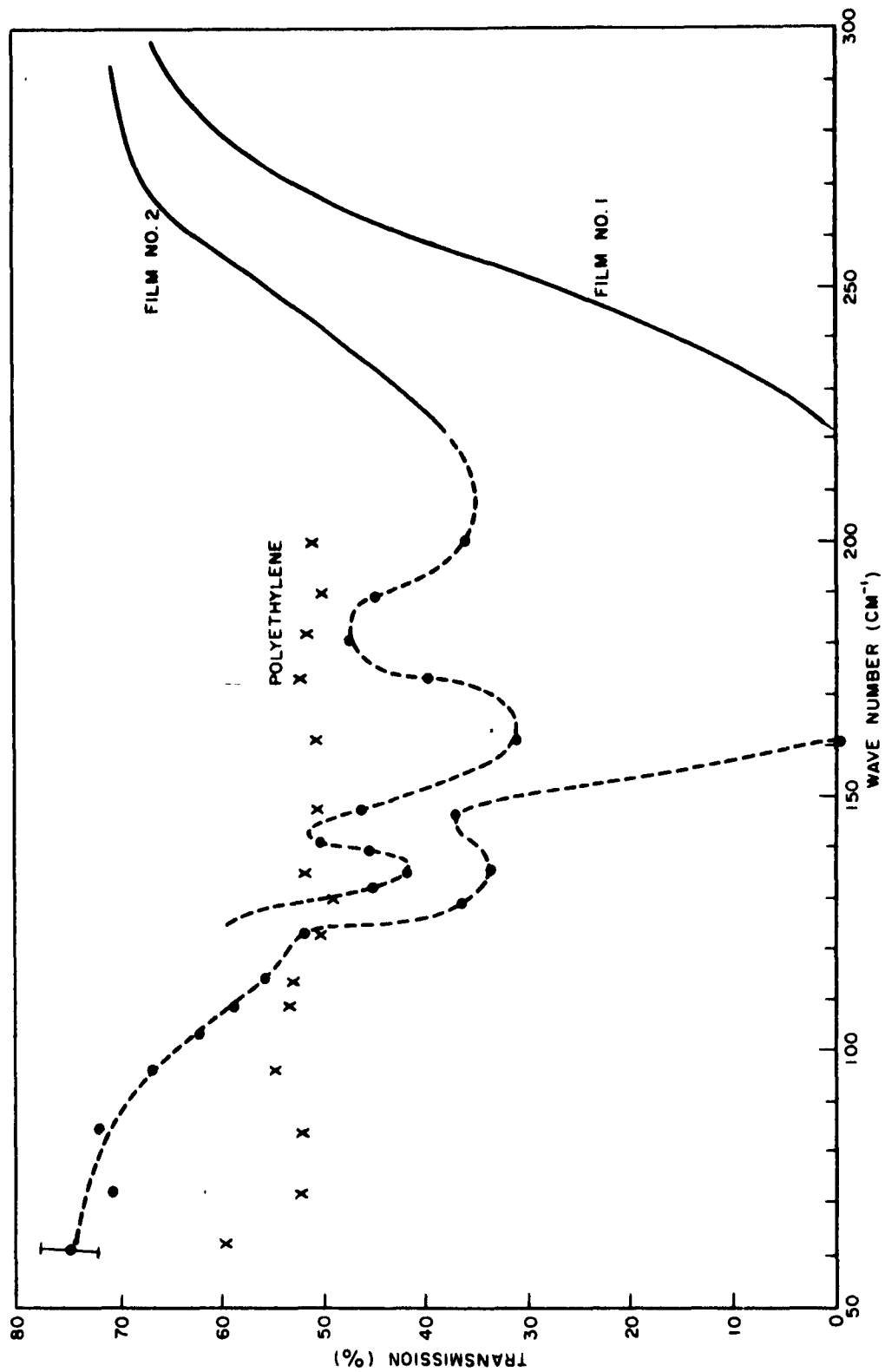


FIGURE 6. Transmission Spectra of Evaporated LaCl_3 Films

Several explanations for the failure of the 165 cm^{-1} mode to be observed in the vibronic spectrum can be presented. Until better far-infrared data actually confirm or reject the wave-number value 165 cm^{-1} , speculation on this matter will be withheld.

CONCLUSIONS

From these observations, it must be concluded that there is strong evidence for the assumption that lattice frequencies of the LaCl_3 host are coupling to electronic levels of the Ce^{3+} ions. As a result of this coupling, many more lines appear in the absorption spectrum in the 4- to 5-micron region than would otherwise exist if only "pure" electronic transitions were involved. No attempt has been made to interpret the groups of lines near 2900 and 3400 cm^{-1} . These lines are too far removed from the 2131 and 2168 cm^{-1} lines to be vibronic lines associated with these electronic transitions. They may be vibronic lines of other electronic transitions, however.

It is tempting to associate some of the lines near 2900 and 3400 cm^{-1} with vibration-induced electronic transitions. The selection rules of Murphy et al.¹ were based on the static crystalline field model and can be shown to break down in the vibrating crystalline field. This assignment leads to a larger crystalline field splitting than is generally observed for rare-earth ions in LaCl_3 . It is, however, consistent with the 1000 cm^{-1} crystalline field splitting observed by Kiss³ for Ce^{3+} in CaF_2 .

The possibility that impurities are present in the spectra has been considered but it is felt that this possibility cannot be the explanation of the additional lines, for the following reasons: (1) The spectral regions in the shorter wavelength infrared and visible have been examined and contain no absorption bands. This would seem to eliminate another rare-earth ion as the impurity. (2) The spectrum of Ce^{3+} in LaF_3 shows a spectrum similar to Ce^{3+} in LaCl_3 . This would seem to imply that the spectra presented are characteristic of Ce^{3+} . The possibility of some other impurity, such as an organic molecule, cannot be positively eliminated at this time.

The Ce^{3+} spectrum seems to defy interpretation in all host lattices in which it has been studied. It is necessary to obtain the positions of the electronic levels and establish the crystalline field parameters before any quantitative understanding of the Ce^{3+} spectrum can be obtained.

ACKNOWLEDGMENTS

The authors wish to thank Professor Eugene Y. Wong of the UCLA Physics Department for preparing the materials studied in this investigation. We also acknowledge very helpful discussions with Professors Wong and Satten with Dr. I. Richmond of the UCLA Physics Department. H. Ronald Marlin of NOLC prepared the LaCl_3 evaporated films used in this research.

SYMMETRY COORDINATES FOR LaCl_3

by

J. Murphy and H. H. Caspers

INTRODUCTION

For processes in which only a single phonon is involved, the maximum intensity of an absorption line in the vibrational spectrum of a lattice corresponds to a $\vec{k} = 0$ mode. This comes about because a $\vec{k} = 0$ infrared active mode has associated with it a large induced electric dipole moment in comparison with a $\vec{k} \neq 0$ mode of the same branch. For a similar reason, the peaks in the Raman spectrum are associated with $\vec{k} = 0$ vibrations. There seems to be good agreement between the absorption peaks found in the infrared lattice spectrum and the "vibronic" lines observed in the optical absorption spectra of rare-earth ions in crystals.^{5,6}

The factoring of the secular determinant for the frequencies of the $\vec{k} = 0$ modes is greatly facilitated by the introduction of symmetry coordinates. These symmetry coordinates reduce the determinant to block diagonal form. The subdeterminants for the frequencies now involve only those symmetry coordinates that transform as the same row of the same irreducible representation of the factor group. It is desirable to establish a procedure for determining sets of symmetry coordinates that form bases in terms of which the normal modes of the lattice can be expressed. The linear combination of symmetry coordinates which form a normal mode depend upon the selection of significant force constants. Naturally, an exact solution would require an infinite

⁵R. A. Buchanan, J. Murphy, and H. H. Caspers, Bull. Am. Phys. Soc., Vol. 7, p. 616, R10 (1962).

⁶I. Richman and E. Wong, Physics Dept., UCLA (private communication).

number of force constants for an infinite lattice. However, it is often a good approximation to consider the interactions only up to a few nearest neighbors. One tries to express all of the vibrational frequencies in terms of as small a number of force constants as possible. As one will discover in applying this formalism, certain lattices prove to be rather difficult because of either too many particles in the primitive cell or too low a symmetry, or both. There are, however, a large number of lattices for which the symmetry coordinates can readily be reduced.

LATTICE VIBRATIONS IN LaCl_3

LaCl_3 crystallizes in a hexagonal dipyramidal type of symmetry and belongs to the space group C_{6h}/m (C_{6h}^2).⁷ Figure 7 shows the particles in the primitive cell. (The x,y,z coordinate system indicated will be used in labeling particle displacements in Table 9.) According to Zachariasen,⁷ the dimensions of the primitive cell are $a_1 = a_2 = 7.468 \text{ \AA}$, $a_3 = 4.366 \text{ \AA}$. The particle positions are expressed as fractions of the dimensions of the primitive cell and are

$$2 \text{ La: } (1/3, 2/3, 1/4), (2/3, 1/3, 3/4)$$

$$6 \text{ Cl: } (a, b, 1/4), (1 - b, a - b, 1/4), (1 - a + b, 1 - a, 1/4) \\ (a - b, a, 3/4), (1 - a, 1 - b, 3/4), (b, 1 - a + b, 3/4)$$

where $a = 0.375$ and $b = 0.292$. The origin of coordinates is chosen as the point marked 0. Figure 8, which is taken from International Tables for X-Ray Crystallography,⁸ shows all of the symmetries of the primitive cell. The symmetry operations that leave Figure 8 invariant are listed in Table 3. The $\vec{k} = 0$ factor group of C_{6h}^2 can be seen to be isomorphic with the underlying point group C_{6h} ; therefore, these two groups have the same character table. From Figures 7 and 8, one can determine that the point symmetry at the site of a La ion is C_{3h} , while the point symmetry at a chlorine site is C_s , i. e., (E, σ_h) . Table 4 lists the irreducible characters of C_{6h}^2 , which is isomorphic with the point C_{6h} . Tables 5 and 6 list, respectively, the irreducible characters of C_{3h} and C_s . The groups C_{3h} and C_s are subgroups of C_{6h} .

It is of interest to determine the transformation properties of these modes at the sites of the La and Cl ions. A mode with given transformation properties can only occur if the particles that make up the lattice can move and maintain those transformation properties. The point group

⁷W. H. Zachariasen, J. Chem. Phys., Vol. 16, p. 254 (1948).

⁸International Tables for X-Ray Crystallography, Vol. I, The Kynoch Press, Birmingham, England (1952).

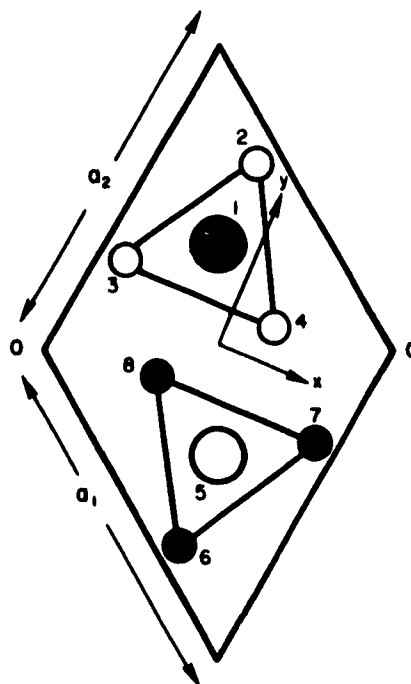
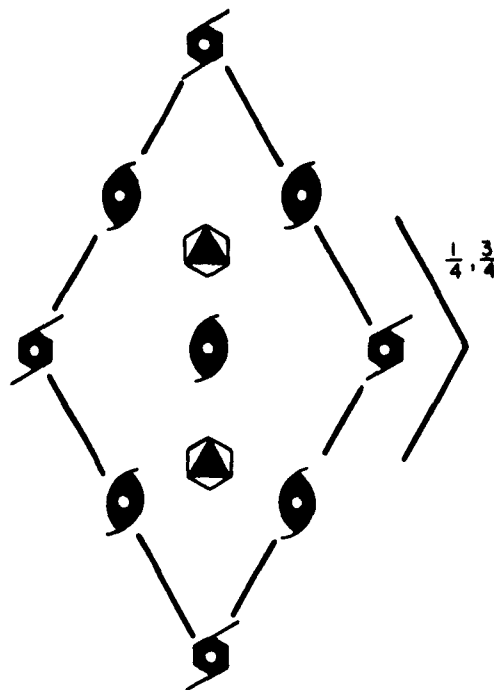


FIGURE 7. Positions of Ions in the Primitive Cell. The large circles represent lanthanum ions and the smaller circles, chlorine ions. Ions in the $1/4$ plane are shown filled in; those in the $3/4$ plane are open. Zero (0) is the origin of coordinates for the ion positions given in the text. The particle displacements listed later in Table 9 are written with respect to the indicated x, y, z coordinate system where the z axis is out of the plane of the paper.



LEGEND:




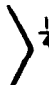

-  -60° rotation followed by inversion
-  -60° rotation followed by translation of $a_3/2$ where a_3 is the z dimension of the primitive cell
-  -180° rotation followed by $a_3/2$ translation
-  $\frac{1}{4}, \frac{3}{4}$ the planes at $1/4 a_3$ and $3/4 a_3$ are reflection planes
-  inversion

FIGURE 8. Symmetry Operations in the C_{6h}^2 Primitive Cell. All rotations are about axes passing through the symbol and perpendicular to the plane of the paper.

TABLE 3. Symmetry Operations of the Space Group C_{6h}^2







Symbol	Description
$\{\epsilon T_n\}$	Lattice translation: $T_n = n_1 \vec{a}_1 + n_2 \vec{a}_2 + n_3 \vec{a}_3$ where $ a_1 = a_2 \neq a_3 $
$\{C_3 0\}, \{C_3^2 0\}$	Three-fold rotation about axes parallel to the c-axis through symbols  and 
$\{S_3 0\}$ $\{S_3^5 0\} = \{I 0\} \{C_6 0\}$	Three-fold rotatory reflection about axis paral- lel to crystalline c-axis passing through 
$\{\sigma_h 0\}$	Horizontal reflection about plane perpendicular to c-axis passing through 1/4 and 3/4 planes
$\{I 0\}$	Inversion through centers indicated by circles o
$\left\{C_2 \left \frac{a_3}{2} \right. \right\}$	Screw diad normal to paper passing through symbols 
$\left\{C_6 \left \frac{a_3}{2} \right. \right\}, \left\{C_6^5 \left \frac{a_3}{2} \right. \right\}$	Screw hexads normal to paper passing through symbols 
$\{S_6 0\}, \{S_6^5 0\}$	Six-fold rotatory reflections with axes parallel to c-axis and passing through symbols 

TABLE 4. Character Table for C_{6h}^2

C_{6h}	$\{\epsilon T_n\}$	$\{C_6 \frac{a_3}{2}\}$	$\{C_3 0\}$	$\{C_2 \frac{a_3}{2}\}$	$\{C_3^2 0\}$	$\{C_6^5 \frac{a_3}{2}\}$	$\{I 0\}$	$\{S_3^5 0\}$	$\{S_6^5 0\}$	$\{\sigma_h 0\}$	$\{S_6 0\}$	$\{S_3 0\}$
A_g	1	1	1	1	1	1	1	1	1	1	1	1
B_g	1	-1	1	-1	1	-1	1	-1	1	-1	1	-1
E_{1g}^1	1	ϵ	$-\epsilon^*$	-1	$-\epsilon$	ϵ^*	1	ϵ	$-\epsilon^*$	-1	$-\epsilon$	ϵ^*
E_{1g}^2	1	ϵ^*	$-\epsilon$	-1	$-\epsilon^*$	ϵ	1	ϵ^*	$-\epsilon$	-1	$-\epsilon^*$	ϵ
E_{2g}^1	1	$-\epsilon^*$	$-\epsilon$	1	$-\epsilon^*$	$-\epsilon$	1	$-\epsilon^*$	$-\epsilon$	1	$-\epsilon^*$	$-\epsilon$
E_{2g}^2	1	$-\epsilon$	$-\epsilon^*$	1	$-\epsilon$	$-\epsilon^*$	1	$-\epsilon$	$-\epsilon^*$	1	$-\epsilon$	$-\epsilon^*$
A_u	1	1	1	1	1	1	-1	-1	-1	-1	-1	-1
B_u	1	-1	1	-1	1	-1	-1	1	-1	1	-1	1
E_{1u}^1	1	ϵ	$-\epsilon^*$	-1	$-\epsilon$	ϵ^*	-1	$-\epsilon$	ϵ^*	1	ϵ	$-\epsilon^*$
E_{1u}^2	1	ϵ^*	$-\epsilon$	-1	$-\epsilon^*$	ϵ	-1	$-\epsilon^*$	ϵ	1	ϵ^*	$-\epsilon$
E_{2u}^1	1	$-\epsilon^*$	$-\epsilon$	1	$-\epsilon^*$	$-\epsilon$	-1	ϵ^*	ϵ	-1	ϵ^*	ϵ
E_{2u}^2	1	$-\epsilon$	$-\epsilon^*$	1	$-\epsilon$	$-\epsilon^*$	-1	ϵ	ϵ^*	-1	ϵ	ϵ^*

Note: $\epsilon = \exp\left(\frac{2\pi i}{6}\right)$

TABLE 5. Character Table for C_{3h}

C_{3h}	E	C_3	C_3^2	S_3^5	σ_h	S_3
A'	1	1	1	1	1	1
E'	$\begin{Bmatrix} 1 \\ 1 \end{Bmatrix}$	$\begin{Bmatrix} -\epsilon^* \\ -\epsilon \end{Bmatrix}$	$\begin{Bmatrix} -\epsilon \\ -\epsilon^* \end{Bmatrix}$	$\begin{Bmatrix} -\epsilon \\ -\epsilon^* \end{Bmatrix}$	$\begin{Bmatrix} 1 \\ 1 \end{Bmatrix}$	$\begin{Bmatrix} -\epsilon^* \\ -\epsilon \end{Bmatrix}$
A''	1	1	1	-1	-1	-1
E''	$\begin{Bmatrix} 1 \\ 1 \end{Bmatrix}$	$\begin{Bmatrix} -\epsilon^* \\ -\epsilon \end{Bmatrix}$	$\begin{Bmatrix} -\epsilon \\ -\epsilon^* \end{Bmatrix}$	$\begin{Bmatrix} \epsilon \\ \epsilon^* \end{Bmatrix}$	$\begin{Bmatrix} -1 \\ -1 \end{Bmatrix}$	$\begin{Bmatrix} \epsilon^* \\ \epsilon \end{Bmatrix}$

Note: $\epsilon = \exp(2\pi i/6)$ TABLE 6. Character Table for C_s

C_s	E	σ_h
A'	1	1
A''	1	-1

at the site of each particle must be a subgroup of the lattice space group. Each representation of the point group with which the factor group is isomorphic (let us call it G) can be expressed as linear combinations of the representations of the point group at each particle site. In other words, the representations of G become reducible representations of the point groups at the particle sites. Let us suppose that the particle coordinates (or displacements) transform according to the representations γ_x , γ_y , and γ_z of the point group g_p , where g_p denotes the point group at the particle site. Upon reducing the representation Γ_i of G to those of g_p , at least one of the γ_x , γ_y , or γ_z must appear at least once in the reduction; otherwise no mode of the lattice that transforms as Γ_i will exist in which the particle at the g_p symmetry site will move. On the other hand, suppose at the La site the representation Γ_i reduces to, say, $\gamma_a + \gamma_b + \gamma_z$, where a and b are not x or y . In the lattice mode that transforms as Γ_i , the La ion can only move in the z direction since only the z coordinate has the right transformation properties for that mode. This situation requires, then, that if a representation of the space group Γ_k does not contain any representation according to which the particle coordinates transform for any type of particles of the crystal, there is no mode of the lattice that transforms as Γ_k . Using these arguments, one can draw a correlation chart⁹ (Figure 9), which shows

⁹D. F. Hornig, J. Chem. Phys., Vol. 16, p. 1063 (1948).

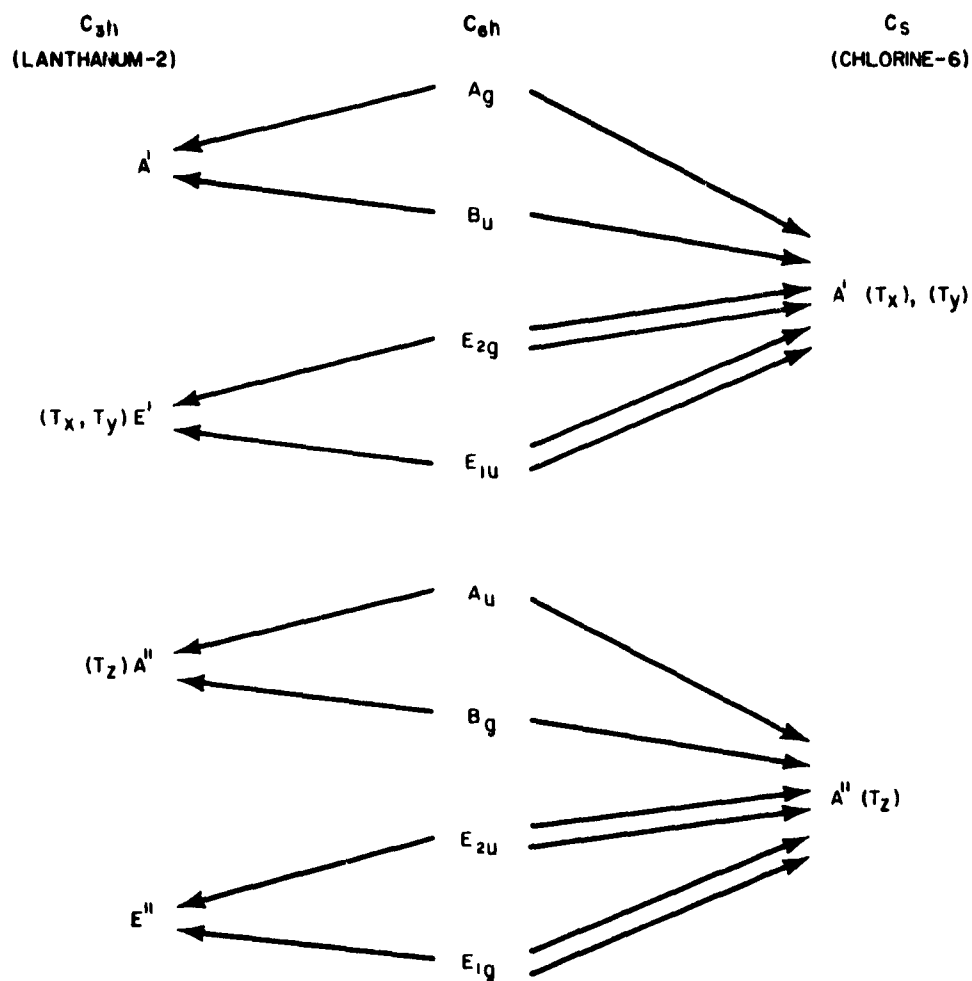


FIGURE 9. Correlation Chart Showing the Reduction of C_{6h} to C_{3h} and C_s Symmetry. The symbol (T_x , T_y) means that x and y translations transform into linear combinations of one another according to the representation next to which they appear. The symbols (T_x), (T_y), and (T_z) mean that the x , y , and z translations transform into themselves times a constant.

the reduction of the space group representations into the representations of the particle site symmetries, and from it determine which particles move in the various modes.

One can, in fact, determine the number of unit cell modes and their transformation properties quite apart from the usual method of reducing the reducible representation of the primitive cell into the irreducible representations of the space group. These two methods serve as a useful check on each other. From Figure 9, we note first of all that modes of vibration (including translations of the whole crystal) are allowed for every representation of C_{6h} . Secondly, in modes that transform as A_g , B_u , E_{1g} , and E_{2u} , only the chlorine ions can take part; the lanthanum ions do not move.

Given a set of n independent coordinates, one can write n linearly independent combinations of these coordinates. This implies that there are n linearly independent modes of vibrations including complete translations and rotations. Therefore, for each degree of freedom we can say there is one mode. In a symmetry coordinate, the particle displacements that transform as an even representation are such that two particles which are related by inversion through an inversion point in the lattice must be moving in opposite directions, whereas the displacements of two such particles in an odd mode are in the same direction. If there is a particle sitting at an inversion point of the primitive cell, an even mode cannot involve the displacements of that particle since it cannot be going in two directions at once. In such a case, the number of even and odd modes would not be equal. In $LaCl_3$, however, there are no particles at the inversion points. In Figure 9, an odd representation is listed under the even representation to which it is related by a change in sign under inversion, i. e., if in an E_{2g} symmetry coordinate the particle displacements on one side of the inversion center are changed in phase by 180 deg, the resulting set of displacements would transform as an E_{1u} representation. Hence, if we can determine all of the even symmetry coordinates, we can find all of the odd ones, and vice versa.

An A_g mode (Figure 9) involves only the x, y motion of the chlorines. In $LaCl_3$ each chlorine ion can be transformed into any other chlorine ion by some operation of the space group. Under such a transformation, the x and y components of the displaced ion become some linear combination of the x and y coordinates of the ion into whose position it has been carried by the symmetry operation. This two-dimensional transformation implies two, and only two, independent solutions or eigenfunctions of the transformation matrices. Hence there are two A_g modes. The number of A_g modes and B_u modes must be equal since the B_u modes can be obtained from the A_g modes by changing the sign of the particle displacements in the lower half of Figure 7. We have

thus used up four linear combinations of the chlorine x,y coordinates, or, as far as numbers are concerned, four out of the twelve coordinates. The E_{2g} and E_{1u} modes (which are equal in number) involve the displacements of both the chlorine and the lanthanum ions in the x,y plane. There are two lanthanum ions in the primitive cell and, therefore, four new x,y coordinates. This means that we once again have twelve coordinates, and so twelve linear combinations or modes must be divided equally among the E_{2g} and E_{1u} representations. There are, therefore, 3 E_{2g} modes and 3 E_{1u} modes $[(3 + 3) \times 2 = 12]$. For the representations at the lower half of Figure 9, the two linear combinations of lanthanum z displacements must be divided equally between the A_u and the B_g representations. The six chlorine z displacements are divided as follows:

$$\begin{array}{ll} E_{2u} \dots 2 & A_u \dots 1 \\ E_{1g} \dots 2 & B_g \dots 1 \end{array}$$

Each E representation must have two linearly independent modes since an E representation is two-dimensional. The remaining two modes are divided between the A_u and the B_g representations. These results, which are tabulated in Table 7, are the same as those that would be determined by the usual group theoretical method of reducing the reducible character of the unit cell.⁹

TABLE 7. Numbers and Species of Modes in $LaCl_3$

Representation	No. of Representations	No. of Modes	Types of Ions Involved	Polarization
A_g	2	2	Cl	(x,y)
B_u	2	2	Cl	(x,y)
E_{2g}	3	6	La + Cl	(x,y)
E_{1u}	3	6	La + Cl	(x,y)
A_u	2	2	La + Cl	z
B_g	2	2	La + Cl	z
E_{1g}	1	2	Cl	z
E_{2u}	1	2	Cl	z

Such a reducible character is shown in Table 8 and is obtained by performing each symmetry operation of the space group on the particles in the primitive cell and finding how many such particles transform into themselves or into particles that are primitive translations away. The set of these numbers multiplied by the traces of the corresponding transformation matrices is the character of the reducible representation and is equal to the sum of the irreducible representations of C_{6h} weighted by the numbers shown in the second column of Table 7.

TABLE 8. Character Table for the Reducible Representation of the Primitive Cell Modes

C_{6h}	E	C_6	C_3	C_2	C_3^2	C_6^5	I	S_3^5	S_6^5	σ_h	S_6	S_3
$\chi(R)$	24	0	0	0	0	0	0	-4	0	8	0	-4

From the correlation chart, we have determined not only the numbers and types of normal modes, but also which particles move and whether the motion is in the x,y plane or in the z direction. This information allows us to find a set of symmetry coordinates—basis functions from which normal modes are determined. For example, we have determined that there are three pairs of modes that transform according to the E_{2g} representation in $LaCl_3$. In each of these modes, both the La and Cl ions are moving. Furthermore, the motion is restricted to be parallel to the x,y plane. Three modes transform as the first row of the representation E_{2g} and three transform as the second row. Any set of displacements of the particles that transform as the first row of E_{2g} must be expressible as a linear combination of normal modes which transform as that first row. Conversely, a normal mode is expressible as a linear combination of linearly independent sets of displacements that transform according to the representation of interest. Consequently, if we can find three linearly independent sets of displacements that transform as the first row of the representation E_{2g} , then the three normal modes will be expressible as linear combinations of these three "symmetry coordinates."

The normal modes are the linear combinations of symmetry coordinates that completely diagonalize the secular determinant. We will not go so far as to calculate the secular determinant in this paper as we are only interested in demonstrating the method of obtaining symmetry coordinates.

DETERMINATION OF SYMMETRY COORDINATES

A symmetry coordinate S , which transforms according to a one-dimensional irreducible representation of the factor group, has the following property:

$$RS = S' = kS \quad (1)$$

where R represents an element of the group and k is a constant factor of unit modules. In the case of an abelian group such as C_{6h} , the factor k can be complex. In a non-abelian group, k is restricted to ± 1 . In the case of complex k 's, the representations that are complex conjugates of one another, i.e., factors k and k^* , are generally taken together and the combination is treated as a two-dimensional representation of the group. In the present study, it is convenient to maintain distinct one-dimensional representation of the C_{6h} point group.

As an example of the procedure to be followed, let us choose the representation listed in Table 4 as E_{2g}^1 , that is, the first row of E_{2g} .

Consider the operation $\{C_6|a_3/2\}$ of Table 3 about the point C of Figure 7. This operation has the following effect on the particles:

$1 \rightarrow 5$	$7 \rightarrow 2' = 2$
$2 \rightarrow 8$	$8 \rightarrow 3' = 3$
$3 \rightarrow 6$	$6 \rightarrow 4' = 4$
$4 \rightarrow 7$	$5 \rightarrow 1' = 1$

The primes indicate particles that are removed from the particles within the unit cell by a primitive translation. Since we are considering $\vec{k} = 0$ modes, the primed and unprimed particles move exactly in phase. This has been indicated by writing $2' = 2$, etc. According to equation (1) and the character table for the representation E_{2g}^1 , the new sets of displacements are related to the old by

$$S' = \exp\left(\frac{2\pi i}{3}\right)S$$

In other words, the transformed particle 2 is leading the untransformed particle 8 by 120 deg. A second application of $\{C_6|a_3/2\}$ or, equivalently, $\{C_3|0\}$, carries particle 2 into particle 3 (or an equivalent position displaced from the first by a primitive translation). We see from the C_{6h}^2 character table and Figure 7 that the transformed particle 2 is lagging the untransformed particle 3 by 120 deg. According to the definition given here of a symmetry coordinate, we are at liberty to choose

the displacement of any particle arbitrarily and then operate on this particle with the group elements to find the displacements of the other particles. It is convenient to choose the motion of our starting particle (say, particle 2 in Figure 7) to be circular. By carrying out the procedure outlined above, we arrive at Figures 10a, 10b, and 10c. Except for modes that involve translations of the whole crystal, the lanthanum motions relative to the chlorine motions are chosen so that the linear momentum of the primitive cell is zero. It can easily be verified that there are three, and only three, symmetry coordinates (barring multiplication of each particle motion by a constant phase factor) that involve circular motion of all of the particles and transform as E_{2g}^1 . The implication is not that this is the only set of symmetry coordinates which transform this way. One can form an infinite number of sets of three linearly independent motions of the three sets shown. The symmetry coordinates that transform as E_{2g}^2 are the complex conjugates of those that transform as E_{2g}^1 and are shown in Figures 11a, 11b, and 11c. It is not convenient for purposes of calculating the vibrational frequencies to use the symmetry coordinates just derived. Linear combinations that are the sum and difference of the complex conjugate pairs turn out to be better, since in these all particles pass through their equilibrium positions simultaneously. Furthermore, the new motions are rectilinear. The sum and difference of Figures 10a and 11a are shown in Figures 12a and 13a respectively. Figures 12b and 13b are the sum and difference of Figures 10b and 11b, while Figures 12c and 13c are the sum and difference of Figures 10c and 11c.

Except that there is only one coordinate for each particle, the analysis of the z-polarized symmetry coordinates is carried out in the same fashion as the x,y motions. The displacement of one of the particles is chosen arbitrarily and the motions of all of the particles are determined with respect to it. In the z-polarized symmetry coordinates that transform as E_{1g} and E_{2u} , the three chlorine ions in each triangle must be 120 deg out of phase with one another. Once again, however, the sums and differences of the symmetry coordinates so derived are more convenient for calculational purposes.

The symmetry coordinate for the $\vec{k} = 0$ modes of LaCl_3 are listed in Table 9. Those shown that transform as E representations are actually the sums and differences of the symmetry coordinates first arrived at, as discussed above.

The particle displacements are listed as (i,j,k) where i, j, and k are the components of the displacement vectors located on the particles and written with respect to the x,y,z coordinate system shown in Figure 7. Some of the lanthanum displacements are multiplied by a factor which is required in order to reduce the linear momentum of the unit cell to zero.

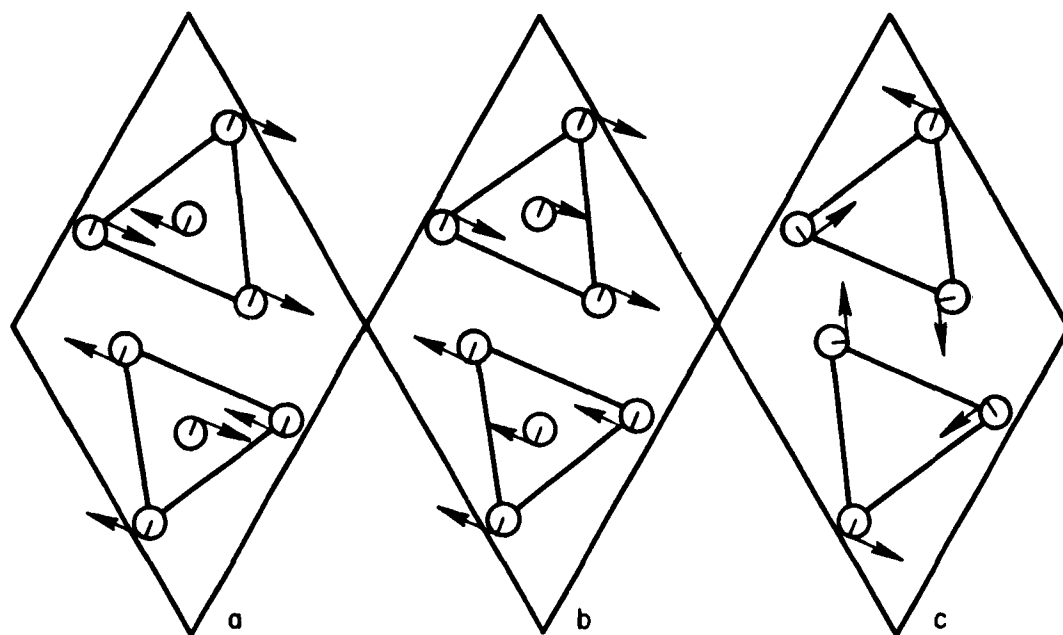


FIGURE 10. Symmetry Coordinates That Transform as E_{2g}^1

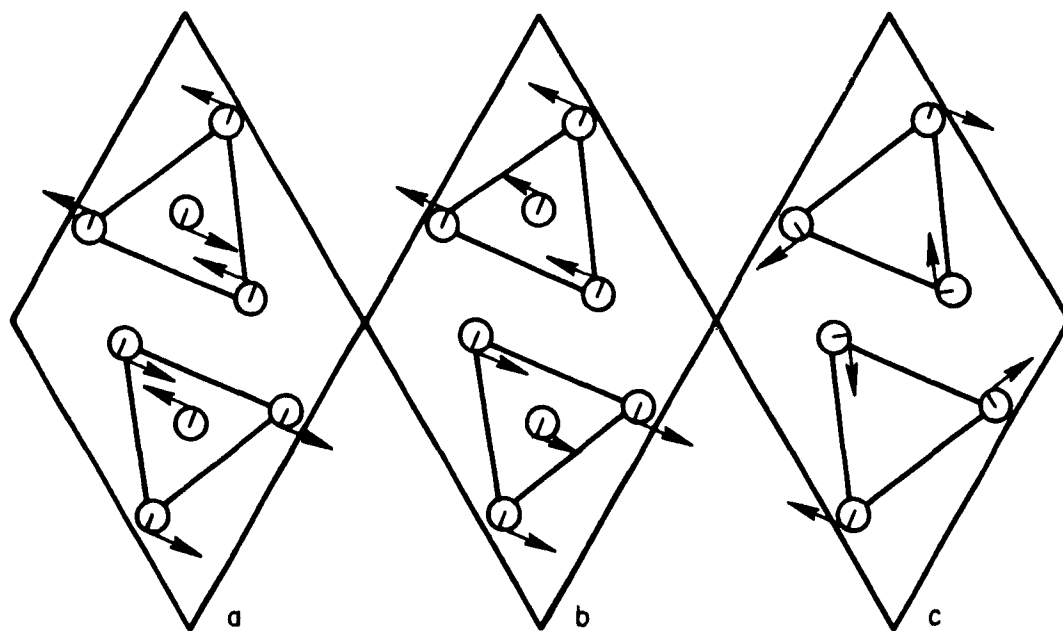


FIGURE 11. Symmetry Coordinates That Transform as E_{2g}^2

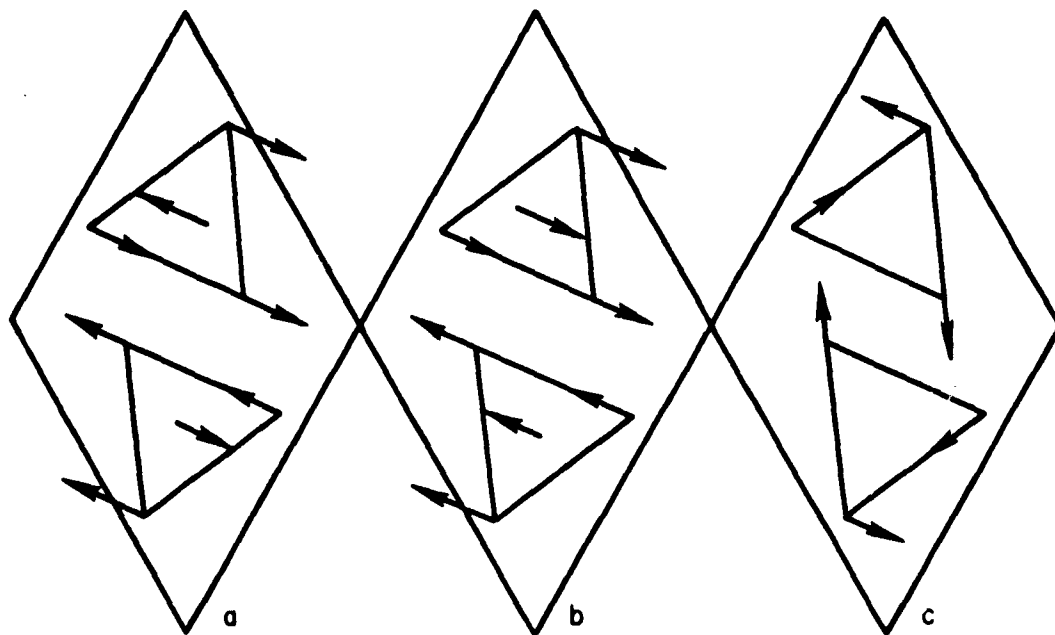


FIGURE 12. Symmetry Coordinates That Transform as $E_{2g}^1 + E_{2g}^2$.
(a, b, and c appear in Table 9 as S_{5a} , S_{5b} , and S_{5c} , respectively.)

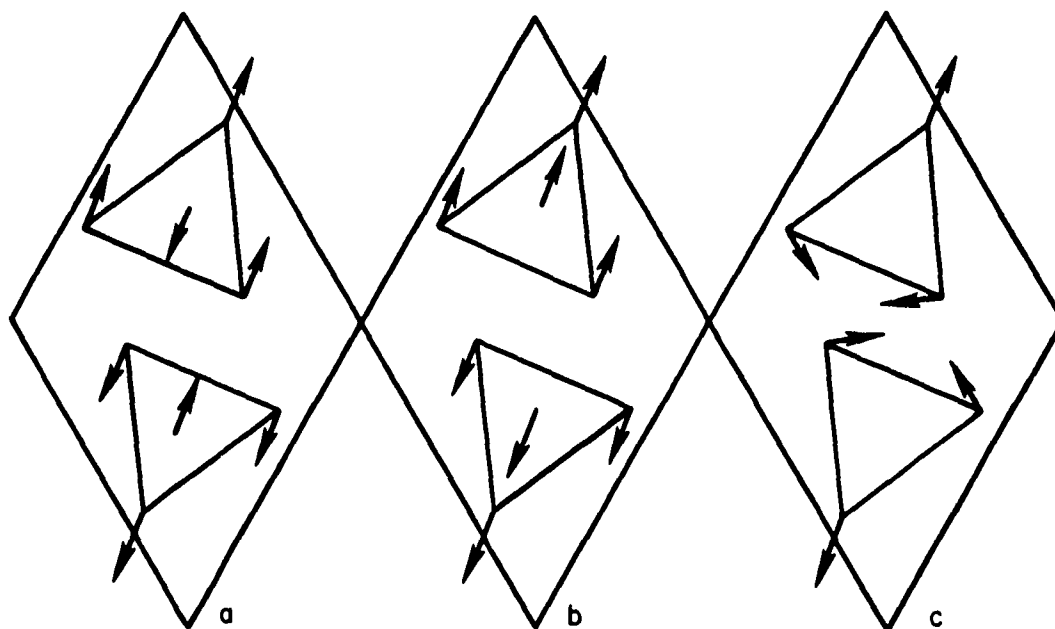


FIGURE 13. Symmetry Coordinates That Transform as $E_{2g}^1 - E_{2g}^2$.
(a, b, and c appear in Table 9 as S_{6a} , S_{6b} , and S_{6c} , respectively.)

TABLE 9. Particle Displacements in Symmetry Coordinates for LaCl_3

Representation	Symmetry Coordinate	Particle Number							
		1	2	3	4	5	6	7	8
A_g	S_1	(0,0,0)	(0,1,0)	$(-\sqrt{3}/2, -1/2, 0)$	$(\sqrt{3}/2, -1/2, 0)$	(0,0,0)	(0,-1,0)	$(\sqrt{3}/2, 1/2, 0)$	$(-\sqrt{3}/2, 1/2, 0)$
	S_2	(0,0,0)	(1,0,0)	$(-1/2, \sqrt{3}/2, 0)$	$(1/2, -\sqrt{3}/2, 0)$	(0,0,0)	(-1,0,0)	$(1/2, -\sqrt{3}/2, 0)$	$(1/2, \sqrt{3}/2, 0)$
B_u	S_3	(0,0,0)	(0,1,0)	$(-\sqrt{3}/2, -1/2, 0)$	$(\sqrt{3}/2, -1/2, 0)$	(0,0,0)	(0,1,0)	$(-\sqrt{3}/2, -1/2, 0)$	$(\sqrt{3}/2, -1/2, 0)$
	S_4	(0,0,0)	(1,0,0)	$(-1/2, \sqrt{3}/2, 0)$	$(1/2, -\sqrt{3}/2, 0)$	(0,0,0)	(1,0,0)	$(-1/2, \sqrt{3}/2, 0)$	$(-1/2, -\sqrt{3}/2, 0)$
E_{2g}	S_{5a}	(0,-1,0)	(0,1,0)	(0,1,0)	(0,1,0)	(0,1,0)	(0,-1,0)	(0,-1,0)	(0,-1,0)
	S_{6a}	(-1,0,0)	(1,0,0)	(1,0,0)	(1,0,0)	(1,0,0)	(-1,0,0)	(-1,0,0)	(-1,0,0)
	S_{5b}	(0,1,0)	(0,1,0)	(0,1,0)	(0,1,0)	(0,-1,0)	(0,-1,0)	(0,-1,0)	(0,-1,0)
	S_{6b}	(1,0,0)	(1,0,0)	(1,0,0)	(1,0,0)	(-1,0,0)	(-1,0,0)	(-1,0,0)	(-1,0,0)
	S_{5c}	(0,0,0)	(0,1,0)	$(\sqrt{3}/2, -1/2, 0)$	$(-\sqrt{3}/2, -1/2, 0)$	(0,0,0)	(0,-1,0)	$(-\sqrt{3}/2, 1/2, 0)$	$(\sqrt{3}/2, 1/2, 0)$
	S_{6c}	(0,0,0)	(-1,0,0)	$(1/2, \sqrt{3}/2, 0)$	$(1/2, -\sqrt{3}/2, 0)$	(0,0,0)	(1,0,0)	$(-1/2, -\sqrt{3}/2, 0)$	$(-1/2, \sqrt{3}/2, 0)$
E_{1u}	S_{7a}	$k(0,-1,0)$	(0,1,0)	(0,1,0)	(0,1,0)	$k(0,-1,0)$	(0,1,0)	(0,1,0)	(0,1,0)
	S_{8a}	$k(-1,0,0)$	(1,0,0)	(1,0,0)	(1,0,0)	$k(-1,0,0)$	(1,0,0)	(1,0,0)	(1,0,0)
	S_{7b}	(0,1,0)	(0,1,0)	(0,1,0)	(0,1,0)	(0,1,0)	(0,1,0)	(0,1,0)	(0,1,0)
	S_{8b}	(1,0,0)	(1,0,0)	(1,0,0)	(1,0,0)	(1,0,0)	(1,0,0)	(1,0,0)	(1,0,0)
	S_{7c}	(0,0,0)	(0,1,0)	$(\sqrt{3}/2, -1/2, 0)$	$(-\sqrt{3}/2, -1/2, 0)$	(0,0,0)	(0,1,0)	$(\sqrt{3}/2, -1/2, 0)$	$(-\sqrt{3}/2, -1/2, 0)$
	S_{8c}	(0,0,0)	(-1,0,0)	$(1/2, \sqrt{3}/2, 0)$	$(1/2, -\sqrt{3}/2, 0)$	(0,0,0)	(-1,0,0)	$(1/2, \sqrt{3}/2, 0)$	$(1/2, -\sqrt{3}/2, 0)$
A_u	S_9	(0,0,1)	(0,0,1)	(0,0,1)	(0,0,1)	(0,0,1)	(0,0,1)	(0,0,1)	(0,0,1)
	S_{10}	$k(0,0,-1)$	(0,0,1)	(0,0,1)	(0,0,1)	$k(0,0,-1)$	(0,0,1)	(0,0,1)	(0,0,1)
B_g	S_{11}	(0,0,1)	(0,0,1)	(0,0,1)	(0,0,1)	(0,0,-1)	(0,0,-1)	(0,0,-1)	(0,0,-1)
	S_{12}	(0,0,-1)	(0,0,1)	(0,0,1)	(0,0,1)	(0,0,1)	(0,0,-1)	(0,0,-1)	(0,0,-1)
E_{1g}	S_{13a}	(0,0,0)	(0,0,1)	$(0,0,-1/2)$	$(0,0,-1/2)$	(0,0,0)	(0,0,-1)	$(0,0,1/2)$	$(0,0,1/2)$
	S_{13b}	(0,0,0)	(0,0,0)	(0,0,1)	(0,0,-1)	(0,0,0)	(0,0,0)	(0,0,-1)	(0,0,1)
E_{2u}	S_{14a}	(0,0,0)	(0,0,1)	$(0,0,-1/2)$	$(0,0,-1/2)$	(0,0,0)	(0,0,1)	$(0,0,-1/2)$	$(0,0,-1/2)$
	S_{14b}	(0,0,0)	(0,0,0)	(0,0,1)	(0,0,-1)	(0,0,0)	(0,0,0)	(0,0,1)	(0,0,-1)

Note: $k = \frac{3m}{M}$ where m = chlorine mass and M = lanthanum mass.

SPECTRAL EMITTANCE OF SOLIDS

SPECTRAL EMITTANCE MEASUREMENTS OF SOME COMMERCIAL TRANSPARENT SOLIDS

by

D. L. Stierwalt, D. D. Kirk, and J. B. Bernstein

A continuing study¹ is being conducted at this Laboratory on the spectral emittance of solids. The theory, techniques, and experimental apparatus used in acquiring the spectral emittance of opaque and transparent solids in the 50-200°C temperature range in the infrared region of the spectrum have been discussed in detail in a previous report.² In this report are presented data on two commercial transparent solids that have some applications in the near infrared region.

Two samples of transparent solids, 1 mm thick, were made available through the courtesy of the Eastman Kodak Company. Termed "Irtran 3" and "Irtran 4," they consist of, respectively, polycrystalline calcium fluoride and polycrystalline zinc selenide. Figure 1 shows the spectral emittance of Irtran 3 at 100°C and Figure 2 shows the emittance of Irtran 4.

¹ NAVWEPS Report 7237, Quarterly Report: Foundational Research Projects, July-September 1962, p. 135 (December 1962).

² NAVWEPS Report 5981 (NOLC 487), Quarterly Report: Foundational Research Projects, October-December 1959, p. 41 (April 1960).

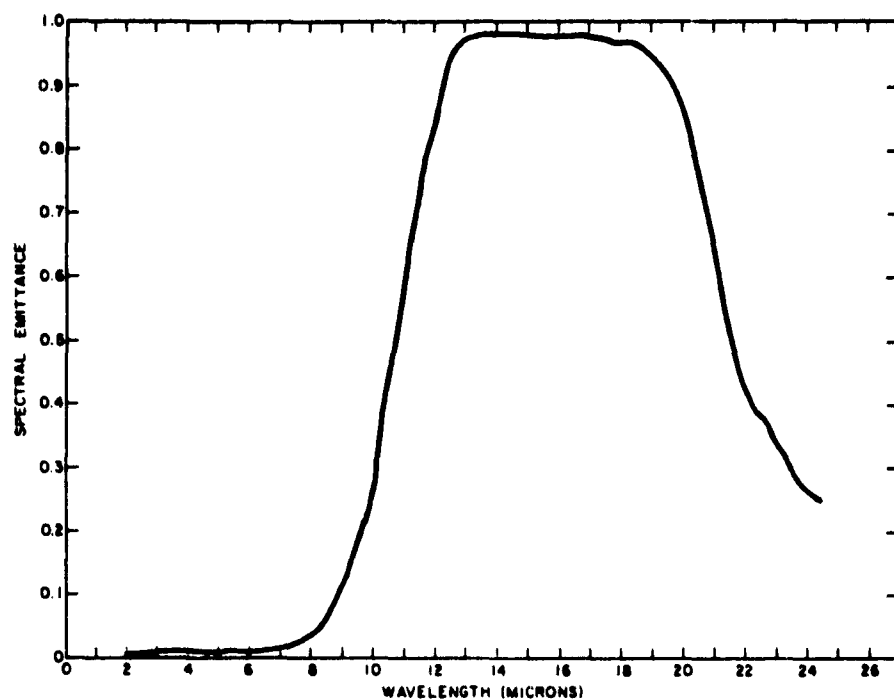


FIGURE 1. Spectral Emittance of Irtran 3 at 100°C

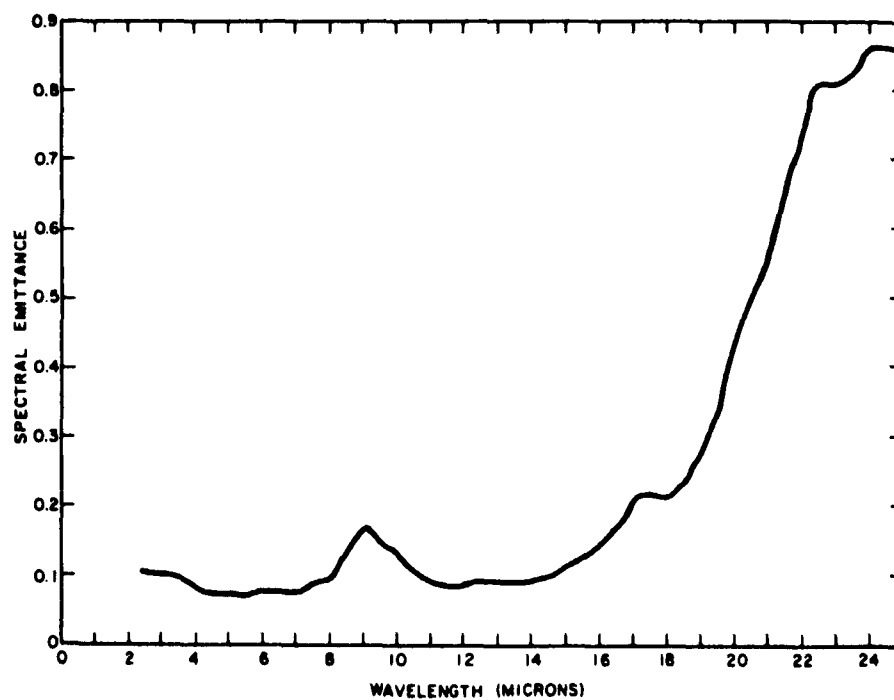


FIGURE 2. Spectral Emittance of Irtran 4 at 100°C

NAVWEPS Report 8141 - WepTasks R360 FR-104/211-1/R011-01-001 and
RMGA-41-031/211-1/F009-07-002

INITIAL DISTRIBUTION

	<u>Copies</u>		<u>Copies</u>
Chief, Bureau of Naval Weapons		Officer in Charge	
Navy Department		Naval Civil Engineering Laboratory	
Washington 25, D. C.		Port Hueneme, Calif.	
Attn: Code R-3	1	Attn: Technical Library	1
R-5	1		
R-12	1	Director	
RM	1	Naval Research Laboratory	
RMMO	1	Washington 25, D. C.	
RMWC	1	Attn: Richard Wallis	1
RRMA-3	1	Commander	1
RRRE	1	Naval Weapons Laboratory	
DLI-31	4	Dahlgren, Va.	
Director		Officer in Charge	
National Security Agency		Naval Weapons Services Office	
Fort George G. Meade, Md.		U. S. Naval Station	
Attn: REMP-2	1	(Washington Navy Yard Annex)	
Chief, Bureau of Ships		Washington 25, D. C.	
Navy Department		Attn: Code 120	2
Washington 25, D. C.		Commander	
Attn: Code 681A	1	Naval Ordnance Laboratory	
687C1	1	White Oak	
694E, D. Wilson	1	Silver Spring 19, Md.	
452F	1	Attn: E. H. Jackson, LX Division	1
Chief of Naval Research		Dr. F. Stern, Solid State	
Navy Department		Division	1
Washington 25, D. C.		Dr. E. P. Trownson, Physics	
Attn: Code 407	1	Research Department	1
420	1	Commander	
Commanding Officer	1	Naval Ordnance Test Station	
Office of Naval Research		China Lake, Calif.	
Pasadena Branch		Attn: Technical Library	1
1030 East Green Street		B. O. Seraphin, Code 5019	1
Pasadena 1, Calif.			

	<u>Copies</u>		<u>Copies</u>
Commanding Officer Naval Ordnance Test Station Pasadena Annex 3202 E. Foothill Blvd. Pasadena 8, Calif. Attn: Library		Commanding General Army Electronics Proving Ground Fort Huachuca, Ariz. Attn: SIGPG-DCGES-2	1
Director Navy Electronics Laboratory San Diego, Calif. Attn: H. E. Lee Technical Library	1	Commander Cambridge Research Center L. G. Hanscom Field Bedford, Mass. Attn: CROTLA	1
Superintendent Naval Postgraduate School Monterey, Calif. Attn: Library E. C. Crittenden, Jr.	1	Armed Services Technical Information Agency Arlington Hall Station Arlington 12, Va.	10
Commanding Officer and Director Naval Radiological Defense Laboratory San Francisco 24, Calif. Attn: L. D. Miller, Code 944A	1	Director National Bureau of Standards Washington 25, D. C. Attn: Dr. H. P. R. Frederikse, Code 4.04	1
Commander Pacific Missile Range Naval Missile Center Point Mugu, Calif. Attn: Technical Library	1	Dr. R. D. Huntoon, Code 30	1
NOLC Washington Office Naval Ordnance Laboratory White Oak Silver Spring 19, Md. Attn: W. F. Stuart	1	Aerojet-General Corporation Advanced Research Division Azusa, Calif. Attn: R. C. Carlston, Bldg. 415	1
Commanding Officer Office of Ordnance Research 55 South Grand Avenue Pasadena, Calif. Attn: Dr. W. N. Arnquist	1	Armour Research Foundation Illinois Institute of Technology Technology Center 10 West 35th Street Chicago 18, Ill. Attn: J. W. Buttrey	1
Commander Harry Diamond Laboratories Washington 25, D. C. Attn: Dr. W. K. Saunders	1	Avco Corporation Research and Development Division Physics Department - T430 Wilmington, Mass. Attn: Dr. T. Wentink, Jr.	1
		Barnes Engineering Company Stanford, Conn. Attn: R. DeWaard	1
	1	Bell and Howell Research Center 360 Sierra Madre Villa Pasadena, Calif. Attn: R. K. Willardson, Solid State	1

	<u>Copies</u>		<u>Copies</u>
Bulova Research and Development Laboratories 6210 Woodside Avenue Woodside 77, Long Island, N. Y. Attn: Dr. T. K. Steele	1	Lockheed Aircraft Corporation Plant B-1 Burbank, Calif. Attn: Dr. L. G. Mundie, Dept. 7210, Bldg. 167A	1
California Institute of Technology 1201 East California Street Pasadena 4, Calif. Attn: I. E. Newland, Reports Group, JPL	1	Lockheed Aircraft Corporation Missile Systems Division Sunnyvale, Calif. Attn: M. Eisenberg Dr. C. Kooi	1 1
Eastman Kodak Company Naval Ordnance Division 50 West Main Street Rochester 14, N. Y. Attn: W. McKusick	1	Massachusetts Institute of Technology Lincoln Laboratory Lexington 73, Mass. Attn: J. H. Chisholm	1
Ford Motor Company Aeronutronics Division Research Operations Newport Beach, Calif. Attn: L. M. Lambert	1	Motorola, Inc. 8201 East McDowell Road Phoenix, Ariz. Attn: J. C. Cacheris	1
General Electric Company One River Road Schenectady 5, N. Y. Attn: G. C. Dodson	1	Pennsylvania State College State College, Pa. Attn: Director, Ordnance Research Laboratory	1
General Telephone and Electronics Laboratory 1015 Corporation Way Palo Alto, Calif. Attn: K. A. Wickersheim	1	Servo Corporation of America 111 New South Road Hicksville, Long Island, N. Y. Attn: I. Melman	1
Hughes Research Laboratory Hughes Aircraft Company Malibu, Calif. Attn: C. Asawa	1	Syracuse University Syracuse 10, N. Y. Attn: Dr. N. Ginsburg, Physics Department H. Levenstein, Solid State Laboratory	1 1
Johns Hopkins University Applied Physics Laboratory Silver Spring, Md. Attn: Dr. A. I. Mahan A. Nagy	1 1	University of Arizona Lunar and Planetary Laboratory Tucson, Ariz. Attn: R. B. Goranson	1
		University of California Riverside, Calif. Attn: A. Lawson	1

	<u>Copies</u>		<u>Copies</u>
University of Michigan		NOLC:	
Willow Run Laboratories		J. A. Hart, Code 04	1
P. O. Box 618		C. J. Humphreys, Code 40	2
Ann Arbor, Mich.		E. Paul, Jr., Code 40	1
Attn: W. Wolfe	1	R. L. Conger, Code 42	1
Washington University		C. A. Roberts, Code 422	1
St. Louis, Mo.		K. I. Crowder, Code 43	1
Attn: Dr. E. U. Condon	1	R. F. Potter, Code 43	1
Royal Radar Establishment	1	D. L. Stierwalt, Code 43	1
Ministry of Aviation		J. B. Bernstein, Code 432	1
St. Andrews Road		D. D. Kirk, Code 432	1
Malvern		R. A. Buchanan, Code 433	1
Worcestershire, England		H. H. Caspers, Code 433	1
Attn: E. H. Putley	1	J. Murphy, Code 433	1
Via: BuWeps, Code DSC-3		H. Piller, Code 433	1
Signals Research and Development		C. P. Haber, Code 44	1
Establishment		W. S. Harris, Code 441	1
Ministry of Aviation		R. E. Panzer, Code 441	1
Christchurch		W. C. Spindler, Code 441	1
Hampshire, England		C. M. Douglas, Code 442	1
Attn: Dr. M. R. Brown		D. L. Herring, Code 442	1
(ZSP/5/08)	1	F. C. Essig, Code 45	1
Via: BuWeps, Code DSC-3		J. R. Alday, Code 452	1
Royal Aircraft Establishment		E. W. Seeley, Code 452	1
Radio Department		R. W. Yancey, Code 452	1
Farnborough, Hants, England		B. F. Husten, Code 50	1
Attn: T. S. Moss	1	L. L. Parker, Code 50	1
Via: BuWeps, Code DSC-3		H. A. Bulgerin, Code 51	1
		R. L. Bauer, Code 53	1
		J. J. Nastronero, Code 54	1
		R. J. Hardy, Code 57	1
		F. C. Alpers, Code 71	1
		W. F. Meggers, Jr., Code 72	1
		T. B. Jackson, Code 73	1
		A. C. Sevy, Code 75	1
		Technical Library, Code 234	2

<p>Naval Ordnance Laboratory Corona. (NAVWEPS Report 8141) QUARTERLY REPORT: FOUNDATIONAL RESEARCH PROJECTS, OCTOBER-DECEMBER 1962. 1 March 1963. 110 pp.</p> <p>During the second quarter of fiscal year 1963, Foundational Research projects were conducted in the following general areas: Ferromagnetic Research; High Temperature Polymers; Infrared Atomic Spectra; Nonaqueous Electrochemistry; Nonlinear Transmission Lines; Semiconductor Microwave Microelectronics; Spectral Emission of Physics; Solid State Spectroscopy; Spectral Emission of Solids.</p> <p>WepTasks: R360 FR-104/211-1/R011-01-011 RMGA-41-031/211-1/F009-07-002</p>	<p>1. Naval research 2. Ferromagnetism 3. Polymerization—Theory 4. Infrared spectrum—Analysis 5. Electrochemistry—Applications 6. Spectroscopy 7. Foundational Research Projects</p>	<p>1. Naval research 2. Ferromagnetism 3. Polymerization—Theory 4. Infrared spectrum—Analysis 5. Electrochemistry—Applications 6. Spectroscopy 7. Foundational Research Projects</p>
<p>Naval Ordnance Laboratory Corona. (NAVWEPS Report 8141) QUARTERLY REPORT: FOUNDATIONAL RESEARCH PROJECTS, OCTOBER-DECEMBER 1962. 1 March 1963. 110 pp.</p> <p>During the second quarter of fiscal year 1963, Foundational Research projects were conducted in the following general areas: Ferromagnetic Research; High Temperature Polymers; Infrared Atomic Spectra; Nonaqueous Electrochemistry; Nonlinear Transmission Lines; Semiconductor Microwave Microelectronics; Spectral Emission of Physics; Solid State Spectroscopy; Spectral Emission of Solids.</p> <p>WepTasks: R360 FR-104/211-1/R011-01-011 RMGA-41-031/211-1/F009-07-002</p>	<p>1. Naval research 2. Ferromagnetism 3. Polymerization—Theory 4. Infrared spectrum—Analysis 5. Electrochemistry—Applications 6. Spectroscopy 7. Foundational Research Projects</p>	<p>1. Naval research 2. Ferromagnetism 3. Polymerization—Theory 4. Infrared spectrum—Analysis 5. Electrochemistry—Applications 6. Spectroscopy 7. Foundational Research Projects</p>